School of Applied Science

Microsphere Distribution and Radiation Dosimetry in Human Liver following Yttrium-90 Microsphere Therapy

Andrew Mark Campbell

This thesis is presented as part of the requirements for
the award of the Degree of Doctor of Philosophy
of the
Curtin University of Technology

August 2000

Abstract

The microscopic distribution of microspheres and the resulting radiation dose deposition patterns in human liver following hepatic arterial infusion of ^{90}Y labelled microspheres have been investigated. Tissue samples from normal liver, the tumour periphery and tumour centre were taken from a patient following infusion of 3 GBq of 32 μm diameter resin microspheres labelled with ^{90}Y as treatment for an 80 millimetre diameter metastatic liver tumour. Microspheres were found to deposit inhomogeneously in tissues, preferentially lodging in a region approximately 6 mm wide around the periphery of the tumour. A relative concentration of microspheres of 50 to 70 times that of normal hepatic parenchyma and 65 to 94 times that in the tumour centre was measured in this region. The deposition of microspheres in the tumour periphery was not uniform, and cluster analysis showed that the spheres could be classified into clusters. The number of microspheres in a cluster was skewed towards low numbers and cluster sizes varied from 20 μm to 1500 μm. Microsphere deposition in normal liver was demonstrated to be non-uniform, there being significant variations in concentration over distances on the order of 3 to 4 millimetres. The observed microsphere distributions in three dimensions were used to calculate radiation dose patterns, and the results showed that heterogeneous doses were delivered to all tissues. Within the tumour periphery average doses ranged from 200 Gy to 600 Gy with minimum doses between 70 Gy and 190 Gy. The maximum and minimum doses for the tumour centre sample were 920 Gy and 3.7 Gy respectively, the median dose was 5.8 Gy. In the normal liver sample the median dose was 7.3 Gy with maximum and minimum doses of 753 Gy and 5 Gy respectively. Less than 1% of the normal liver tissue volume received more than 30 Gy, the level above which complications have resulted for whole liver exposure using external beam radiotherapy. These calculations suggest that preferential deposition of microspheres in the well vascularised periphery of large tumours will lead to a high proportion of the tumour volume receiving a therapeutic dose, with most of the normal liver tissue being spared substantial damage.

Acknowledgments

A number of people have contributed many helpful suggestions and useful discussions during the course of this work. Mr. Livio Mina contributed many hours of debate and advice on statistical methods and provided much practical and pragmatic assistance in other areas. Dr. Richard Fox and Mr. Peter Klemp contributed many helpful suggestions that were much appreciated. The contributions of my associate supervisor, Dr. David Causer, are also acknowledged. Thanks are also due to Dr. Mark Burton who supplied the tissue samples analysed in this work that made the whole thesis possible.

Finally, I would like to thank my supervisor, Dr. Ian Bailey. His continued supervision after his retirement from full time employment at the university is greatly appreciated.

Table of Contents

List of Figures

List of Tables

List of Publications/Conference Presentations Arising from this Thesis

Campbell, A., and Bailey, I. H. 1998. Analysis of the distribution of intra-arterial microspheres in human liver following selective internal radiation therapy, 13th National Congress of the Australian Institute of Physics, Fremantle, Western Australia.

Campbell, A., and Bailey, I. H. 1998. Tumour dosimetry in human liver following hepatic yttrium-90 microsphere therapy. EPSM98, Wrest Point Casino Conference Centre, Hobart, Tasmania.

Campbell, A. M., and Bailey, I. H. 1999. Dosimetry in normal human liver following hepatic yttrium-90 microsphere therapy. EPSM99, Marriott Hotel, Surfers Paradise, Qld.

Campbell, A. M., Bailey, I. H., and Burton, M. A. 2000. Analysis of the distribution of intra-arterial microspheres in human liver following hepatic yttrium-90 microsphere therapy. Phys. Med. Biol. 45(April), 1023-1033.

Campbell, A. M., Bailey, I. H., and Burton, M. A. 2001. Tumour dosimetry in human liver following hepatic yttrium-90 microsphere therapy. Phys. Med. Biol.46 (2), 487-498.

1. Introduction

The treatment of primary and metastatic neoplasms of the liver has been the subject of much effort over the last twenty or so years. Primary liver cancer, although relatively rare in the western world, is one of the most common cancers world wide. Primary hepatocellular carcinoma (HCC) is the fourth most frequently occurring gastrointestinal tract cancer in the United States (Groen, 1999). Lau et al. (1998) noted that HCC is the second most common cancer in males and the seventh most common in females in Hong Kong, and that its prognosis is poor with a mean survival time of only three months in high incidence areas. Although the exact aetiology of HCC is unknown, exposure to hepatitis B and hepatitis C viruses shows a strong correlation with the disease. The prevalence of hepatitis in Asia and parts of Africa is thought to be related to the high incidence of HCC in these areas (Groen, 1999). In western countries metastatic hepatic tumours, arising from primary tumours of the gastrointestinal tract, breast and lung are the most frequent cause of malignant hepatic disease, but metastatic liver cancer has the potential to occur from any primary tumour site (Groen, 1999). A majority of patients dying of cancers originating in structures whose venous drainage is through the portal circulation will show evidence of metastatic liver disease at the time of death (Russell et al., 1993, Leen et al. 2000). Russell et al. (1985) retrospectively studied 53 patients who had died following diagnosis of adenocarcinoma of the proximal colon and who had undergone potentially curative surgery. 58% of these patients showed liver metastases on post mortem examination and liver failure due to parenchymal metastases was the principal cause of death in 13 patients (25%). Leen et al. (2000) noted that approximately two thirds of patients who present with colorectal cancer have potentially curative surgery, but that up to 30% of these patients have undetectable hepatic metastases at the time of initial presentation.

1.1 The Liver

The liver is the largest gland in the body, weighing about 1500 g in the adult. It functions both as an exocrine gland, secreting bile through a system of bile ducts

into the duodenum, and as an endocrine gland, synthesising a variety of substances that are released directly into the bloodstream. The liver is uniquely positioned across the venous blood system, interposed between the GI tract as well as the pancreas, spleen and heart. It receives a large volume of blood from the GI tract via the portal vein and a small volume of arterial blood from the hepatic artery and it is drained by the hepatic veins that empty into the vena cava near the heart (Fawcett, 1986)). The organ has many functions and although it is often damaged by disease, it has enormous functional reserves and significant regenerative capabilities (Hamilton, 1999).

Figure 1 shows a diagrammatic view of the liver. It is divided into two principal lobes, the right and left, that are separated by the falciform ligament. The right lobe further divides into two more lobes known as the quadrate lobe and the

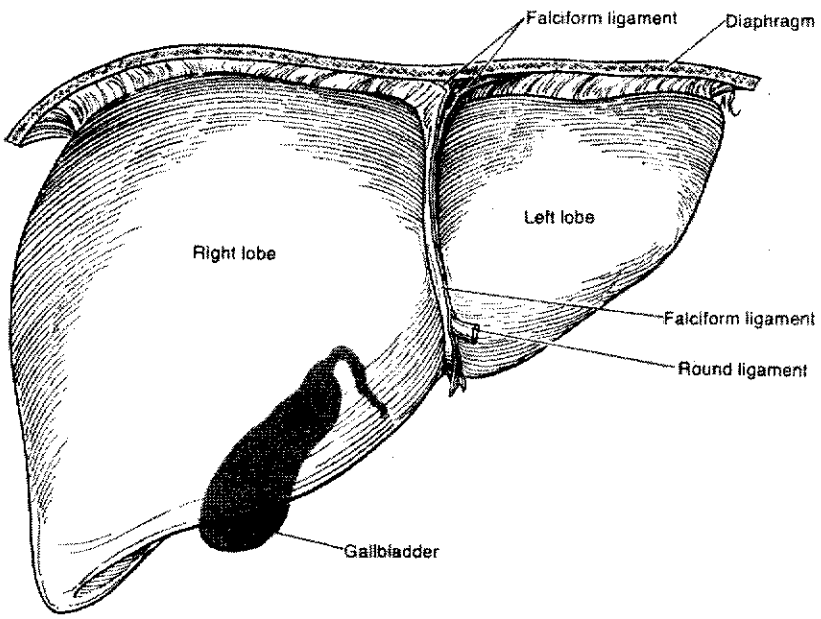

Figure 1. Diagrammatic view of a human liver showing the principle lobes. (from Tortora, 1983)

caudate lobe (Tortora, 1983). Viewed microscopically, the lobes of the liver are made up of numerous structural units known as hepatic lobules (or more often called simply lobules). It has been estimated there are approximately 1 million lobules in a human liver. The liver is covered with a connective tissue capsule

(Glisson's capsule) that branches and extends throughout the substance of the liver as septa. The connective tissue tree provides a scaffolding of support for the blood vessels, lymphatic vessels and bile ducts that traverse the liver.

The liver is composed of cells called hepatocytes. These are large (20-30 μm) polyhedral epithelial cells that form the mass of the parenchyma of the liver. The hepatocytes are arranged in plates or laminae that are interconnected to form a continuous tridimensional lattice. The cell plates are disposed radially with respect to terminal branches of the hepatic veins, which are known as central veins because of their location in the centre of roughly hexagonal shaped units of the liver parenchyma that constitute the liver lobules. In animals, such as pigs and camels, a well defined layer of connective tissue clearly demarcates the lobules. In most mammals however there is no boundary between the lobules. The radial pattern of sinusoids and the regularly distributed central veins and other anatomical landmarks allows imaginary boundaries to be assigned.

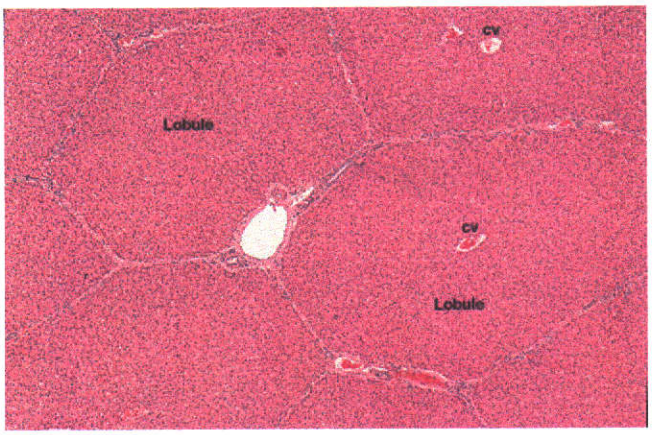

Figure 2. Low magnification view of liver tissue from a pig (magnification x40). The lobule structures can be clearly seen. The central vein (CV) is labelled for two of the lobules. (Adapted from *HB134 - Liver (low power)*, 1998).

Figure 2 shows a low magnification view of porcine liver tissues in which the lobule arrangement can be seen clearly. Between the cell plates are channels called sinusoids through which blood from terminal branches of the portal vein and hepatic artery flows into the central vein. The sinusoids form a system of thin walled vessels that provide a very large surface area for exchange of nutrients. Figure 3 provides a higher magnification view of a liver tissue section in which sinusoids can be seen radiating outwards from the central vein.

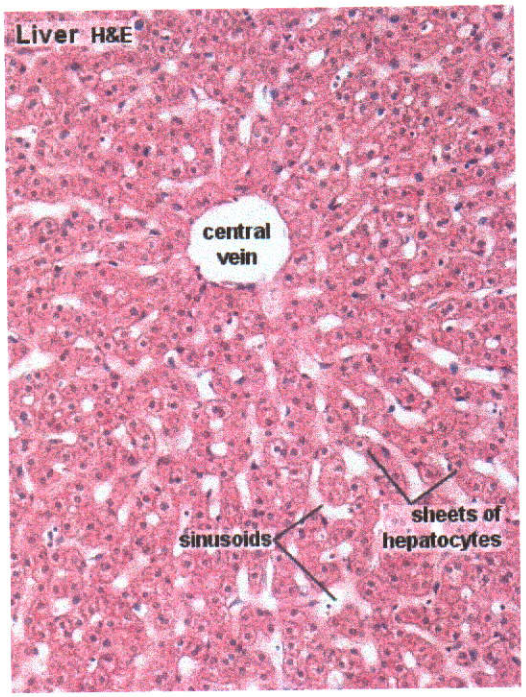

Figure 3. Higher magnification view of a liver lobule. The central vein (CV) is marked at the centre of the lobule and sinusoids can be seen radiating outwards from this vein between sheets of hepatocytes. (adapted from Blue Histology - Accessory Digestive Glands, 2000) ..

1.1.1 Hepatic Lobules

Lobules are polyhedral prisms of tissue approximately 1 - 2 mm in diameter (Last, 1978) and shown diagrammatically in Figure 4. Lobules appear to be randomly arranged and are roughly hexagonal in cross section with the vertices of each occupied by a portal triad (canals, areas, tracts and radicles are also used as synonyms for triads). The portal triads consist of small branches of the portal vein and hepatic artery as well as a bile duct enclosed in a common investment of connective tissue. An example is shown in Figure 5. Blood enters the hepatic sinusoids from small branches of the hepatic artery and portal vein, flows through the lobule and leaves via the central vein (see Figure 6). This arrangement allows arterial blood and portal venous blood, containing nutrients absorbed in the gastrointestinal tract, to mix as the blood flows from the periphery of the lobule to the central vein. Bile is produced in the liver by hepatocytes and secreted into

thin channels, known as bile canaluculi, within each hepatic plate. Bile in the canaluculi drains into the bile ducts in the portal triads.

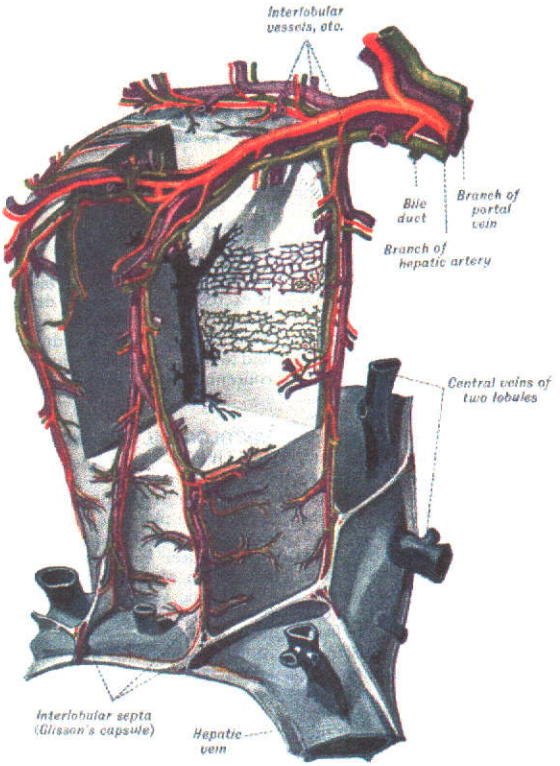

Figure 4. A wax reproduction of a lobule of the liver of a pig. A portion has been cut away to show the bile capillaries and sinudoids x400 (from Fawcett ,1986).

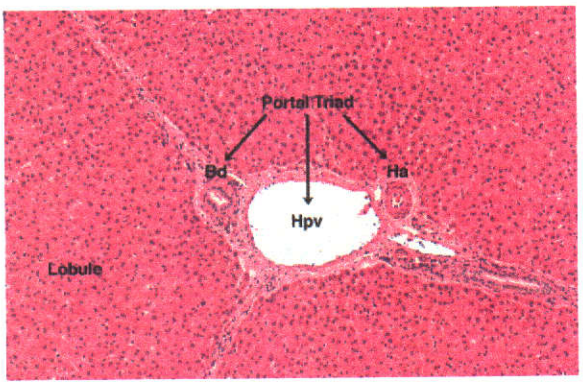

Figure 5. View of a portal triad.(x400 mag.). A portal triad consists of branches of the hepatic vein (Hpv), hepatic artery (Ha) and bile duct (Bd). (Adapted from *HB134 - Liver (high power)*, 1998)

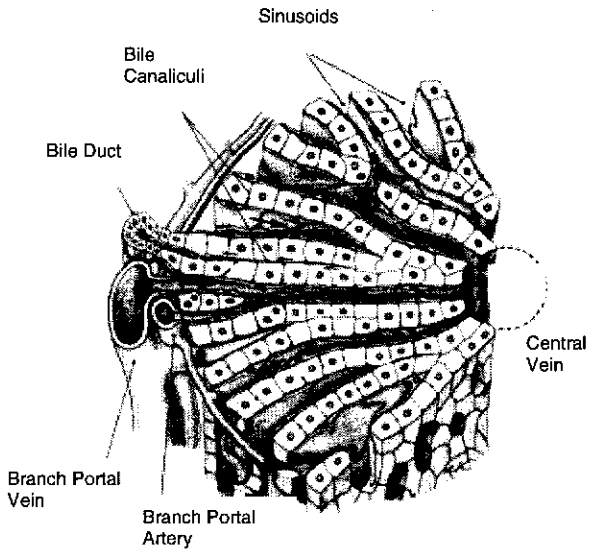

Figure 6. Diagrammatic representation of hepatic cell plates, blood vessels and sinusoid representation. (from Fawcett ,1986).

1.1.2 Hepatic Vascular System

The circulatory system of the liver is unique in the body. It is a very vascular organ and the total hepatic blood flow is about one quarter of the total cardiac output (Paton, 1999). Approximately 75% (70 - 80%) of the blood entering the liver is venous blood from the portal vein, and only 25% of blood is delivered by the relatively small hepatic artery (Groen, 1999).

The portal vein branches into interlobar veins on entering the liver and these in turn into conducting veins 400 μm or more in diameter. The conducting veins then branch into the interlobular veins. The terminal portal venules arise from the interlobular veins and are 280 μm in diameter and very thin walled. These, accompanied by a terminal branch of the hepatic artery and a small bile duct, are the axial structures of the smallest portal canals. Small lateral branches given off at frequent intervals from these terminal venules become continuous with the sinusoids of the neighbouring liver lobules (Fawcett, 1986).

On entering the liver, the hepatic artery branches into interlobar and then into intralobular arteries. The majority of the flow from these vessels is distributed to capillaries in the connective tissue of the liver. A small volume continues into the terminal hepatic arterioles of the smallest portal canals. These give off collateral branches to the hepatic sinusoids.

The primary function of the hepatic circulation is carried out in the sinusoids. These form an elaborate three-dimensional plexus that presents an enormous surface area for interchange of metabolites with the hepatic parenchyma. Blood leaves the sinusoids through the central vein of the lobule. Its wall is penetrated by numerous openings through which blood flows from the surrounding sinusoids into the vessel. The central veins drain into sublobular veins and several of these unite to form collecting veins. These in turn join to form hepatic veins which eventually drain into the inferior vena cava.

1.2 Treatment Methods for Liver Cancers

Treatment of liver neoplasms has traditionally been delivered using surgical resection, systemic and regional chemotherapy, chemoembolisation, cryosurgery and external beam radiotherapy. None of these methods is without problems.

Surgical Resection

Hepatic resection offers the best curative hope for primary liver cancers. However, hepatocellular carcinoma is typically asymptomatic during the early stages of the disease and consequently patients do not present with symptoms until the cancer is at an advanced stage (Groen, 1999). This results in only a small percentage of patients (10% to 20%) being suitable candidates for resection due to large tumour size and the presence of metastases on diagnosis (Ballantyne and Quin, 1993, Pillai et al., 1991, Groen, 1999). Unfortunately patients with hepatocellular carcinoma often develop recurrences following resection, indicating that tumour cell dissemination must have occurred preoperatively or intraoperatively (Kienle et al., 2000).

Surgical resection may also offer a chance of long term survival for some

patients presenting with metastatic liver cancer arising from primary colorectal cancer, provided the liver is the only site of metastatic disease (Scheele et al., 1991). However, liver metastases are usually diffuse at the time of diagnosis, and surgical resection is rarely feasible (Ruszniewski & Malka, 2000).

Systemic chemotherapy

Systemic chemotherapy involves the administration of chemotherapeutic drugs intended to induce toxicity in tumour tissues. Fluorinated pyrimidines, for example fluroxidine and 5-fluorouacil, are frequently used in systemic chemotherapeutic treatments of liver cancers (Archer and Gray, 1990, Robertson et al., 1997, Ho et al., 1998). Response rates to systemic chemotherapy are generally between 10% and 20% (Groen, 1999), with only a marginally improved survival rate (Ruszniewski & Malka, 2000, Chang et al., 1987). This is probably due to the fact that toxic chemotherapeutic drugs, in order to prevent toxicity to non-target tissues, have to be applied at sub therapeutic doses and thus tend to be of minimal effect (Pillai et al., 1991).

While systemic chemotherapy alone has not been shown to be effective in prolongation of patient survival, it is frequently included as an adjuvant therapy to enhance the effects of the primary treatment (Leen et al. 2000, Groen, 1999). For example, fluroxidine and 5-fluorouacil are frequently administered in conjunction with radiotherapy as they are radiation sensitisers (Robertson et al.,1997; McGinn et al., 1998).

Regional Chemotherapy

Regional chemotherapy can be delivered by hepatic intra-arterial infusion of chemotherapeutic drugs. This treatment relies on the fact that liver metastases derive most of their blood supply from the hepatic artery, while normal liver parenchyma is perfused primarily from the portal vein and receives only about 25% of its blood from the hepatic artery. Therefore higher levels of chemotherapeutic agents are absorbed by tumour cells when the drug is infused via the hepatic artery. Additionally, many chemotherapy drugs are completely removed from circulation by the liver during first-pass metabolism (Groen,

1999). This allows for much higher concentrations of the drug to reach the tumour with reduced systemic side effects, but the treatment is associated with hepatic toxicity (Cascinu at al., 1998).

While response rates of 50% to 80% have been reported for this type of therapy using fluorodeoxyuridine and 5-floxuridine (Ho et al., 1998, Groen, 1999), prolongation of survival has only been on the order of months (Ho et al., 1998). In addition, candidates for this therapy must have no evidence of extrahepatic metastases (Groen, 1999).

Chemoembolisation

Chemoembolisation involves the injection of embolizating agents into the hepatic arterial system in order to block the small arterioles and capillaries leading to the tumour, resulting in ischaemic necrosis of the tumour (Groen, 1999). While this treatment has been shown to reduce tumour growth, it has not been demonstrated to improve survival and often causes episodes of liver decompensation.

Cryosurgery

Cryosurgery involves the circulation of liquid nitrogen through a cryoprobe placed in the centre of liver metastases. A cycle of rapid freezing followed by gradual thawing of the tumour, as well as a narrow rim of normal liver causes cell death (Weaver, Atkinson and Zemel, 1995). This treatment has been used mainly to treat liver metastases from colorectal cancer, but other types of metastases and primary liver cancer have been treated as well (Groen, 1999). Tumours greater than 6 cm in size are difficult to destroy because of the size of the ice ball required (Cascinu at al., 1998).

External Beam Radiotherapy

While external beam radiotherapy is widely used in the treatment of malignant neoplasms, the relative radiosensitive of liver parenchyma, and consequent radiation induced hepatic toxicity, limits treatment using external beam radiotherapy to palliative doses (Ho et al., 1998). Delivering excessive radiation

doses to the liver results in the potentially fatal complication of radiation hepatitis (Lawrence et al., 1995). A discussion of the tolerance of liver tissues to radiation is presented in section 1.5.1. Doses delivered by external beam radiotherapy may be further limited by exposure to other critical organs such as the spinal wall, heart and pancreas (Andrews et al., 1994).

1.3 Treatment for liver cancer using targeted radioactive microsphere therapy

The drawbacks and limitations of traditional treatment methods for liver cancer have led researchers to investigate other methods of delivering therapeutic agents to tumours whilst sparing normal hepatic parenchyma. Over the past decade there has been a resurgence of interest in using radiotherapy to treat liver malignancies. Targeted radioactive microsphere therapy is a treatment technique that aims to deliver therapeutic doses of radiation to tumours whilst keeping doses to normal hepatic parenchyma below its tolerance limit.

Radiation has been used as a cancer treatment for nearly 100 years. Radium was discovered in 1898 by Marie and Pierre Curie and within 5 years its effectiveness as a cancer treatment had been histologically proven in two patients suffering from basal cell carcinoma of the face. Implantation of a radioactive source directly into a tumour was first suggested by Alexander Graham Bell in 1903 (Mould, 1994a). The term *brachytherapy*, with *brachy* from the Greek for 'short-range', is used for this type of treatment where a radioactive source having short-range tissue penetration is placed close to a tumour in order to try and effect a cure. Brachytherapy treatment methods have increased in sophistication in the areas of dosimetry, source placement and delivery in recent years. However they still mainly involve placement of radioactive sources external to the body, either close to the skin surface or within body cavities, or use implantation of radioactive sources directly into tumours. An excellent compendium of current brachytherapy practice is given in Mould et al. (1994b).

Targeted radioactive microsphere therapy attempts to target liver tumours whilst sparing normal hepatic parenchyma (see for example Anderson et al., 1992, Burton and Gray, 1995, Lau et al., 1998). This method utilises the unique blood supply mechanism of the liver in which normal liver tissue receives only about 25% of its blood supply from the hepatic artery, while hepatic tumours derive their blood supply almost exclusively from this source (Ridge et al., 1987, Mumper, Ryo, and Jay, 1991). Infusing microspheres that have been sized to trap in the precapillary circulation of tumours via the hepatic artery will result in preferential uptake of microspheres in tumour tissues, resulting in favourable tumour to normal tissue ratios (Gray et al., 1989). Meade et al. (1987) found a mean tumour to normal liver (T/N) arterial perfusion ratio of 3:1 for microspheres having diameters of 15 and 32.5 μm, but no increase in the ratio for 50 μm diameter microspheres for hepatic arterial infusions in rats. Hafeli et al. (1999) performed hepatic arterial infusion of glass microspheres in rats and reported average T/N ratios of 2. Archer and Gray (1989) reported that lesions as small as 0.5 mm had developed a rich internal circulation fed almost exclusively via the hepatic artery and found T/N ratios of 1.5 for hepatic infusion of microspheres. The preferential uptake of microspheres by tumour tissues means that normal liver tissues receive a lower radiation exposure than tumour tissues, helping to reduce the limitations on tumour doses imposed by liver toxicity effects when using external beam radiotherapy that typically exposes the whole liver. The same rationale has also been applied to microspheres labelled with chemotherapeutic agents (see for example Ciftci et al., 1997, Codde et al., 1993).

Relative blood flow to tumours, and hence uptake of microspheres, can be enhanced by infusion of microspheres in conjunction with a vasoconstrictive agent (Endrich and Vaupe, 1998, Burton et al., 1985). As discussed in section 1.4.1, while neoplastic vessels develop anatomically under stimulation by angiogenic factors, they do not retain normal physiological function. Burton, Gray, and Coletti (1988), noted that this provides the opportunity to exert a degree of blood flow control to tumours via vasoactive manipulation of the surrounding hepatic vasculature which retains normal innervation. They used the powerful vasoconstrictive drug Angiotensin II at the time of microsphere infusion

and found significant increases in T/N ratios both in the tumour periphery and the tumour centre for transplanted squamous cell carcinomas in sheep. Goldberg et al. (1991) used Angiotensin II during hepatic infusion of cytotoxic loaded albumin microspheres in patient with colorectal liver metastases and found a doubling of the T/N ratios. Anderson et al. (1992) also used Angiotensin II to enhance tumour uptake in human patients treated with glass ^{90}Y microspheres as a treatment for colorectal liver metastases.

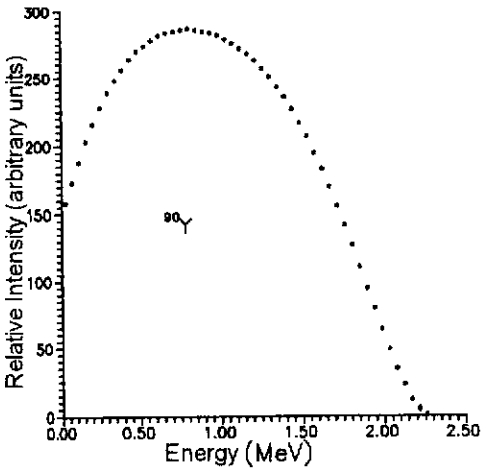

Figure 7. Beta particle energy spectrum for ^{90}Y. (adapted from Simpkin and Mackie, 1990)

The microspheres are most often labelled with a pure beta emitting isotope, with ^{90}Y being the most commonly used (see, for example, Dancey et al., 2000, Lin et al. 2000, Gray et al., 1992, or Andrews et al., 1994), although the use of isotopes emitting gamma and beta radiation such as ^{166}Ho (Mumper et al., 1991, Turner et al., 1994, Nijsen et al., 2000) and ^{188}Re or ^{186}Re (Wang et al., 1998, Hafeli et al., 1999) have been reported. β particles emitted from a radioactive material are simply energetic electrons. The electrons emitted are not monoenergetic but consist of a range of energies up to a maximum value characteristic of the radionuclide. Figure 7 depicts the beta energy spectrum for ^{90}Y, which is a pure β emitter with a physical half life of 64 hours. The β particles have a mean energy of 0.937 MeV with a maximum energy of 2.2 MeV.

Bichsel (1968) has discussed methods by which electrons interact with matter and his work can be summarised as follows. For electrons having energies up to 100 MeV the major interactions with matter can be broken into three main types: interactions with the individual electrons of the atoms and molecules, interactions with the nuclei, and interactions with the atoms as a whole. The last interaction

method occurs when the electron energies are below the excitation energies of the atoms, the electron interacts with the coupled system of nucleus plus atomic electrons. This is in contrast to the situation at higher energies where the coupling between the particle struck and the rest of the atom has a negligible effect on the energy transfer. The electron's low mass means that it can lose a large fraction of its energy in a single collision within the medium and can be deflected through large angles. This means the path of an electron can be tortuous, depending on the angles through which it is scattered. The distance a charged particle travels through matter before losing all its kinetic energy is known as the path length, and the penetration distance is defined as the linear distance travelled from the point of emission. For electrons the path length may be much greater than its penetration distance. The average penetration distance for many particles from a radiation source is the range of the particles in the medium. The fact that electrons can be deflected through large angles means that, even for monoenergetic electron sources, there is a great variation in penetration distances and consequently electrons do not have a well defined range. The presence of a spectrum of electron energies for beta emitting radioisotopes further compounds this effect. There is however a maximum distance beyond which no electrons will penetrate. For ^{90}Y in tissue the maximum penetration distance is approximately 10 mm (Andrews et al., 1994). Few electrons reach this distance and 90% of the energy from β emissions for ^{90}Y is deposited within 5.34 mm of the source (Simpkin and Mackie, 1990).

The finite range of beta radiation means there is no significant exposure of sensitive structures, such as the spinal cord, heart or pericardium, as may occur with external beam irradiation, when using targeted microsphere therapy (Andrews et al., 1994).

Hepatic intra-arterial infusion of ^{90}Y labelled microspheres has been reported to improve tumour to normal therapeutic ratios (Burton et al., 1989b, Roberson et al., 1992, Lau et al., 1998) and to lead to regression of liver metastases (Gray et al. 1992, Andrews et al., 1994, Lau et al., 1998, Hafeli et al., 1999, Dancey et al., 2000). The treatment method might be more effective against tumours of a

few centimetres or more in size as shown by modelling of dosimetry by Nahum (1996). This work, and more recent modelling of tumour control probabilities by Ebert and Zavgorodni (2000), suggests that tumours which are small compared to the range of the β particles being used are harder to cure than larger ones, and that delivering curative radiation doses to microscopic sized metastases is impossible. However Burton and Gray (1995) noted that microscopic tumours have not developed their own arterial supply and are fed by diffusion from the portal circulation They found, in a study in rats, that infusion of ^{90}Y labelled microspheres into the portal vein was effective in treating microscopic sized metastases, suggesting there may be a role for portal infusion of microspheres as an adjuvant treatment for patients at high risk of developing liver metastases.

1.3.1 Patient suitability for ^{90}Y microsphere treatment

Prior to ^{90}Y microsphere administration, a patient's suitability for the treatment is normally assessed using nuclear medicine imaging, as the presence of a significant amount of arterio-veneous shunting to the lungs via the liver precludes treatment using this method. This is because an unacceptable lung radiation dose would be delivered (Lau et al., 1998, Andrews et al., 1994). The expected distribution of microspheres is normally assessed by infusion of ^{99m}Tc labelled macroaggregated albumin (^{99m}Tc-MAA), using the same techniques as for the therapeutic microspheres, and imaging the resulting MAA distribution. ^{99m}Tc-MAA has a similar particle size to the microspheres and is assumed to distribute in the same manner. As ^{90}Y is a pure beta emitter, post-treatment imaging is only possible using bremsstrahlung radiation. The problems of imaging with bremsstrahlung radiation from high energy beta emitters precludes accurate quantitative information from being obtained (Shen et al., 1994), but such images are normally obtained to ensure no gross variation exists between the preliminary ^{99m}Tc-MAA scan and the actual ^{90}Y microsphere distributions.

1.4 Distribution of microspheres

Microspheres are carried to their ultimate deposition sites by blood flow, so it is to be expected that deposition patterns will reflect blood perfusion. An understanding of how microspheres will distribute is then dependent on an understanding of blood perfusion patterns to tumours, a discussion of which follows.

1.4.1 Tumour vascularisation model

The cells of solid tumours grow in densely packed populations that form into spheroidal or ellipsoidal aggregates. This geometry means that the absorption of oxygen and nutrients is diffusion limited, restricting tumour sizes to approximately 1 mm^3 (about 10^6 cells) unless the neoplasm can somehow tap into the capillary bed of the vascular network (Shilling et al., 1999, Konarding et al., 1999). Studies have shown that tumours reach a stage in their growth in which they themselves can stimulate the growth of new capillaries from the host vascular system.(Hayes, Li and Lippman, 2000). Prior to this, the tumour grows in what is known as the avascular stage. After this time, growth is in the vascular stage (Cravalho et al., 1980). While neoplastic vessels in the vascular stage develop anatomically under stimulation of angiogenic factors, such vessels do not retain normal physiological function (Burton et al., 1988). The vessels are relatively physiologically inert - they do not have the ability to regulate blood flow, direction and capacitance and do not have normal neural innervation (Song, 1998).

In the early avascular stage, absorption of nutrients and elimination of wastes is effected by diffusion. Newly developed capillaries supply the tumour after it reaches a certain diameter. Archer and Gray (1989) found that liver metastases as small as 0.5 mm had well developed internal circulation. Recent studies have shown that the process of angiogenesis can occur at the earliest stages of tumour growth. Li et al., 2000 observed formation of new vessels when tumours consist of only approximately 100 cells. After this, growth occurs at an exponential rate limited only by vascular supply (Schilling et al., 1999, Hayes et al., 2000).

During this period, capillaries penetrate the tumour volume, and may occupy up to 10% of the volume (Jain, 1994). However the extent of vascularisation is extremely dependent upon tumour type. Brain tumours are the most vascularised followed by carcinomas and then sarcomas (Cravalho et al., 1980). Tumour blood vessels grow in a chaotic manner. Fukumura et al. (1997) observed liver tumour microvasculature that was tortuous and frequently branching. They also noted that some vessels showed abrupt diameter changes and formed shunts or loops. Kondering et al (1998) also noted that abrupt changes in vessel diameter, leaking sprout tips and blind ends are common in tumour microvasculature. Tumour vessels also have spatially and temporally heterogeneous blood supplies (Fukumura et al., 1997), and Song (1998) noted that not all vessels visible on histological sections may function.

Once a tumour diameter of around 10 mm is reached, the initial rapid growth has begun to decay, and beyond this size the growth rate varies inversely with tumour size. As a tumour grows larger, there is a deterioration of the vascular network in the tumour core (Fukumura et al., 1997) while the periphery remains well perfused at a level well above that of the normal surrounding tissue (Kondering et al., 1998). Thus larger tumours display heterogeneous blood perfusion (Cravalho et al., 1980, Jain, 1994). Growth is confined to the outer periphery and this region is the most highly vascularised in any given tumour (Hayes et al., 2000, Burton et al., 1985). However, it has been noted that while the central portions of a tumour are relatively dormant, they do have the potential for further tumour growth, especially if their blood supply is re-established (Burton et al., 1985, Kondering et al, 1999).

A tumour model can therefore be put forward in which the neoplasm is divided into a number of regions. At the tumour centre there is a necrotic core which has little vascularisation. This is surrounded by a region in which perfusion increases, proceeding outward from the tumour centre. Cravalho et al. (1980) further divides this area into two regions - the first being a semi-necrotic area that contains long capillaries with no branching followed by a region of stabilised

tumour microcirculation. Surrounding this is the advancing tumour front which is highly perfused, even more so than normal tissue.

1.4.2 Distribution of microspheres following targeted microsphere therapy

The macroscopic distribution of microspheres in tumour and normal tissues is in agreement with typical blood perfusion models, although microsphere deposition may not be directly proportional to blood flow as Anderson et al. (1992) reported that a greater proportion of microspheres were delivered to tumours than would be expected from baseline arterial flow measurements. It has been observed that microspheres lodge preferentially in the periphery of tumours in rats and rabbits (Burton et al., 1985) and also in sheep (Burton et al., 1988). Lau et al. (1998) treated patients suffering from hepatocellular carcinomas with ^{90}Y microspheres. They observed small numbers of microspheres in the necrotic centre of tumours, but saw large aggregations of microspheres in the periphery of the tumours.

There have only been limited studies on the distribution of microspheres at sub millimetre scales following hepatic radioactive microsphere infusion. Fox et al. (1991) examined the distribution of 32 μm microspheres in normal liver in a human patient following targeted hepatic radioactive microsphere therapy. They serially sectioned a tissue sample taken from normal liver into 10 μm thick sections and determined the spatial distribution of microspheres using microscopic analysis. They observed that microspheres were deposited along small arteries which had lengths of the order of 1 millimetre and that this introduced considerable correlation between microsphere positions in adjacent sections. Fox et al. (1991) reported that this correlation in microsphere position meant that for radiation dose calculations using ^{90}Y, it was not necessary to determine microsphere positions in all sections. Accurate radiation doses could be calculated by taking slices at 500 μm intervals and ignoring intervening sections.

Perhaps the most comprehensive study of this nature has been carried out by Pillai et al. (1991) using a rabbit model. They infused 27 μm diameter microspheres into three New Zealand white rabbits that had hepatic VX2 tumour

implants. Microspheres were infused via the hepatic artery in two of the rabbits, with one receiving 15 x 10^6 microspheres and the other double this number. The third received 300 x 10^6 microspheres via the left ventricle by intra-cardiac puncture. Tissue samples were taken from both normal liver and tumour nodules within the liver, serially sectioned, and the sections subjected to microscopic analysis in order to determine the spatial distribution of microspheres. Pillai et al. (1991) observed that while individual microspheres were dispersed throughout normal hepatic parenchyma and tumour tissues, the majority aggregated into clusters of various sizes. They defined a microsphere cluster as a group of microspheres separated from adjacent microspheres by a distance of less than 50 μm, and analysed microsphere deposition patterns to quantitate parameters defining the clusters such as number of microsphere per cluster, size of clusters, the minimal distances separating clusters and the number of clusters per unit volume of tissue. They reported that 6 - 12 times as many microspheres deposited in tumours compared with normal tissue. Analysis of microsphere clustering showed that cluster populations were skewed towards low numbers, with 50% of clusters consisting of one or two microspheres, although some aggregations in excess of 25 microspheres were observed. They observed a higher concentration of clusters within tumour than in normal liver tissues, and clusters in tumour tissues were separated by smaller distances. Pillai et al. (1991) also reported that infusing greater numbers of microspheres via the hepatic artery did not increase the number of microsphere clusters per unit volume but simply increased the number of spheres in each cluster, thus infusing increasing numbers of microspheres is unlikely to result in more uniform microsphere deposition.

1.5 Tolerance of normal liver to radiation and radiation dosimetry for radioactive microspheres

1.5.1 Tolerance of the liver to radiation

The tolerance of normal liver to external beam irradiation has been the subject of considerable research, as excessive exposure to radiation can lead to the

potentially fatal complication of radiation hepatitis. The situation for radiation doses delivered using targeted radioactive microsphere therapy is more uncertain.

Russell et al. (1993) studied patients with hepatic metastases arising from gastrointestinal tract primary tumours using a hyperfractionated irradiation protocol of the whole liver. They found patients who received 27 - 30 Gy showed no evidence, either clinical or biochemical, of radiation induced liver injury while patients receiving 33 Gy whole liver exposures, delivered in 1.5 Gy fractions, had a substantial risk of delayed radiation injury. Radiation dose levels delivered in this study were not curative. No increase in the median survival time of treated patients was observed, nor was there a reduction in the frequency with which liver metastases were reported as the cause of death. Lawrence et al. (1992) reported a significant incidence of radiation hepatitis in patients who received whole liver irradiation which delivered a mean dose of over 37 Gy.

The consensus in the literature is that the whole liver can be treated safely only by doses up to about 30 - 35 Gy using conventional fractionation. Such doses are not curative but can produce palliation (Lawrence et al., 1995). Donath et al. (1990) noted 70-90% of patients who receive whole liver doses of 30 Gy, delivered in 15 fractions over a three week period, experience significant palliation and an increase in the quality of life with negligible toxicity for the duration of their survival.

Heterogeneity of radiation dose distribution has also been recognised as affecting potential organ toxicity (Caudry et al., 1993). For partial liver irradiation, radiation doses that could be expected to cause toxic effects if delivered to the whole liver can be applied without increased incidence of liver injury (Lawrence et al., 1995, Robertson, 1997). Until recently, estimates of the volume of liver irradiated and the dose it received were relatively crude, making characterisation of threshold doses difficult (Lawrence et al., 1995). The development of three dimensional treatment planning has allowed much more precise estimates of dose and volume to be achieved (Lawrence et al., 1992) and this, combined with the development of more precise and flexible treatment facilities, has caused a resurgence of interest in models predicting relationships between dose volume

and normal tissue complications (Caudry et al., 1993). Lawrence et al. (1992) used three dimensional dose volume histograms to examine normal tissue complication probabilities in patients treated using external beam radiotherapy for hepatic tumours. They found the fraction of liver treated strongly affected the dose that could be applied without radiation hepatitis developing. For patients having less than one third of the whole liver exposed, mean doses of 67 Gy were delivered without complication, while for exposure of one half of the liver mean doses of 48 Gy were tolerated without any occurrence of toxic effects. These dose levels are in agreement with the experience of Robertson et al. (1997) who delivered doses of 66 Gy for less than 33% whole liver exposure, and 48 Gy for 33 to 66% whole liver exposure without any effects of late hepatic toxicity being observed in patients with primary hepatobillary carcinomas.

1.5.2 Dosimetry for Radioactive Microspheres

Dosimetry estimates to tissues following hepatic infusion of microspheres are often at best estimates of mean tissue dose. As discussed by Feinendegen (1994), the conventional method of determining absorbed tissue dose uses the Medical Internal Radiation Dose Comittee (MIRD) concepts (Synder et al., 1975) which are based on the average energy deposited per mass of tissue. For radioactive microsphere treatment, this assumes all the activity infused is delivered uniformly throughout the liver (Andrews et al., 1994). Assuming a uniform activity distribution ignores the benefits of preferential uptake of microspheres in tumour tissue gained by the method of administration. It also neglects the fact that the radioactivity is attached to the microspheres and will not deposit uniformly in tissues, even if microsphere deposition happened to be uniform, violating one of the MIRD assumptions of homogeneous radiation dose deposition. Ho et al. (1996) used a partition model to allow for the preferential uptake of microspheres in tumours by using pre-treatment distribution studies performed using ^{99m}Tc labelled macroaggregated albumin (^{99m}Tc-MAA) to estimate the relative uptake of microspheres by tumour and normal liver and tissues. They used CT scans to determine tissue volumes and hence masses for the two tissue types and calculated radiation doses to tumour and normal liver

tissues using MIRD principles. Burton et al. (1989a) performed intraoperative dosimetry using direct beta-probing of the liver and tumour surface during laparotomy in order to estimate mean radiation doses to tumour and normal tissues. This technique appears more likely to provide an estimate of average doses near the surface of the tissues probed, as activity in these tissues will have the most influence on the readings.

Mean radiation doses tolerated by normal hepatic parenchyma to radiation delivered using this technique appear to be much higher than those tolerated using external beam radiotherapy (Gray, 1990). Assuming that all infused activity distributed uniformly throughout the liver, Andrews et al. (1994) calculated that doses of 50 to 150 Gy to normal liver tissue could be tolerated without any evidence of hepatic toxicity. Lau et al. (1998) used the partition model of Ho et al. (1996) to calculate normal liver tissue doses. They reported delivery of doses between 25 Gy and 136 Gy in single treatments and cumulative doses of up to 324 Gy using multiple treatments to patients without any developing radiation hepatitis. Burton et al. (1989a), using direct beta-probing of the liver surface, calculated normal liver radiation doses of up to 75 Gy in patients without observing any evidence of radiation damage.

1.5.3 Microdosimetry

Dosimetry based on mean delivered doses does not adequately consider the heterogeneous distribution of microspheres in tissues (Feinendegen, 1994). However, there have only been a limited number of studies done on the distribution of microspheres and the resulting radiation dose distributions in the liver at sub-millimetre scales following the hepatic infusion of microspheres. Pillai et al. (1991) infused microspheres into rabbit liver and carried out a detailed analysis of microsphere distributions in both tumour and normal liver tissue. Using this data, Roberson et al. (1992) performed radiation dosimetry calculations for a 2 mm tumour nodule and a similar volume of normal liver. Fox et al. (1991) examined microspheres in a sample of normal human liver and performed radiation dosimetry calculations using the observed microsphere

distributions. In these studies, it was found that the distribution of spheres was inhomogeneous, causing the resulting dose distributions to be inhomogeneous also. Fox et al. (1991) estimated that one third of normal liver will receive less than 33.7% of the dose predicted by assuming a homogeneous distribution of ^{90}Y. Zavgorodni (1996) developed a model for dose estimation from radioactive microspheres based on the distribution studies of Pillai et al. (1991) and formed similar conclusions. This is the most likely reason why liver tissue shows a greater tolerance to radiation delivered in this manner compared with external beam radiotherapy (Gray et al., 1990).

1.6 Radiation dose required to kill tumours

The goal of radiotherapy treatment is to deliver sufficient radiation dose to a tumour to destroy the whole tumour, while at the same time attempting to spare normal tissues to avoid significant damage and later complications (Lowry, 1974). Assuming that a tumour requires a certain minimum number of cells for regrowth, then sufficient radiation dose must be delivered to reduce the number of tumour cells below this critical number (Moss, Brand, and Batifora, 1973).

The biological effect of radiation depends on a number of factors. The type of cell and the cell's environment both have an effect. More rapidly dividing cells are, in general, more radiosensitive (Moss et al., 1973). On average, cells are less sensitive to radiation if there is inflammation, necrosis or hypoxia present. More intercellular contact also increases radioresistance (Moss et al., 1973).

The manner in which the radiation dose is delivered and its spatial variation also impacts its biological effect (Ebert and Zavgorodni, 2000). Increasing the dose rate increases the effectiveness of irradiation (Trott. 1987). Walter, Miller, and Bomford (1979) noted that delivery of radiation dose continuously may be advantageous. The length of treatment also influences the outcome because repair of sublethal damage and tumour regrowth can occur. In general the longer the treatment time, the higher the dosage required to achieve comparable results (Ebert and Zavgorodni, 2000). Permanently implanted sources, such as ^{90}Y microspheres, deliver a radiation dose rate that decays exponentially with time.

Longer lived radioisotopes deliver radiation doses over a long period and at low dose rates compared with external beam radiotherapy. As a result, larger absorbed doses must be prescribed to achieve the same biological effect (Ling, 1992). For example, when using ^{125}I, which has a 60 day half life, a delivered radiation dose of 160 Gy has the same biological effect as 60 Gy delivered in 2 Gy fractions using external beam radiotherapy (Donath et al., 1990). Ling (1992) noted that for permanent implants at least the following factors influence the final outcome: cell inactivation by protracted irradiation, repair of sublethal damage during the radiation delivery, tumour regrowth and the exponentially decreasing radiation dose rate. He discussed that the combined influence of these factors means that beyond a certain effective time, T_{eff}, there is no increase in the biological effect or decrease in the surviving tumour cell fraction, even though additional radiation dose continues to be delivered. If, by T_{eff}, sufficient dose has not been delivered to control the tumour, then regrowth will occur and the treatment will be unsuccessful.

Most radiotherapy treatment is performed using external beam radiotherapy. Treatment is not normally delivered using a single acute exposure, but in a number of small fractions given over a period of time, usually 5 – 6 weeks. The standard fractionation regime is to give 2 Gy per fraction and to treat 5 days per week. Fractionated treatment regimes have proven to be superior in both safety and curative effect (Walter et al., 1979). Curative radiation doses vary with the type of cancer. Table 1 provides a summary, compiled from Walter et al. (1979), Moss et al. (1973) and Lowry (1974), of typically prescribed doses for a variety of tumours for fractionated external beam radiotherapy treatments.

A general rule of thumb is that 60 Gy delivered in 2 Gy fractions over a 5 to 6 week period is a tumourcidal radiation dose.

Table 1. Typical prescribed radiation doses for external beam radiotherapy treatments. (Compiled from Walter et al. (1979), Moss et al. (1973) and Lowry (1974))

Cancer Type	Prescribed Dose (Gy)	Treatment Period
Skin	40-55	5 weeks
Tongue	55-70	5-7 weeks
Mouth	55-65	5-6 weeks
Neck	55-60	5 weeks
Thyroid	45-55	4-5 weeks
Oesophagus	50	4 weeks
GI Tract	30-50	4-5 weeks
Lung	45-50	4-5 weeks

1.6.1 Radiation dose required to kill liver tumours

As discussed in section 1.5, the radiosensitivity of normal liver parenchyma limits radiation doses to palliative levels when using external beam radiotherapy. As a consequence no information about the tumourcidal dose required for liver tumours is available from experiences using this treatment technique. Studies using targeted radioactive microsphere therapy often only report total infused activity due to the difficulties in making dosimetry estimates using this technique. (See section 1.5.2 for further discussion of radiation dosimetry using radioactive microspheres.)

Lau et al. (1994) examined tumour response of patients with inoperable hepatocellular carcinoma that were treated with ^{90}Y microspheres. They estimated tumour doses by assuming a uniform distribution of activity throughout the tumour and applied MIRD principles. They reported that patients

demonstrated a better tumour response if the tumour dose exceeded 120 Gy. Yoo et al. (1989) also suggested the tumourcidal dose for hepatocellular carcinomas to be at least 120 Gy from their experiences using intra-arterial infusions of ^{131}I-lipiodol. Yan et al. (1993) reported good responses after hepatic infusion of ^{90}Y glass microspheres in eighteen patients with primary liver cancer. They delivered a mean tumour dose of 88 Gy (highest tumour dose was 186 Gy). Ebert and Zavgorodni (2000) modelled tumour control probabilities for simulated ^{90}Y labelled microsphere treatments of liver metastases using both uniform and clustered activity distributions for a number of tumour sizes. Their calculations suggest that an activity concentration of 5 MBqg^{-1} is required in spherical tumours of 1 or 2 cm radius to achieve a 99% tumour control probability. They calculate this activity concentration results in minimum tumour doses of 107.5 Gy and 120 Gy respectively in clustered microsphere simulations.

However the work of Donath et al. (1990) suggests that tumourcidal dose estimates of 100-120 Gy would appear to be unduly pessimistic. Donath et al. (1990) implanted ^{125}I seeds in solitary colorectal liver metastases in six patients. They used a prescribed absorbed dose of 160 Gy, which is biologically equivalent to 60 Gy delivered in 2 Gy per day fractions. Local control was achieved in 5 out of 6 patients, the one failure was attributed to the implant delivering only 135 Gy to the tumour. This study would suggest that radiation doses equivalent to 60 Gy delivered in 2 Gy fractions will be a tumourcidal dose for liver metastases

Ling (1990) calculated that for ^{198}Au ($t_{1/2}$ = 64.8 hrs) implants, delivering a radiation dose of 60 Gy will have approximately the same biological effect as a 60 Gy dose delivered in 2 Gy fractions. He calculated an effective treatment time (T_{eff}), beyond which additional dose delivered is wasted, to be between 14 and 20 days, depending on whether the tumours were fast or slow growing. For ^{90}Y microsphere therapy similar results are expected as the half life of ^{90}Y is 64 hours, virtually the same as ^{198}Au. Delivering a 60 Gy total radiation dose from ^{90}Y labelled microspheres should produce a tumourcidal effect in liver cancers.

1.7 Outline of thesis

As discussed in the preceding sections of this chapter, while there are a number of published reports containing qualitative information about the distribution of microspheres following hepatic arterial microsphere infusion, there are few that present quantitative information, and even less that have studied such distributions on sub millimetre scales. The work reported here examines in detail the distribution of microspheres in human liver resulting from targeted microsphere therapy and the resulting radiation doses arising from the observed distributions.

Tissue samples from a patient who had received treatment with 32 μm diameter ^{90}Y labelled microspheres as treatment for an inoperable metastatic cancer in one lobe of the liver were used for this study. Subsequently, the tumour reduced in size and was resected along with the liver lobe in which it was situated. Tissue samples were taken from the resected tissues from normal liver, the tumour centre, the interface between tumour and normal hepatic parenchyma, and the serosal surface of the tumour. The tissue samples were serially sectioned and a representative selection of these slices were subjected to analysis to determine the microsphere locations within the tissue. Chapter 1 presents further details about the tumour and the regions from which tissues samples were taken and covers the methods used in determining microsphere positions within the sections. The measured microsphere locations were analysed to determine parameters which characterise the distribution patterns of microspheres in the tissue. The number density of microspheres within each region was determined and the distribution of microspheres in the periphery examined. Clustering of microspheres in the tumour periphery was carried out with a view to refining the criteria used by Pillai et al. (1991) of simply taking a microsphere cluster as those microspheres separated from adjacent microspheres by a distance of less than 50 μm. The analysis of microsphere distribution studies are presented in Chapter 4.

The observed microsphere positions were used to carry out radiation dosimetry calculations and the results compared with values that would have been obtained using dosimetry calculations based on MIRD concepts. These results are found

in Chapter 5 along with a discussion of treatment implications arising from the results.

A summary of results and conclusions is found in Chapter 7 together with recommendations for future work.

2. Tissue Section and Patient Details

The tissue samples used in this work were taken from the right lobe of a liver resected from a patient who had received treatment with 32μm diameter ^{90}Y labelled resin microspheres. The patient had presented with unresectable metastatic colorectal liver cancer of volume 970 cm^3 in the superior region of the right liver lobe . Subsequently the patient underwent treatment with ^{90}Y labelled microspheres using the Selective Internal Radiation therapy (SIR-therapy) technique described by Gray et al. (1992).

One month prior to microsphere infusion the patient underwent laparotomy at which time an infusion catheter was placed in the hepatic artery and connected to a port attached to the subcutaneous tissue of the right chest wall. Material injected into the port would thus enter the liver via the haptic artery.

Before ^{90}Y microsphere infusion the degree of arterio-veneous shunting to the lungs via the liver was assessed using Nuclear Medicine imaging. A significant amount of shunting would have precluded treatment using this method as an unacceptable lung radiation dose would be delivered (Lau et al., 1998, Andrews et al., 1994). The expected distribution of microspheres was assessed by infusion of ^{99m}Tc labelled macroaggregated albumin (^{99m}Tc-MAA) using the same techniques as for the therapeutic microspheres. ^{99m}Tc-MAA has a similar particle size to the microspheres and was assumed to distribute in the same manner. Using this technique a lung shunting ratio of 20% was measured.

Approximately 6×10^7 microspheres having a total activity of 3.2 GBq were injected into the port and hence infused via the hepatic artery Angiotensin II was used to enhance the tumour-to-normal tissue ratio. From the measured lung shunting ration of 80%, it was expected that 80% of the infused activity (2.56 GBq) would have lodged in the liver. The distribution of microspheres following infusion is expected to remain fixed as they become extravascular soon after embolisation and their porous structure becomes embedded in the tissue making

it difficult to dislodge. The patient also received hepatic perfusion chemotherapy using floxuridine (FUDR) commencing the day following microsphere administration.

Six months post therapy the volume of the tumour had decreased to 336 cm^3 (approximately 80 mm diameter), allowing for curative resection of the right liver lobe to take place.

The resected lobe was cut into 10 mm thick slices, as shown in Figure 8. Samples from the slice labelled 4 in Figure 8 were taken and subjected to analysis. Section 4 was chosen as the centre of the tumour was included in this section. Samples were taken from four sites within the section. These sites were chosen to include representative samples from normal liver, the tumour centre, the interface between tumour and normal hepatic parenchyma and the serosal surface of the tumour. A diagrammatic representation of the liver section and the locations from which tissue samples were taken is shown in Figure 9.

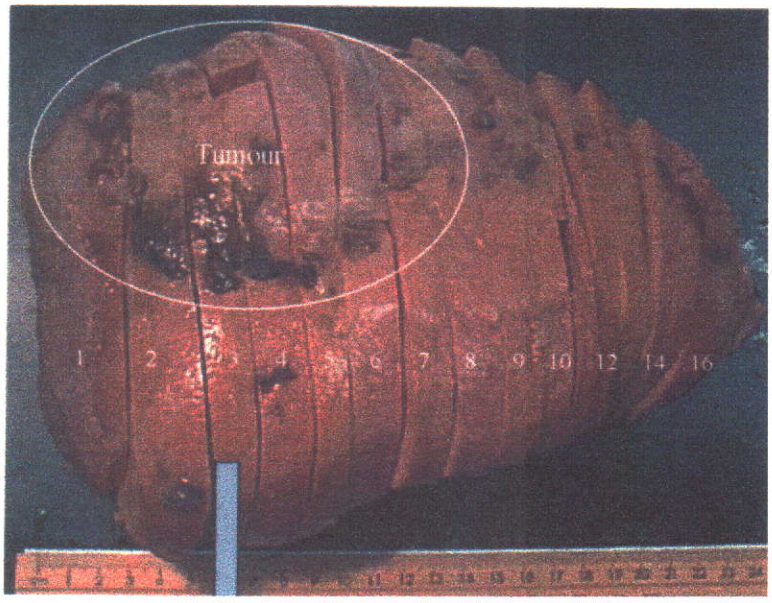

Figure 8. Resected right liver lobe. This picture is reproduced from Halley (1999).

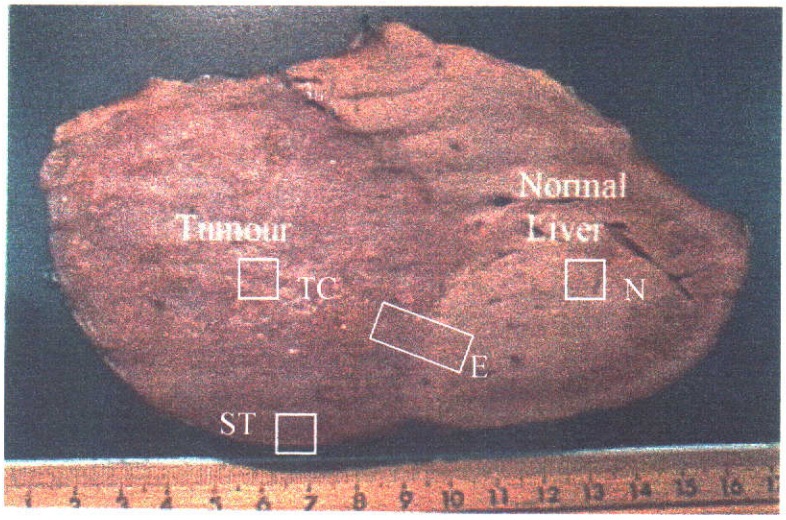

Figure 9. Liver lobe section from which tissue samples were taken for microsphere distribution analysis. Samples were taken from normal liver (N), tumour centre (TC), tumour-normal tissue boundary (E) and serosal tumour (ST). The picture of the liver section shown is reproduced from Halley (1999).

The tissue samples were sectioned serially, each section having a thickness of 10 μm. Every 20th section was retained, stained with haematoxylin eosin and mounted on microscope slides using standard techniques (Sheehan and Hrapchak, 1980). Table 2 gives the dimensions of each tissue sample and the number of sections examined from each area. Microspheres stained significantly darker than tissue and were easily visible using transmission light microscopy. Samples taken from the tumour peripheries were sectioned approximately perpendicularly to the tumour boundary to facilitate subsequent analysis.

Each tissue section was examined using transmission light microscopy. Since the whole section could not be included in a single field of view, it was necessary to divide it into a matrix of adjoining fields. Images of these fields were obtained by moving the section with a computer controlled microscope stage and capturing

capturing images with an attached video camera. A detailed discussion of this procedure is presented in Chapter 3.

Table 2. Tissue Sample Dimensions

Sample Region	Dimensions (millimetres) (width x height x thickness)	Volume (mm^3)	Number of sections examined
Normal Liver	8.7 x 10.7 x 6.4	596	31
Tumour Centre	7.7 x 8.9 x 8.0	548	42
Serosal Surface	7.0 x 9.5 x 7.6	505	41
Tumour-Normal Tissue Interface	16.8 x 9.1 x 4.0	612	22

3. Acquisition of Microsphere Position Data

3.1 Computer collection of Section Images

The distribution of microspheres was assessed using transmission light microscopy. Sections were viewed using a Nikon microscope with a x20 objective and an Ikegami CCD black and white camera (Model ICD-44AC) mounted on one eye piece. The video signal from the camera was digitised using a Perceptics frame grabber fitted in a Macintosh Quadra 700 computer. An image processing program (NIH Image) running on the Macintosh was used to display and save images acquired from the frame grabber. The microscope was fitted with variable magnification in addition to its objective capable of providing additional magnification continuously variable in the range x1 to x4.

The video camera provided a standard PAL video signal. The frame grabber digitised a single video frame into an image 768 x 512 pixels in size with one byte of storage per pixel. Pixel values were in the range 0 to 255, with 0 representing black and 255 white. A 10 pixel wide column on the left side of each digitised image contained incorrect data due to a signal timing incompatibility between the frame grabber and video camera and was discarded. Images used for analysis were thus 758 x 512 pixels and each required 379 kbytes of storage space.

3.1.1 Selection of microscope magnification

When digitising images of an object, each pixel in the resulting image corresponds to a certain area of the original image. For monochrome image capture, the value assigned to each pixel represents the average brightness of the object over the area that the pixel covers. The larger the magnification used, the smaller the area represented by each pixel in the original image. In general, the height and width of a pixel may represent different distances on the original object. For the system used here this was not the case, and the pixel height and

width were equal; ie. the pixels were square. For the purpose of detection of microspheres in tissue sections, if the pixel size of the image was too large the area of a microsphere on the digitised image would be represented by too few pixels for reliable detection. As the number of pixels in a digitised image was fixed by the frame grabber hardware, the pixel size was altered by changing the magnification of the microscope.

The pixel size of images digitised with the microscope system was determined by imaging a graticule. The graticule had graduations at 100 μm intervals over a length of 10 000 μm. An image of the graticule was acquired and stored. Two graduations in the image lying at least 1 000 μm apart were selected and the number of pixels between them determined. The known distance between the graduations then enabled the pixel size to be determined. This process was repeated several times using different pairs of graduations and the average value of the readings taken as the best estimate of the pixel size.

Selection of a microscope magnification that enabled an image of a whole section to be captured in a single image proved insufficient for visualising microspheres within the section. In order to digitise an image of a section at a magnification sufficient to permit visualisation of microspheres, a matrix of adjoining frames was captured. It was considered desirable to store permanently, for later reference and processing, all the frames captured. The choice of magnification impacts the storage requirement needed. While higher magnification makes identification of microspheres in the captured section images easier, there is a trade off with the number of frames required to cover the area of each section. The higher the magnification the more frames are needed to cover the whole section, demanding an increased storage requirement. In order to minimise storage requirements, a magnification was selected for the microscope just sufficient to identify microspheres unambiguously in the captured images.

A suitable setting was chosen by acquisition of a variety of images at different magnifications. A magnification corresponding to a pixel size of 4.156 ± 0.005 μm was found to be sufficient for reliable identification of

microspheres. With this pixel size each 758 x 512 pixel image covered a 3150 ± 3.8 μm x 2128 ± 2.6 μm area. To completely digitise a typical section required approximately 16 images, requiring 5.92 Mbytes of storage. The storage requirement for each region of the liver from which tissue samples were taken was a little under 200 MB and while this is large, it was not an intractable problem with the computer equipment that was available.

3.1.2 Digitisation of section images

Since a whole tissue section could not be included in a single field of view of the video camera, multiple adjoining images were captured and then joined together in order to digitise a complete section image. An example of this process is shown in Figure 10, where the individual frames that form the overall image are outlined. Tissue to the right of the image is tumour tissue while that on the left is normal liver.

In order to digitise a complete tissue section it had to be moved across the field of view of the camera/microscope combination between image captures. The movement had to be precisely equal to the width or height of the camera field view, depending on the position of the next image to be acquired. It was judged that for this to be accomplished in a reliable and sufficiently accurate manner some type of automatic control of the microscope stage was required. A computer controlled microscope stage was developed 'in-house' to serve this function. This stage permitted automatic acquisition and saving of a predefined image collection sequence to cover a tissue section.

A microscope stage capable of manual motion in two axes via rack and pinion type gearing systems was modified to allow it to be able to be controlled using a personal computer. The stage was fitted with stepper motors, each attached so as to drive one axis of the stage through a gear box and toothed belt arrangement. Hard limit micro switches were mounted on the stage and were designed to cut power to the motors when the stage reached the limits of its motion in order to prevent mechanical damage to the mechanism should it be over driven. An optoelectronic sensor was fitted to each axis near one end of the direction of

motion to act as a software detectable reference point (a soft limit). This enabled a known physical position to be referenced via the computer.

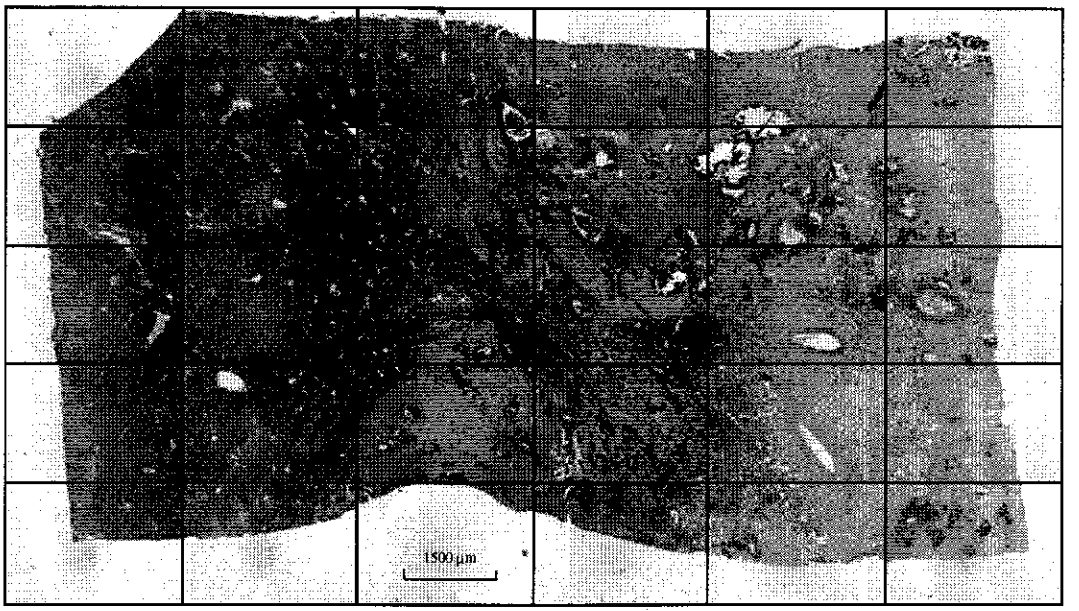

Figure 10. Division of a tissue section into adjoining video camera fields of view.

Motors were driven via an interface box that contained three stepper motor driver boards that allowed independent control of up to three motors. The box accepted standard TTL level signals as inputs to step each motor and to control the stepping direction. It also provided signal conditioning to TTL levels for a number of switch inputs that could be used for sensing hard and soft limit switch status.

A dedicated stepper motor controller card was not available for the controlling computer. Use was made of the standard PC parallel printer port to control the stepper motors. Printer port data lines were toggled under software control to

step the motors and control their direction of motion. Inputs used normally for sensing the printer status outputs (such as paperout, fault, etc.) were used to read hard limit switches and the soft reference point switches. Software written in Microsoft QuickBasic v4.5 was used to directly read and write data to the computer's printer port, allowing computer control of the microscope stage.

Prior to each use, the stage was initialised by moving to the soft limit point on each axis. This was taken as the origin for the stage coordinates and at all times the position of the stage relative to this reference point was maintained. The stage construction meant that it was not backlash free. This meant that when the direction of motion was reversed the stepper motor would turn for a number of steps before the stage actually began to move. The effect of the backlash was counteracted by always moving in the same direction during data collection.

In order to use the microscope stage to accurately move a microscope slide known distances, the distance moved by the stage for each pulse sent to the stepper motor needed to be known. This distance, referred to hereafter as the step size, had to be measured for each axis. Preliminary estimates of the step size indicated that around 2000-3000 steps would be required to move the stage through distances on the order of the size of the microscope's field of view. It was thus important that the step size was measured with sufficient precision to avoid unacceptably large errors accumulating after movements of approximately 3 000 steps.

The step size for each axis was measured using the same graticule as employed for pixel size determinations (see section 3.1.1). The graticule was aligned to be parallel to the stage axis for which step size was to be determined. The stage was positioned such that the 0 μm graduation was visible in the microscope's field of view and an image captured. The pixel location on this image of the bottom of the 0 μm graduation was noted. The stage was then sent steps until the bottom of the 6 000 μm graduation moved to the same pixel location as originally occupied by the 0 μm graduation. Knowing the number of steps required to move the stage through this 6 000 μm distance thus enabled the step size to be calculated. It was

estimated that the 6 000 μm graduation could be positioned to the required pixel location with an uncertainty of ± 3 steps. This arose because the stage could be sent around three steps with no apparent shift in the pixel location of the 6 000 μm graduation.

Step size results were :

x-axis	0.9315 ± 0.0004 μm/step
y-axis	1.5851 ± 0.0012 μm/step

The number of steps to move the stage across the microscope's field of view will thus be 3328 and 1343 steps for the x and y axis respectively. The precision of the step sizes given above is such that the accumulated positioning error due to step size will be less than 2 μm in each axis for movements of this number of steps.

In order to check the step size values, a complete image of the graticule was acquired. This was captured using 18 images in a 6 x 3 image array. The image produced showed an obvious problem with adjoining images for the y-axis of the stage. In some positions the stage appeared to have advanced too far while at others it had not moved far enough. Further investigation revealed that the y-axis step size varied with the absolute position of the stage. This was most likely due to mechanical variations in the drive system with position. The variations in step size were however repeatable. Step sizes calculated by moving the stage through distances of 600 μm were found to be repeatable for the same absolute stage position. This enabled the step size to be measured across the range of stage positions used in the data collection process and a lookup table generated to determine an appropriate step size to be used for the current stage position. Step sizes were determined for a range of y-axis stage positions, using the technique already described, but this time only sending sufficient steps to move the stage through a 600 μm distance. The stage position was referenced as the distance from the y-axis soft reference position. Figure 11 shows the variation of y-axis step size with position. The range of positions shown was sufficient to cover all

stage position used in digitising the liver tissue sections. Figure 12 shows an image of the scale collected using the y-axis step size lookup table. Any misalignments were too small to be observed.

Mechanical variations no doubt also existed in the x-axis stage. However these must have been sufficiently small to be undetectable in this application.

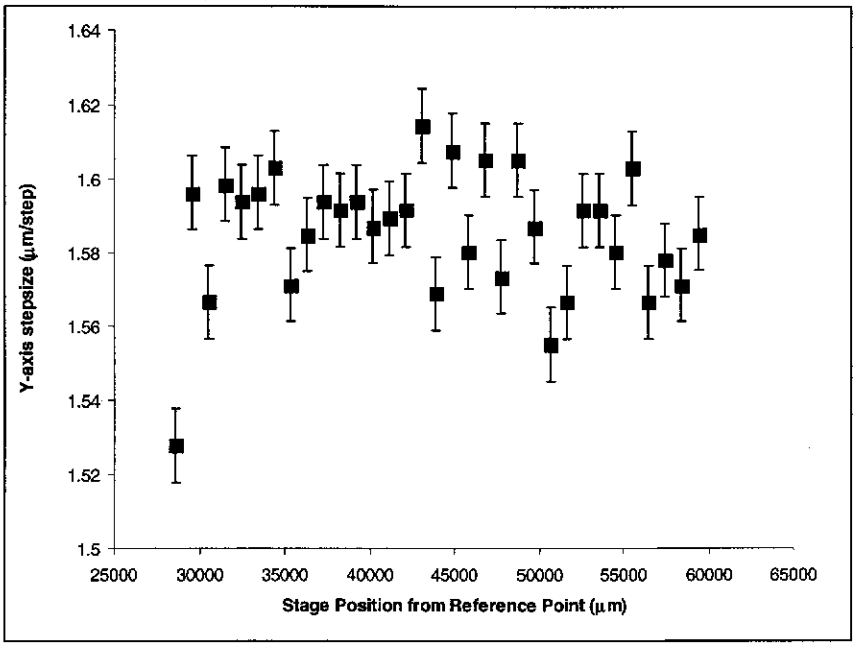

Figure 11. Variation of y-axis step size with absolute stage position. Distances are measured from the y-axis soft reference point.

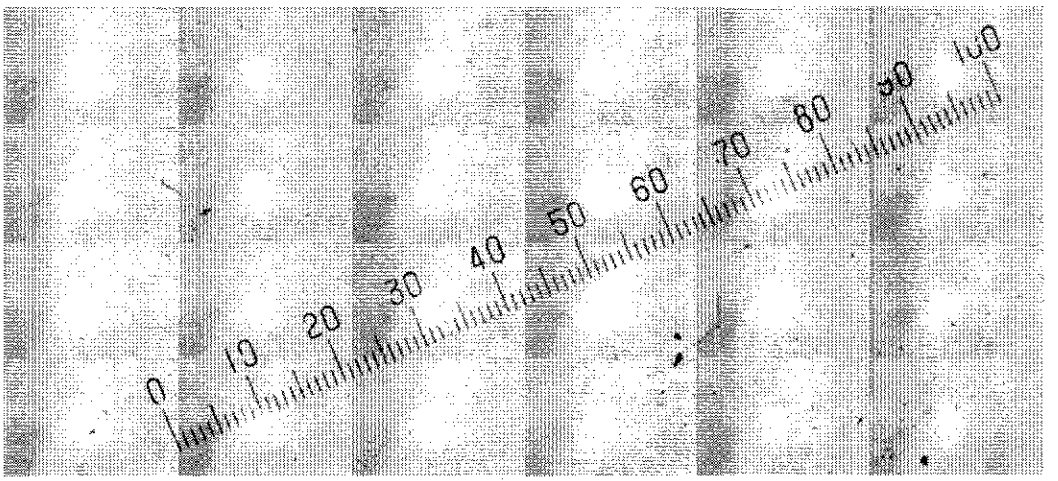

Figure 12. Composite image of the calibrated scale collected using the y-axis step size lookup table.

3.2 Alignment of Sections

In order to reference microsphere positions in different sections cut from the same tissue sample to the same coordinate system, the sections needed to be aligned. This is not an uncommon requirement in microscopy work and would normally be achieved by the inclusion of fiducial markers prior to sectioning of a tissue block (Russ, 1995). The fiducial markers are included such that the spatial relationship between them is the same for all slices. Alignment of the fiducial marks then achieves alignment of the tissue sections. Unfortunately, the tissue sections analysed in this work were sectioned without such fiducial markers being included. Alignment was achieved by identification of the same histo-anatomical features in successive sections.

As all images were acquired with the same pixel size, the possible differences between two section images reduced to rotations and translations. The mapping of a point on an image at position (x,y) to its equivalent position (x',y') in another image by rotation through an angle θ and translation x_t and y_t in the x and y axis respectively can be written in homogeneous matrix form as (Hearn and Baker, 1986)

$$(x' \; y' \; 1) = (x \; y \; 1)\begin{pmatrix} \cos\theta & \sin\theta & 0 \\ \sin\theta & \cos\theta & 0 \\ x_t & y_t & 1 \end{pmatrix}$$

Alignment was performed by selecting the first section from a tissue sample volume as a reference section and aligning all other sections in the sample volume to this reference. Starting with the section closest to the reference, each section was aligned with the immediately preceding section by choosing two histo-anatomical features apparent in both sections. The rotation/translation required to align the two features in the section to their positions in the preceding section was then determined. The alignment was checked by overlaying the rotated and translated section image with the reference. If most histo-anatomical features on the sections did not coincide the process was repeated until this was achieved.

Successive sections were aligned with their immediate neighbour and not directly to the reference section as while histo-anatomical features were sufficiently constant in successive sections to allow for good alignment, this was not true for more widely separated sections. The alignment process was carried out using NIH Image and macros were written to semi-automate the process. Alignment was performed using a reduced resolution view of each section. This was acceptable as histo-anatomical features whose dimensions were on the order of 200 μm were used for alignment purposes. The mapping of microsphere coordinates to the reference section was achieved by successively applying the transformation from one section to the preceding one until the reference was reached.

3.3 Determination of Microsphere Positions

Microsphere positions were determined manually in each tissue section. Tissue section images were loaded into an image processing program (NIH Image) running on the MacIntosh computer used for image acquisition. The position of each microsphere in an image was recorded by positioning the mouse pointer over the centre of the microsphere and clicking the mouse to record its pixel location in the image. The pixel location was then converted to a coordinate position in micrometres using the known image pixel size. Microsphere coordinates for sections in the same tissue volume were then aligned to the same coordinate system as described in section 3.2.

A variety of automated and semi-automated methods for detection of microsphere positions in section images were investigated. None proved sufficiently reliable for accurate microsphere detection. Microspheres stained significantly darker than surrounding tissues raising the possibility of microsphere detection using a thresholding technique. However, there were other structures present that had similar grey level values in the images, making this unsuitable. Microspheres presented a circular cross section in the images. Selection of circles in section images using Hough transforms (Leavers, 1992) was investigated. Image noise and the presence of other circular features similar in size to the microspheres caused problems with this technique.

4. Microsphere Distribution Studies

There have been a limited number of studies on the distribution of microspheres and the resulting radiation dosimetry in the liver at sub-millimetre scales following the hepatic infusion of microspheres. Pillai et al. (1991) infused microspheres into rabbit liver and carried out a detailed analysis of microsphere distributions in both tumour and normal liver tissue. Using this data, Roberson et al. (1992) performed radiation dosimetry calculations for a 2 mm tumour nodule and a similar volume of normal liver. Fox et al. (1991) examined microspheres in a sample of normal human liver and performed radiation dosimetry calculations using the observed microsphere distributions. Both studies found that the distribution of microspheres was inhomogeneous, however the distribution observed by Fox et al. (1991) was more non-uniform than that seen by Roberson et al. (1992). This was reflected in the calculated radiation dose distributions. The dose distribution determined by Roberson et al. being more uniform that the one calculated by Fox et al., although both distributions showed dose inhomogeneities. This is the most likely reason why liver tissue shows a greater tolerance to radiation delivered in this manner compared with external beam radiotherapy (Gray et al., 1990).

In order to determine the effect of microsphere distributions on radiation dose delivered following hepatic microsphere therapy, microsphere distribution patterns in the tissue samples described in Chapter 2 were examined in detail. The measured microsphere locations were analysed to determine parameters which characterise the distribution patterns of microspheres in the tissues. The dimensions of the tissue samples analysed are shown in Table 2.

4.1 Visual Appearance

Typical microscope images from tissue sections in normal liver and the tumour periphery are shown in Figure 13. In normal liver microspheres appeared to deposit around the periphery of liver lobules, lodging in vessels approximately the same diameter as the microspheres. There were also many lobules that had

no microspheres at their periphery. Figure 13a shows four microspheres lodged within a distance of about 500 μm in normal liver. Although the appearance is typical, it was much more common to see between zero and two microspheres in areas of the size shown in the Figure rather than the four apparent in the example given. There was a high density of blood vessels near the edge of the tumour but their distribution around the periphery was not uniform. These vessels were distended compared with those in normal liver, allowing microspheres to aggregate in numbers within a single vessel as evidenced in Figure 13b.

Microspheres were not deposited in all vessels in the tumour periphery, there were areas with a high concentration of blood vessels that contained no microspheres. The lack of microspheres in some vessels visible on the histological sections is probably due to the fact that tumours have temporally heterogeneous blood supplies (Fukumura at al., 1997) and the vessels without microspheres may not have been perfused at the time of microsphere infusion. Since the vascular beds of different parts of the tumour will be functionally perfused on a microscopic level at different times, these aggregations are likely to occur at random throughout the periphery. An additional reason for microspheres not being present is that not all vessels visible in the tumour periphery will have been functional (Song, 1998). As non-functional blood vessels receive no blood supply, no microspheres would deposit in those vessels.

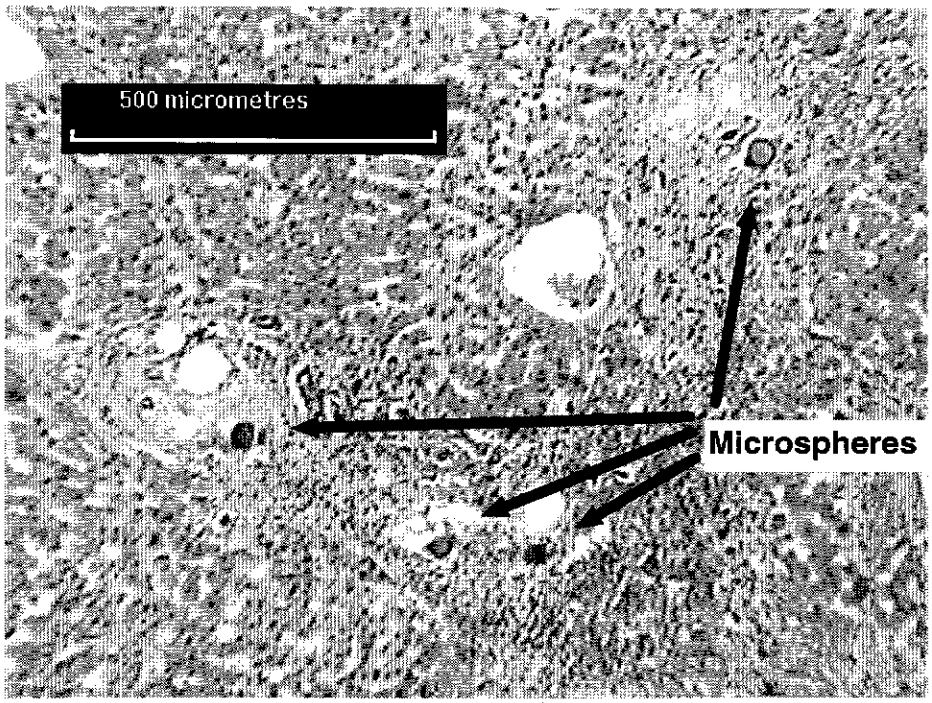

(a)

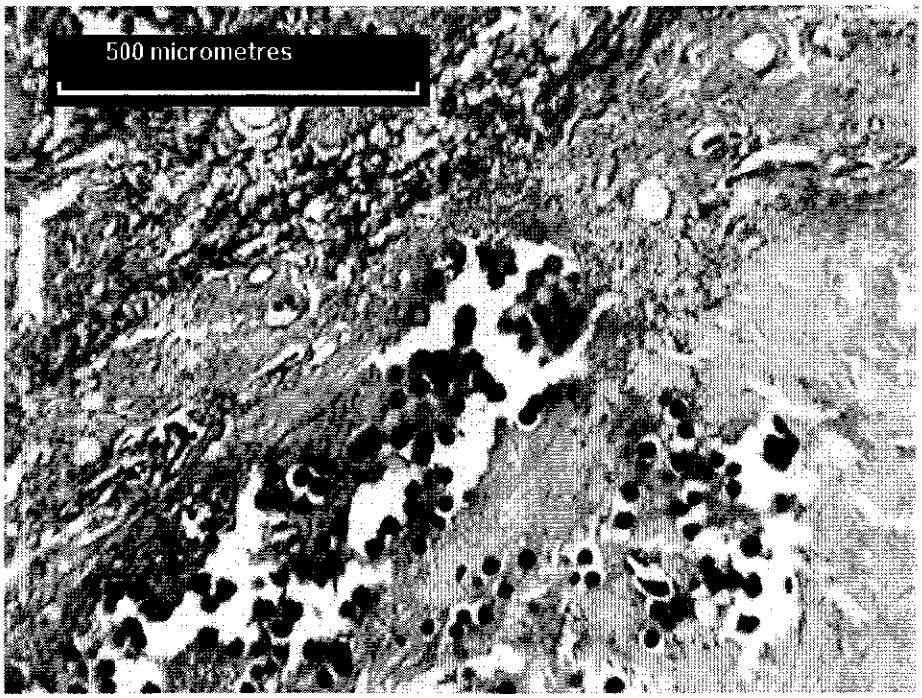

(b)

Figure 13. Light microscope view of 32 μm diameter resin microspheres in normal liver (a), and the tumour periphery (b). A total of four microspheres can be seen in (a).

4.2 Distances from the Tumour Boundary

For the two tissue samples taken from the tumour periphery, the deposition pattern of the microspheres was analysed in terms of their distance from the tumour boundary. For the sample containing the tumour-normal tissue interface, the boundary between the two was drawn by eye on the digitised image of each section. The shortest distance between each microsphere and the boundary was then computed. This distance was assigned a positive value if the microsphere was on the tumour side of the boundary and a negative value if the microsphere was on the normal tissue side. For the serosal sample, a similar process was carried out, although in this case the tumour boundary was clear, and as there was no normal tissue present, no negative distances were assigned.

Figure 14 shows a histogram of the distance of the microspheres from the serosal boundary. This is a composite histogram using position data from all sample sections. It is clear from the Figure that the concentration of spheres is greatest immediately adjacent to the boundary and falls away towards the interior of the tumour. The concentration is very low towards the centre of the tumour. Since this is serosal tumour, no spheres occurred outside the tumour.

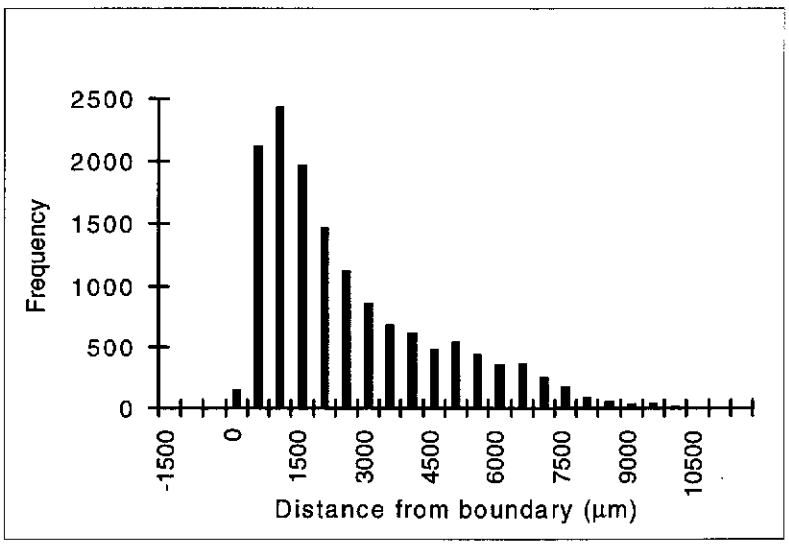

Figure 14. Distance of microspheres from the tumour boundary for the serosal surface tissue sample. The tumour boundary is at 0 μm and positive distances are towards the tumour centre.

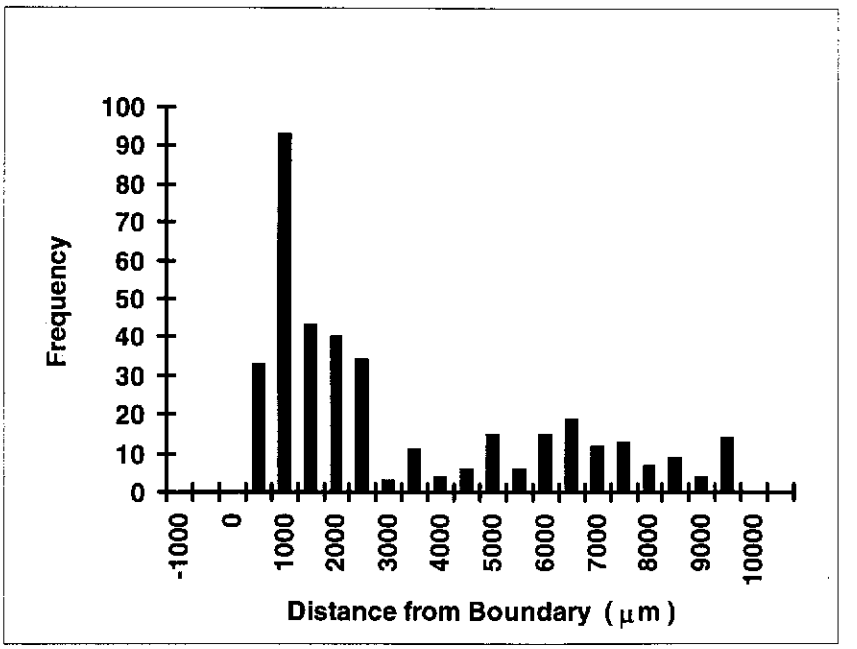

Figure 15. Distance of microspheres from the tumour boundary for one section in the serosal surface tissue sample. The tumour boundary is at 0 μm and positive distances are towards the tumour centre

Figure 15 shows an example of a histogram of the distance of the microspheres from the serosal boundary for a single section. This histogram demonstrates that while most microspheres are deposited close to the tumour boundary, there can be concentrations of microspheres further into the tumour.

Figure 16 shows a histogram of the distances of the spheres from the tumour - normal tissue interface. The distribution has similar characteristics to those noted for the serosal surface, except that the spheres were deposited further into the interior of the tumour. Although spheres were also deposited in normal tissue, the concentration observed was very much less than in the tumour - in this section, 97% of the spheres lay within the tumour, only 3% were in normal liver tissue.

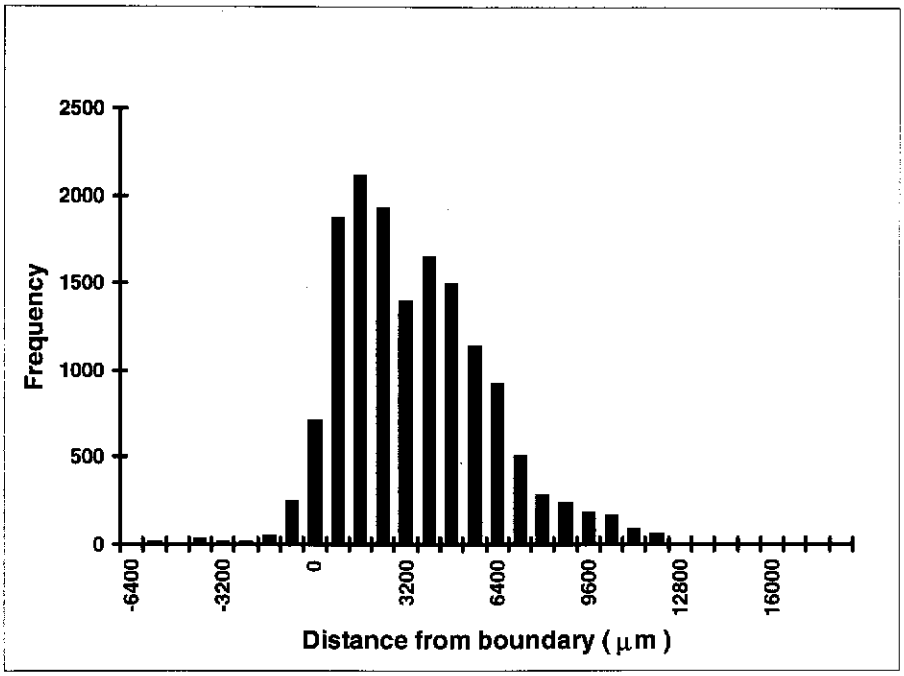

Figure 16. Distance of microspheres from the tumour boundary for the tumour normal tissue interface sample.

The confidence limits for distances from the tumour boundary which contain a certain percentage of the microspheres can be determined using a χ^2 goodness of fit test.

For an arbitrary distance from the boundary, X, the observed frequency of spheres closer to and further from the boundary than X is given by the sample data. How well these frequencies match assumed theoretical values can be tested using the χ^2 goodness of fit test for observed and expected frequencies (Hunstberger and Billingsley, 1981).

Let N be the total number of sphere positions observed and E the theoretical or expected frequency of spheres lying closer than a distance X_E to the boundary. E can be expressed as a fraction of the total number of spheres as

$E = eN$ where e is the fraction of spheres lying closer to the boundary than the distance X_E.

When the value e is expressed as a percentage, the value X_E is referred to as the e^{th} percentile (Hunstberger and Billingsley, 1981). From the sample data a point

estimate of X_E can be determined directly (by using the cumulative frequency polygon). An interval estimate (confidence interval) for a percentile can be estimated by using the χ^2 statistic as follows.

Let O be an observed frequency of spheres and define o to be the fraction of the total number of spheres that is O, ie. O = oN. If E is the expected frequency and again taking E = eN as above, the χ^2 value will have one degree of freedom and is given by

$$\begin{aligned}\chi^2 &= \frac{(O-E)^2}{E} + \frac{[(N-O)-(N-E)]^2}{(N-E)} \\ &= \frac{(oN-eN)^2}{eN} + \frac{[(1-o)N-(1-e)N]^2}{(1-e)N} \\ &= \frac{N(o-e)^2}{e(1-e)}\end{aligned} \qquad (1)$$

For a specified theoretical frequency E, a value of O can be determined such that χ^2 assumes the critical value for a specified significance level α. Two values of O will exist, one less than E and one greater than E. These will be the two end points of a confidence interval containing a range of frequencies which may be considered to be statistically indistinguishable from the theoretical frequency E, with confidence (1 - α).

The percentiles associated with these critical O frequencies allow the determination of a confidence interval for the expected percentile value, X_E.

The range of distances from the boundary associated with these critical O values define an interval which has a probability of (1-α) of containing the actual distance, X_E, at which E spheres will be found.

For the tumour-normal tissue boundary sections, 13000 microsphere positions were observed. The distance from the boundary within which 90% of the spheres are found (the 90^{th} percentile) estimated from the data is 6.48 mm. The critical o values calculated at a significance level of 0.05 are 0.905899 and 0.894101. These correspond to distances from the tumour boundary of 6.61 mm and 6.38

mm respectively. Thus the 95% confidence interval for the 90th percentile is 6.61 mm to 6.38 mm.

Some results for the serosal and tumour-normal tissue boundary sections are summarised in the Table 3 and Table 4.

Table 3. Tumour-normal tissue interface sections

% of microspheres	Estimate of distance from tumour boundary within which this percentage of spheres will be found (mm)	95% Confidence Interval (mm)
50%	2.56	2.47 - 2.66
90%	6.48	6.38 - 6.61
95%	7.93	7.73 - 8.15

Table 4. Serosal sections

% of microspheres	Estimate of distance from tumour boundary within which this percentage of spheres will be found (mm)	95% Confidence Interval (mm)
50%	1.66	1.61 - 1.71
90%	5.46	5.35 - 5.57
95%	6.43	6.35 - 6.53

4.3 Concentration of microspheres

4.3.1 Determining the concentration of microspheres

The 10 μm thick sections observed with a transmission light microscope form essentially a two dimensional sample. In order to extend this to a three dimensional distribution, allowance has to be made for the fact that any piece of a microsphere that is cut and remains in the section, and is not too small to be resolved by the imaging system, will appear in the image. This means that the number of microspheres observed in a particular area of a section is not the actual number normally present in a 10 μm thick sample of equivalent area, but a higher number due to the affect of counting spheres whose centres do not lie within the 10 μm thickness of the slice.

This effect can be corrected by recognising that any sphere whose centre lies within one radius of the edges of the slice will have some portion of itself included in the slice. This is illustrated in Figure 17a which shows microspheres, of radius r, on either side of a slice whose centres are positioned a distance r

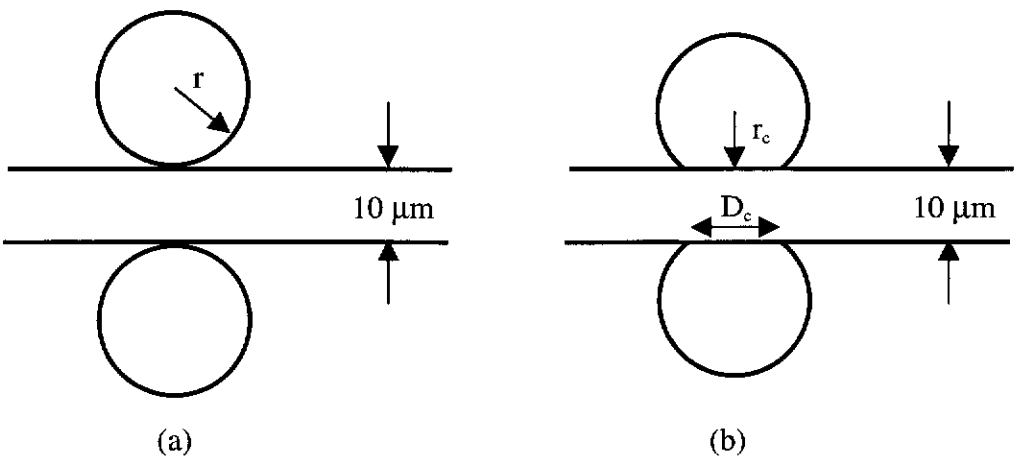

Figure 17. Finite resolution effects in concentration measurements. (a) is the idealised case where microspheres, of radius r, can just touch the cut slice and be visualised in that slice. (b) represents the real case where the finite spatial resolution of the imaging system requires that there is a minimum cut diameter, D_c, for the microsphere piece to be detected. The cut diameter D_c corresponds to microspheres whose centres lie a distance r_c from the edge of the cut.

above and below the edges of the slice. Thus a tissue sampled with a slice thickness of 10μm is effectively 10μm plus twice the radius of a microsphere, or 42 μm for 32 μm diameter microspheres. This is an idealised situation and in reality uncertainty can arise from two sources. The first is the finite spatial resolution of the system and the second is that the cross-section of a sphere is very small when the cut occurs close to the surface of the sphere. The combination of these two facts means that microspheres that are cut close to their surface may not be visualised. This is illustrated in Figure 17b where microspheres whose centres are a distance r_c from the edge of the section present a cut section of diameter D_c that is just resolved by the microscope system. This reduces the effective slice thickness. The errors introduced by ignoring the finite resolution effects are small as the cross-sectional area of a sphere increases rapidly as the cut moves away from the sphere surface. For a sphere of radius r, the distance r_c as a function of the cut diameter, D_c is given by

$$r_c = \sqrt{r^2 - D_c^2/4}$$

Microspheres whose cut area was as small as 2 pixels could be marked with confidence, thus to estimate r_c, D_c can be taken as 2 pixels which equates to 8.312 μm for a 4.156 μm pixel size. For 32 μm diameter microspheres the value of r_c, for this D_c, is 15.45 μm, giving an effective slice thickness of 40.9 μm. The true effective slice thickness, allowing for finite resolution effects, must thus be somewhere between 40.9 μm and 42 μm. The difference between these two numbers is less than 3%, so using an idealised slice thickness of 42 μm to determine microsphere concentrations should result in an error, due to the effects discussed above, of less than 3%

Thus observing the microsphere numbers and measuring the tissue area in which they lie allows the volume density of microspheres to be calculated by assuming that the thickness of the section is 42μm.

4.3.1.1 Verification using an independent method

Microsphere position data obtained by Fox et al. (1991) for closely sectioned samples of normal liver was available and was used as an independent verification of the previous reasoning. They obtained a sample of normal human liver, approximately 14 x 10 x 0.38 mm^3, from a patient following infusion of 32 μm diameter ^{90}Y labelled microspheres. The sample was sectioned parallel to the side having the largest area contiguously into 10 μm thick slices and every second section was retained. These sections were stained and microsphere positions recorded using a computerised microscope system to identify microsphere centres in each section.

When sectioned in this manner microspheres will be cut so as they have a portion in either two or three of the retained sections, the possibilities are illustrated in Figure 18. For the case shown in Figure 18(a) the microsphere must be cut in just the right position, a vertical shift in its centre of only 1 μm will result in the

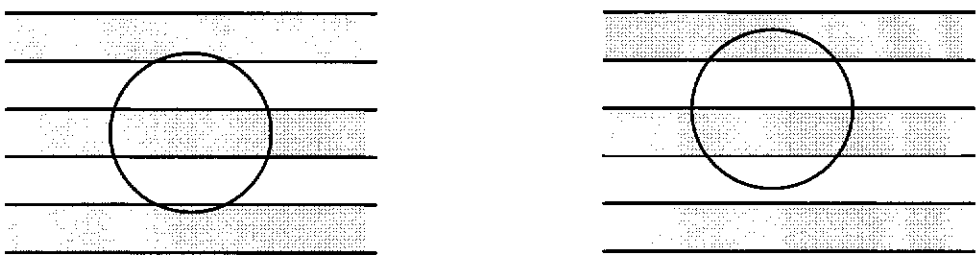

(a) (b)

Figure 18. Possibilities for cutting a microsphere, in each case the shaded sections are retained for analysis. (a) the microsphere is positioned so that portions will appear in three sections. (b) the microsphere will only appear in two sections.

case degenerating to that shown in Figure 18(b). It would appear reasonable to believe the situation of Figure 18(a) will occur relatively infrequently and to take as a good approximation for all microspheres the situation in Figure 18(b). Thus a portion of each microsphere will appear in two sections. Using the total

number of microspheres counted in for the whole tissue sample will then result in each microsphere being 'double counted', the true number of microspheres within the volume will be half the number observed.

The total number of microsphere positions recorded was 1700, implying the number of spheres within the tissue sample was 850. This equates to a volume density of 16 microspheres/mm^3.

The average number of microsphere positions for each section was 89.2. Using this number, and taking a section has having an effective thickness of 42 μm, the volume density of microspheres would be estimated at 15.2 microspheres/mm^3. The close agreement of these two density estimates gives confidence in the technique discussed in section 4.3.1.

4.3.2 Results

The average concentration of microspheres is given in Table 5 for the four regions from which the samples were taken. The figures quoted for the tumour boundaries are those for the regions in which 90% of the microspheres were observed. For normal liver and the tumour centre the concentration is the average for the whole of the tissue section. It is clear that the concentrations in the normal tissue and the tumour centre are very much less than those near the surface of the tumour. There is a significant difference between the concentration values for the tumour-normal tissue interface and the serosal edge at the 2% level using a Student's t-test. This implies that there is higher tumour blood perfusion in the periphery of the tumour adjacent to normal tissue than on the serosal surface. While there is a difference in the mean concentrations observed for the normal liver parenchyma and tumour centre samples, this was not found to be significant at the 5% level using a Student's t-test.

In order to check that the microsphere concentration measurements were assessed correctly, the total number of microspheres deposited was approximated. To do this, the tumour was assumed to be spherical, with an overall diameter of 80 mm, and divided into an inner zone 68 mm in diameter surrounded by a 6 mm thick

periphery zone. Microspheres were considered to deposit with a concentration matching that observed for the tumour centre tissue sample in the inner zone and with the average value seen in the samples from the tumour periphery in the periphery zone. Normal liver was assumed to have a volume of 1800 cm^3 and a microsphere concentration the same as observed in normal hepatic parenchyma. The total number of spheres calculated was 3×10^7. The patient received 3.2 GBq of ^{90}Y microspheres and the activity per microsphere was estimated to be 50 Bq. The number of microspheres actually infused was thus approximately 6×10^7. A lung shunting ratio of 20% was measured for this patient, so that the number of microspheres expected to lodge in the liver was 4.8×10^7. Because of the assumptions made, there is a large uncertainty in the figure obtained, but it is in substantial agreement with the expected number.

Table 5. Microsphere Concentrations

Sample Region	Microsphere concentration (spheres/mm^3)	Concentration relative to normal liver tissue
Normal Liver	3.5 ± 0.5	1.0
Tumour Centre	2.7 ± 0.2	0.77
Serosal Surface	175 ± 9	50
Tumour-Normal Tissue Interface	254 ± 18	72

Using this model for the tumour permits an estimation of the ratio of the number of microspheres lodging in the tumour to number lodging in normal tissue (referred to as the T/N ratio). A ration of 4:1 was calculated. This T/N ratio is also encouraging as it is within the range reported for other studies (see the discussion in section 1.3

4.4 Clustering of microspheres

Microsphere concentrations clearly varied with location in the liver (normal liver compared with the edge of the tumour for instance) but moreover within a given region of the tumour near the tumour boundary variations are also evident. Near the tumour boundary within a single tissue section microsphere concentrations are seen to vary with spatial location with spheres appearing to aggregate into clusters. Pillai et al. (1991), after infusing 25 μm diameter microspheres into rabbits' liver, also observed that microspheres did not distribute uniformly, but tended to group into clusters. They determined microsphere clusters within tissue sections by taking any microspheres found within 50 μm of another microsphere as belonging to the same cluster.

A variety of methods were used in an attempt to quantify the clustering observed in the periphery of the tumour for the observed microsphere positions. An extension of the basic method employed by Pillai et al. (1991) was used to try and identify clusters but achieved equivocal results. Cluster analysis, which is a standard statistical technique that attempts to classify a set of data, which could be homogeneous, into groups based on selected characteristics was also used to identify clusters.

4.4.1 Characterising clustering via a cluster parameter

Pillai et al. (1991) investigated the clustering of microspheres in rabbit liver both in tumour and in normal tissue. They noted that spheres tended to cluster and looked at the number of microspheres in a cluster and the distance between clusters in different areas of the liver. Pillai et al. (1991) defined spheres as belonging to the same cluster if any two spheres in the cluster were within a certain maximum distance of each other, this distance he referred to as the cluster size, but will be referred to here as the cluster parameter. Spheres not belonging to a cluster will be at a distance greater than the cluster parameter from all spheres within that cluster.

The algorithm for assigning spheres to a cluster is then as follows:

> A sphere is selected at random. Any spheres within the cluster parameter distance are marked as being in the same cluster. Each of these spheres is then examined and any spheres within the cluster parameter distance are assigned to the same cluster. This process then repeats until no more spheres are added to the cluster.
>
> A sphere not already assigned to a cluster is then chosen and the process in the above paragraph repeated.
>
> This continues until all spheres have been assigned to a cluster.
>
> A cluster may consist of a single sphere.

The question then arises as to what is an appropriate cluster parameter. Pillai et al. (1991) investigated microsphere distributions using a cluster parameter of 50 μm. This was apparently an arbitrary choice. In this analysis an attempt was made to determine a cluster parameter for microspheres in the tumour periphery.

As an example of how the choice of cluster parameter can affect the calculated clustering of spheres consider the case of two clusters of spheres as depicted in Figure 19.

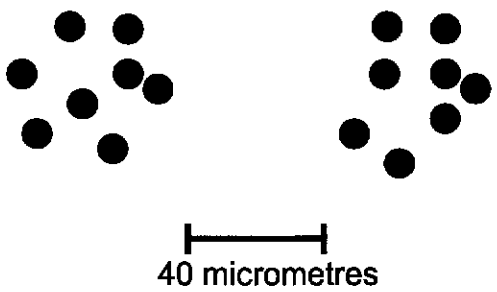

Figure 19. Effect of the choice of cluster parameter on cluster determination.

If a cluster parameter of less than 40 μm were chosen then the spheres would be correctly classified into two separate clusters. A choice of a larger cluster parameter would see all the spheres incorrectly classified into a single cluster.

The variation of the number of clusters classified in a section with cluster parameter might be expected to allow quantification of the cluster parameter. The expectation is that for a cluster parameter smaller than a single sphere each sphere will form its own cluster, so that the number of clusters will equal the number of spheres. As the cluster parameter is increased the number of clusters seen should rapidly fall as spheres near to each other are included in the same cluster. As the "true" cluster parameter is reached the number of clusters would be expected to plateau as no more spheres are being included into clusters. As the cluster parameter is made larger a point will be reached where neighbouring clusters are amalgamated, and so the number of clusters will again begin to fall. Eventually, for an extremely large cluster parameter, all spheres will be allocated to the same cluster.

Graphs of number of clusters identified versus cluster parameter, referred to as cluster parameter histograms, were generated to assist with this process. Initially some numerical simulations were carried out to gain some insight into the type of cluster parameter histograms that might be expected when spheres distribute in clusters.

4.4.1.1 Simulation of Clustering of Spheres

4.4.1.1.1 Randomly placed spheres

Sphere locations were randomly generated to lie on a 5000 μm x 5000 μm plane. No clustering was imposed.

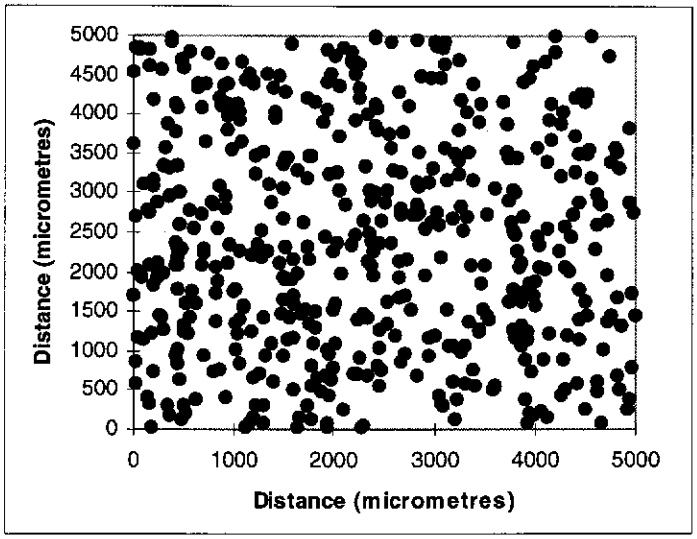

Figure 20. Distribution of randomly positioned spheres.

The spatial distribution of the spheres is shown in Figure 20 and its cluster parameter histogram in Figure 21. Cluster parameter histograms for actual sphere locations in liver would not be expected to show this type of curve.

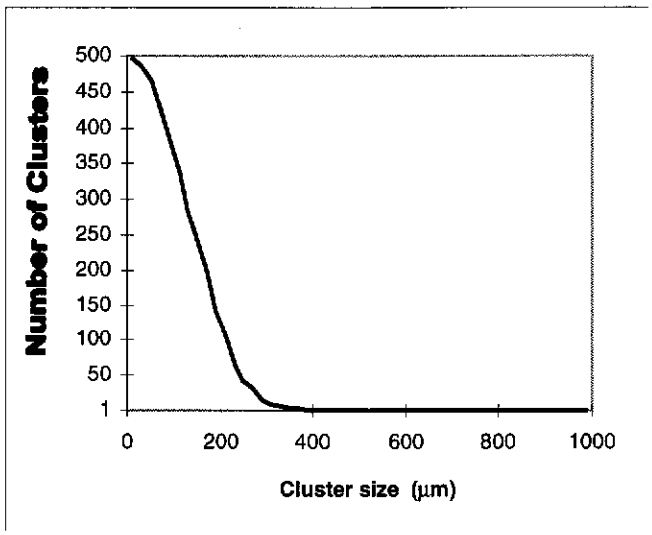

Figure 21. Cluster parameter histogram for randomly distributed spheres.

4.4.1.1.2 Non-Overlapping Clusters of Spheres

A distribution of spheres grouped into clusters was produced by hand by placing coordinate locations onto an image. The distribution formed is shown in Figure 22.

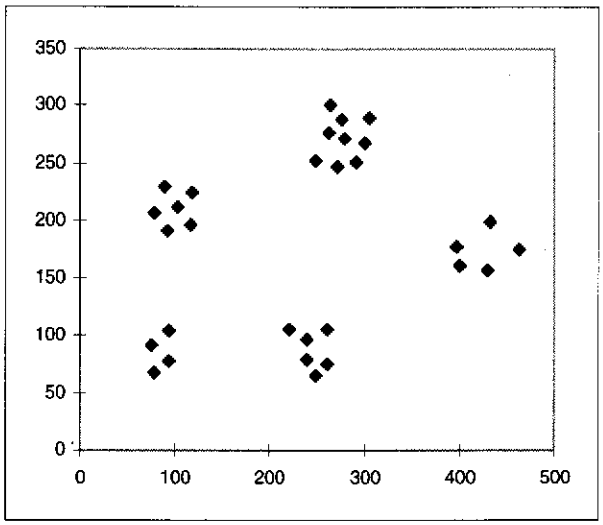

Figure 22. Simulated distribution of non-overlapping microsphere clusters

There are 30 spheres grouped into 5 clusters. The cluster parameter histogram for the above distribution is shown in Figure 23. This curve shows the expected features, viz

- at a small cluster parameter the number of clusters equals the number of spheres.
- as the cluster parameter increases the number of clusters falls rapidly.
- a plateau of 5 clusters is reached at around 50 μm when all spheres have been grouped into their own clusters.
- as the cluster parameter rises above around 90 μm clusters begin to amalgamate and the number of clusters falls again.

- for cluster parameters above about 150μm all spheres have been grouped into a single cluster.

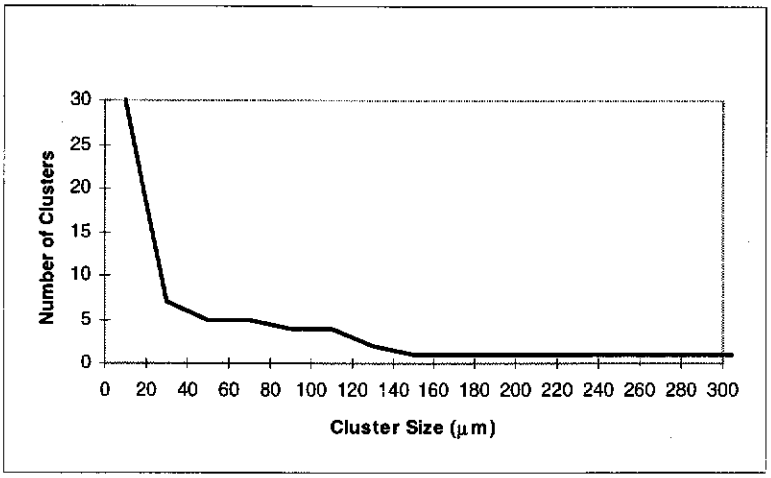

Figure 23. Cluster parameter histogram for a simulated distribution of non-overlapping sphere clusters.

4.4.1.1.3 Random clusters of spheres

Spheres were placed into randomly generated clusters on a 2000 μm x 2000 μm plane. The process was to randomly determine the centre of a cluster within the plane, and then to assign a random number of spheres to that cluster (up to a specified maximum number). These spheres were positioned randomly within a specified cluster radius of the cluster centre. The possibility exists that some clusters could overlap each other. Note that the cluster radius is not defined in the same manner as the cluster parameter and the two are not equivalent.

A simulation was performed with the following parameters

30 clusters

100 μm cluster radius

10 spheres/cluster maximum

The distribution of spheres produced is shown in Figure 24 , the cluster parameter histogram is shown in Figure 25.

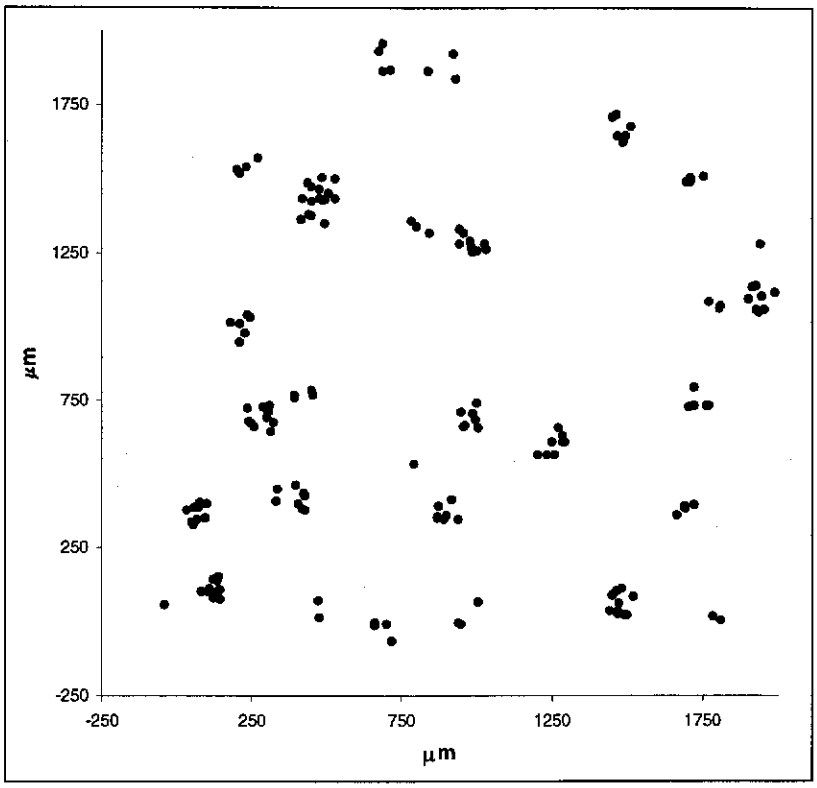

Figure 24. Distribution of randomly distributed clusters with a 100 µm cluster radius.

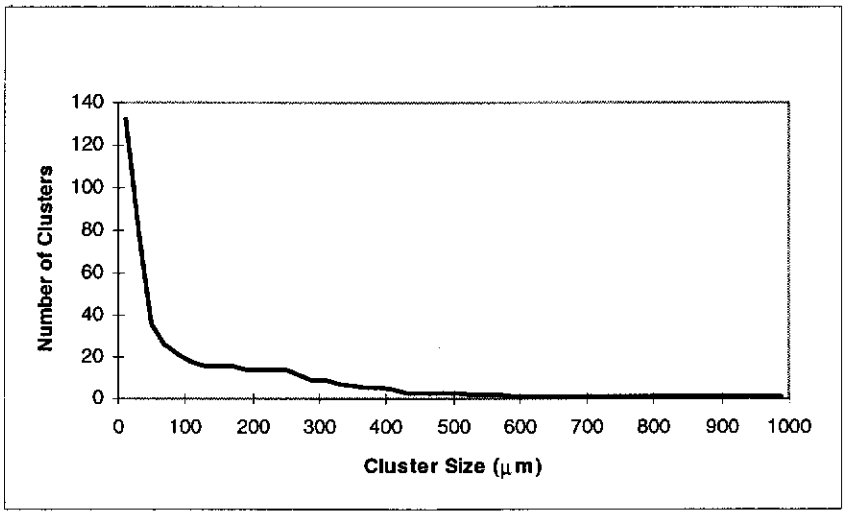

Figure 25. Cluster parameter histogram for randomly distributed clusters with a 100 µm cluster radius.

This graph shows features similar to that of Figure 23 for strictly non overlapping clusters.

Further simulations were conducted with cluster radii from 80 to 200 μm in steps of 20 μm. Three examples of the cluster parameter histograms for these simulations are presented in Figure 26 to Figure 28. Examination of these graphs would indicate that the selection of a suitable cluster parameter is not obvious - the first plateau encountered as cluster parameter is increased would seem to not always correspond to the expected value and sometimes the plateau is not present.

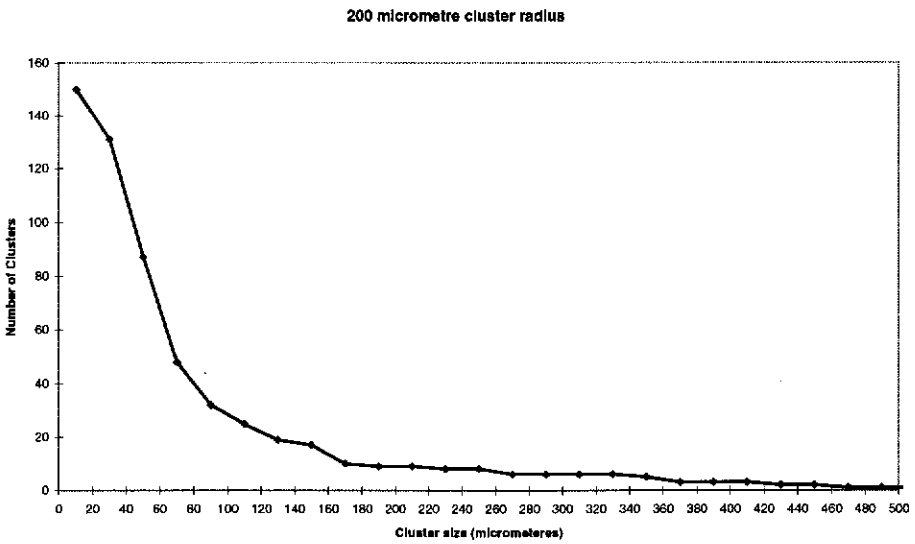

Figure 26 Cluster parameter histogram for randomly distributed clusters with a 200 μm cluster radius.

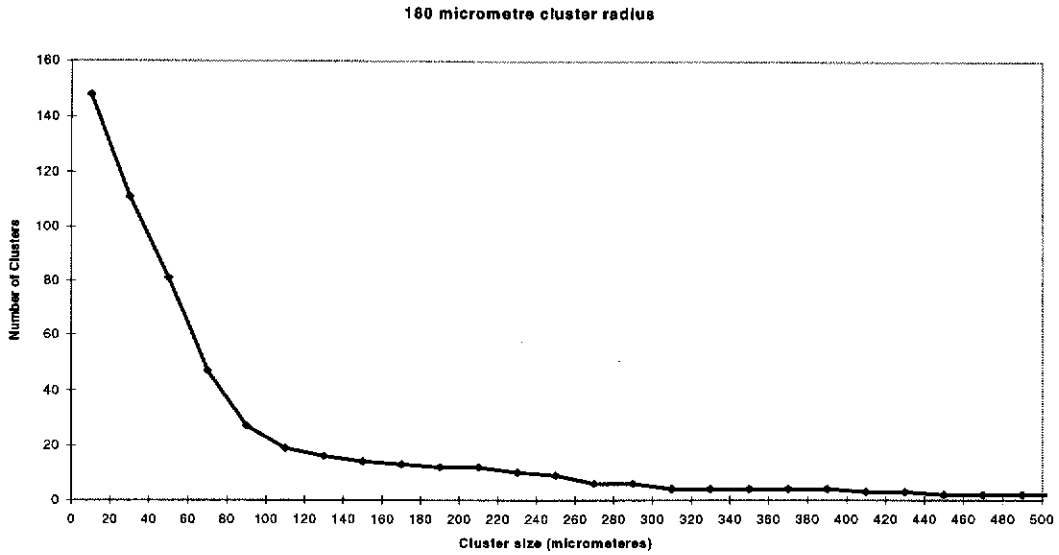

Figure 27 Cluster parameter histogram for randomly distributed clusters with a 180 μm cluster radius.

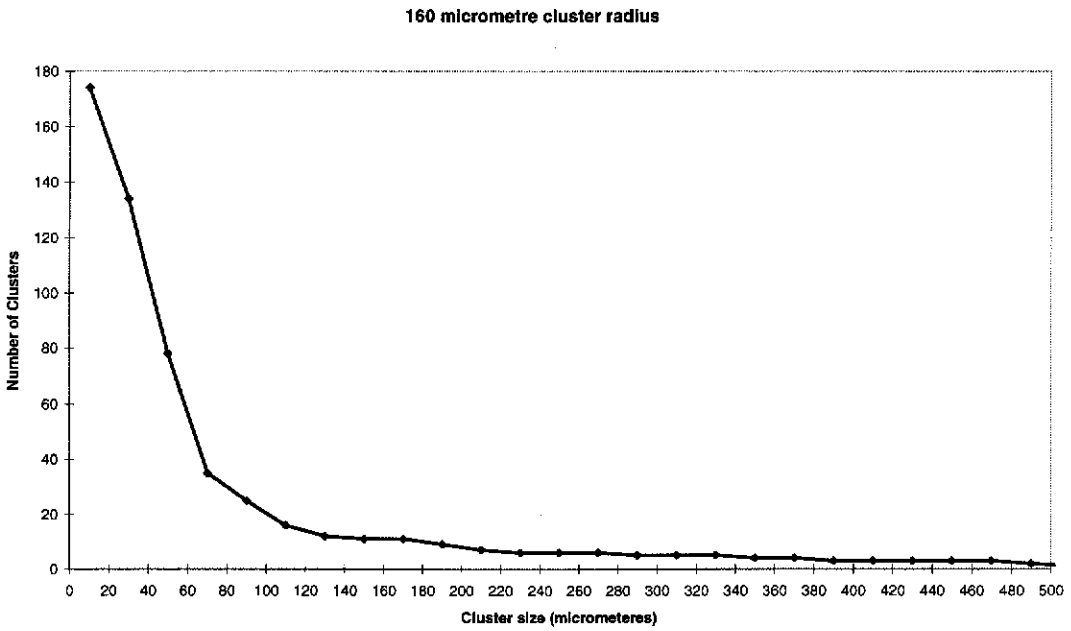

Figure 28 Cluster parameter histogram for randomly distributed clusters with a 160 μm cluster radius.

4.4.1.2 Cluster parameter histograms for tumour section data

Selection of a cluster parameter value appeared difficult for simulated data as discussed in the previous section. The difficulties did not diminish when examining real data.

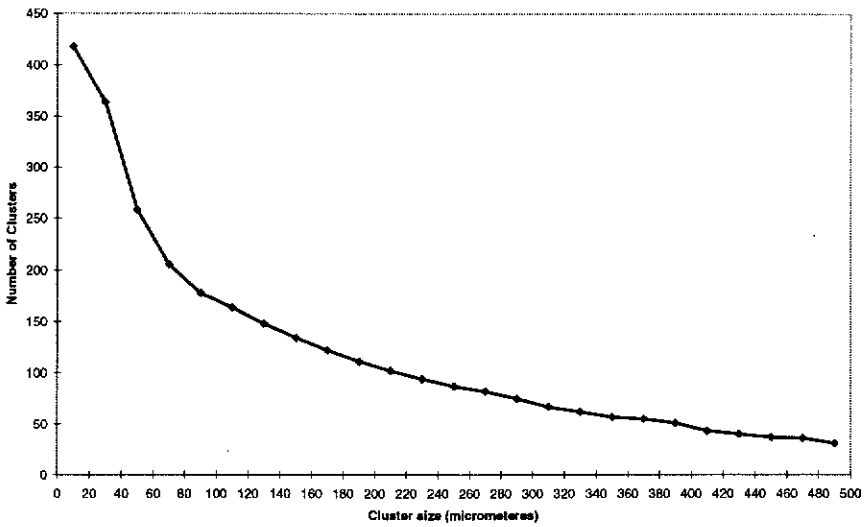

Figure 29 Example cluster parameter histogram for the tumour serosal surface tissue sections.

A typical example of one cluster parameter histogram is shown for the serosal surface and tumour-normal tissue interface sections in Figure 29 and Figure 30 respectively.

The shape of the cluster parameter histograms provides qualitative evidence of clustering as the shapes are similar to the simulated cluster histograms. However, no quantitative information regarding the cluster parameter is apparent from the histograms.

The equivocal results achieved using this analysis lead to investigation using an alternative approach, that of cluster analysis. This is discussed in the next section.

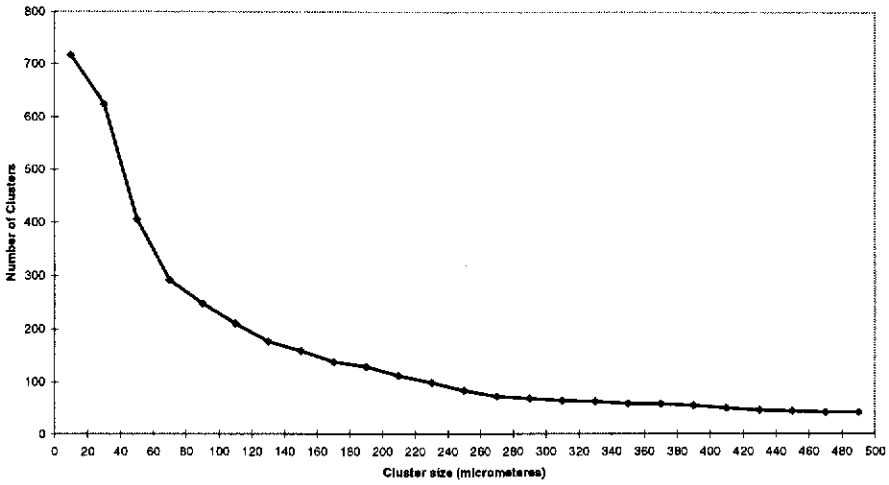

Figure 30 Example cluster parameter histogram for the tumour-normal tissue boundary sections.

4.4.2 Analysis of microsphere distributions using Cluster Analysis

Cluster analysis was employed in order to generate a quantitative measure of clustering of spheres in the tumour periphery. This is a standard statistical technique that attempts to classify a set of data, which could be homogeneous, into groups based on selected characteristics.

The purpose of cluster analysis was described by Gitman and Levine (1970) as being to place objects into groups (or clusters) in a manner suggested by the data itself. Objects in the same cluster tend to be 'similar' in some sense, objects in different clusters tend to be dissimilar. Several types of clusters are possible, these being

Disjoint where each object is a member of only one cluster

Hierarchical where one cluster may be entirely contained within another cluster but no other kind of overlap is permitted.

Overlapping objects can have membership of more than one cluster. This type of clustering can be constrained to limit the number of objects that belong simultaneously to two cluster or unconstrained allowing any degree of overlap.

Fuzzy where each object is assigned a probability of belonging to each cluster. Depending on how this probability is used, disjoint, hierarchical or overlapping clusters may be generated.

Hierarchical clusters appeared to be the most suitable type from visual examination of the data. The statistical package SAS (SAS Institute Inc.) was used to perform the analysis, using the Euclidean distance between spheres as the characteristic parameter. The process involves initially considering each observation to be a cluster by itself. The distance between all clusters is determined and the two 'most similar' clusters are merged to form a new cluster that replaces the two previous ones. The process then iterates, merging the closest two 'most similar' clusters at each iteration, until only a single cluster remains. A variety of clustering methods are discussed in the literature (a summary is given in Anderberg, 1973). The methods differ in the manner with which the similarity between clusters is determined. Three clustering methods were employed in analysing microsphere position data. They were the median, average linkage, and centroid methods. Each is summarised briefly below.

Average Linkage The similarity measure between two clusters is the average distance between pairs of observations, with one observation in each cluster.

Centroid The similarity measure between two clusters is the Euclidean distance between their centroids. When two clusters are merged the centroid of the merged cluster is used in further similarity measures. The centroid of the new cluster is a sum of the original centroids weighted according to the relative number of elements in each merged cluster.

Median — This is a variation of the centroid method. Distances between cluster centroids are used as the similarity measure but when two clusters are merged the centroids of each cluster contribute equally in determining the centroid of the merged cluster, irrespective of the number of entries in the original two clusters.

Determining the number of clusters present in a set of data is difficult (see for example Hardy, 1996). Ordinary significance tests, such as analysis of variance F tests, are not valid for testing differences between clusters (SAS, 1982). The SAS Institute have described a graphical method based on some 'goodness of clustering' parameters generated at each iteration. The parameters are the cubic clustering criterion (CCC), pseudo F and pseudo t^2 parameters. Their suggested method of use is described in SAS (1982) and SAS (1988) and is summarised in the following.

The CCC is plotted against the number of clusters from 2 clusters to approximately one tenth the number of observations. Peaks on the plot with a CCC greater than 2 or 3 are indicative of good clustering. Several peaks may be observed if the data clusters hierarchically. Very disjoint non-hierarchical clusters show a sharp rise before the peak followed by a gradual decline. SAS suggest that peaks between 0 and 2 should be interpreted with caution. Peaks in the CCC graph that are real clusters should also have a local maximum in their pseudo F score and a minimum in their pseudo t^2 score. The SAS Institute recommends performing clustering using a number of methods and examining the variation of the goodness of clustering parameters for each method. The median, average linkage and centroid methods were all used on data analysed in this work. The 'true' number of clusters present in the dataset should exhibit valid peaks in the CCC curve at the same number of clusters for all methods. The SAS Institute believe the power of the CCC to be at least a good as the human eye in two dimensions with 100 observations.

Hardy (1996) recommends always examining the clusters ultimately chosen to ensure they appear to be those naturally suggested by the data, as clustering

methods may select the correct number of clusters, but the resulting classifications may not be the ones the data would naturally suggest.

4.4.2.1 Preliminary Investigations

4.4.2.1.1 Application of cluster analysis to simulated clusters of microspheres

In order to gain a feel for the type of results produced by cluster analysis, the method was applied to the simulated microsphere clusters discussed in sections 4.4.1.1.2 and 4.4.1.1.3.

Cluster analysis was applied to the microsphere positions for non-overlapping clusters generated by hand shown in Figure 22. The CCC, pseudo F and pseudo t^2 variations with number of clusters for the median clustering method are presented in Figure 31. Starting with a single cluster the CCC increases with the number of clusters, rising sharply before peaking at 5 clusters and then falling beyond this point. The pseudo F is a maximum at 5 clusters while pseudo t^2 is low at this point. Thus five clusters would appear to be indicated from the clustering parameters. The average linkage and centroid methods showed similar curves to the median and provided corroborating evidence for the existence of five clusters. Figure 32 illustrates the cluster assignments using the median method with five clusters. The clusters correspond to the natural groupings.

Applying cluster analysis to the randomly generated microsphere positions of Figure 24 produced the curves shown in Figure 33 for the variation of CCC, pseudo F and pseudo t^2 with number of clusters for the average linkage method.

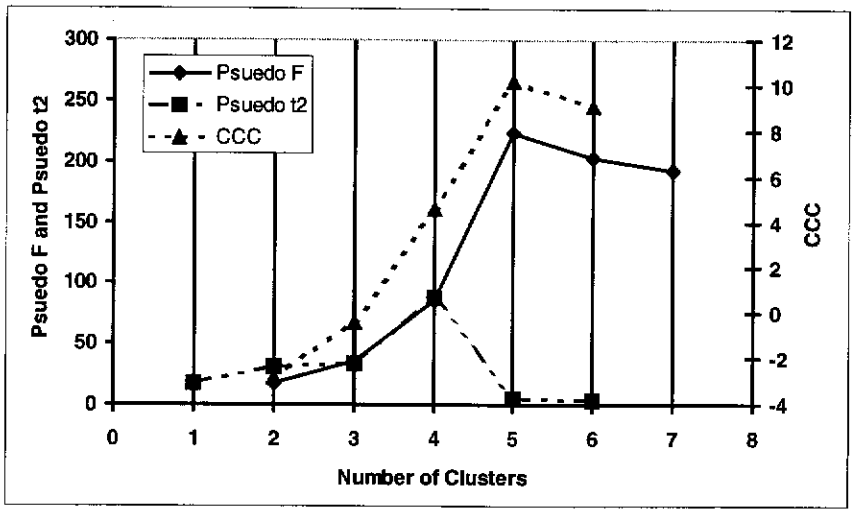

Figure 31. Variation of CCC, pseudo F and pseudo t^2 parameters with number of clusters for the non-overlapping clusters of Figure 22

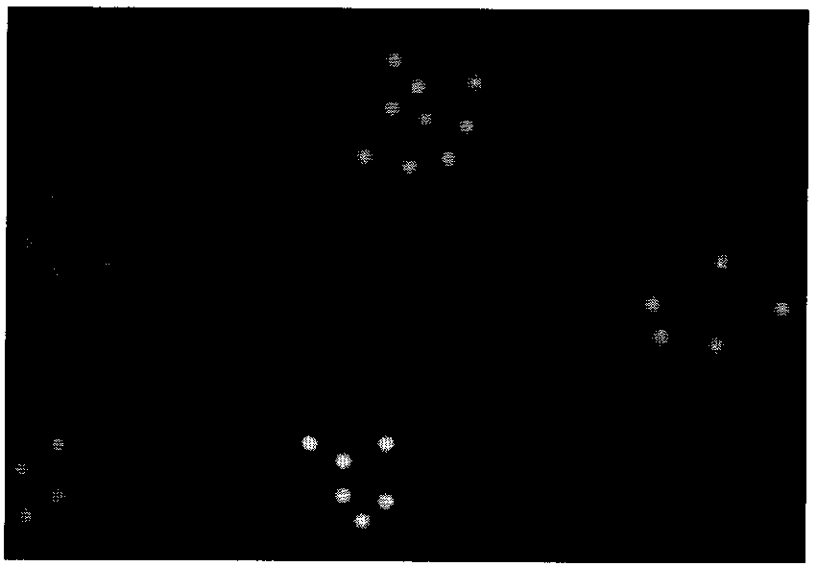

Figure 32. Clusters identified using the median clustering method for 5 clusters on the microsphere positions from Figure 22. Microspheres in different clusters appear in different colours.

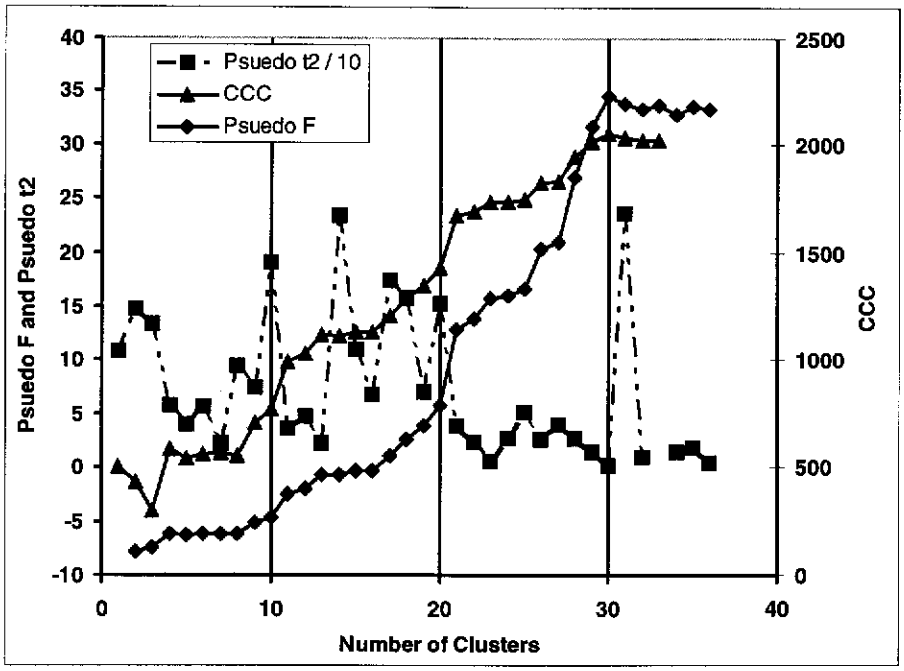

Figure 33. Variation of clustering parameters with number of clusters for the average linkage clustering method applied to the simulated microsphere positions of Figure 24

The CCC peaks at 30 clusters and the pseudo F value is also a maximum at this number while the pseudo t^2 is a minimum. The other methods provide corroborating evidence for 30 clusters. Figure 34 presents the cluster assignments for 30 clusters. The clusters chosen would appear to be the natural ones.

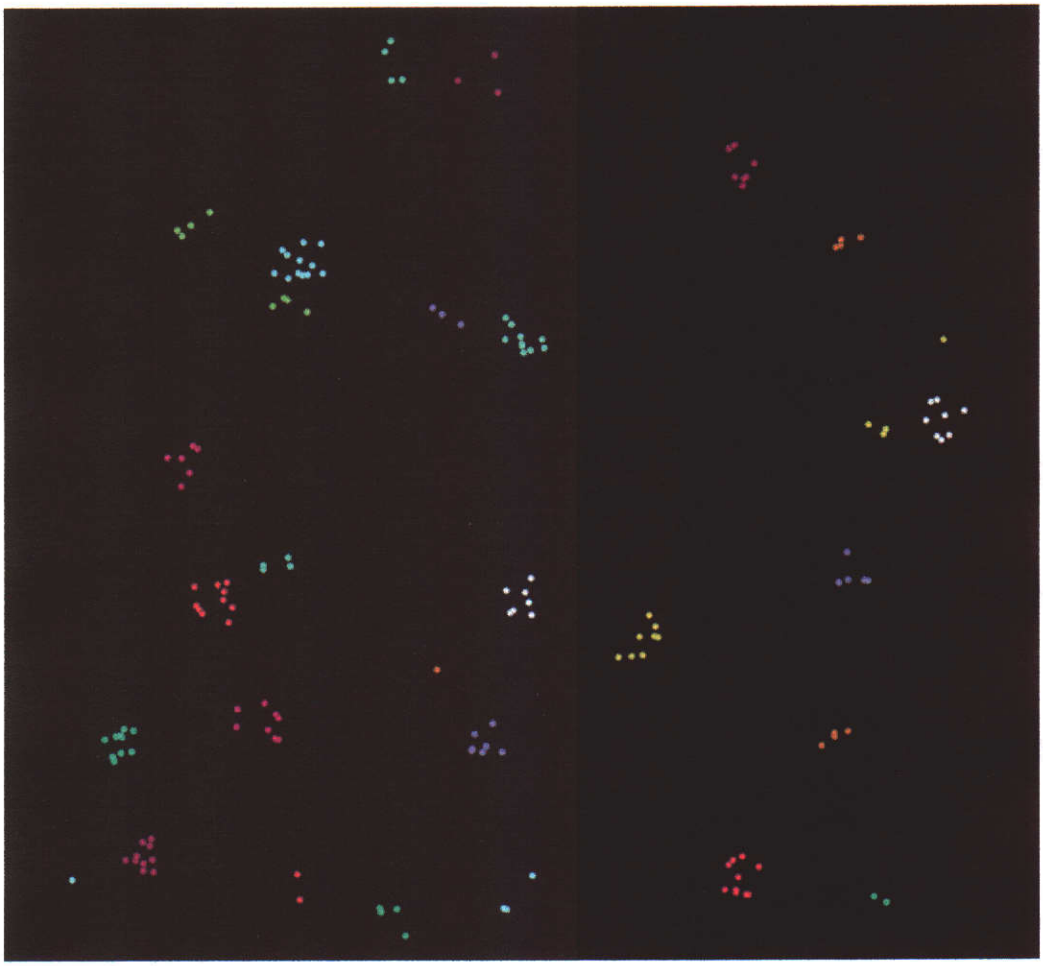

Figure 34. Cluster classifications for the microsphere positions of Figure 24 using the average linkage method with 30 clusters. Microspheres in different clusters are shown as different colours (colours are reused for some non-adjacent clusters).

4.4.2.1.2 Cluster analysis applied to observed microsphere positions

The results of the application of cluster analysis to simulated data indicated that this technique was capable of identifying actual clusters in this type of data. Its applicability to real microsphere distributions was tested by analysing microsphere positions in a tissue section from the sample volume containing the tumour-normal tissue interface. Figure 35 shows the variation of clustering parameters with number of clusters using the centroid method. Its appearance is typical of results obtained for the other clustering methods. A common feature was the presence of multiple peaks in the CCC curve and such peaks frequently coincided with pseudo F maxima and pseudo t^2 minima. This is indicative that the clustering of microspheres is hierarchical, with clusters of clusters occurring, and is consistent with visual observation of microsphere positions. The approach taken in determining how many clusters were present in a section was to choose the largest number consistent with good clustering.

The situation in Figure 35 suggests that the largest number of clusters occurring is 49. The CCC rises to a sharp maximum at this point and then falls away, the pseudo F value also has a maximum at this point and the pseudo t^2 is a minimum.

Figure 36 demonstrates the assignment of microspheres to clusters for the section. The grouping of microsphere clusters into larger clusters is evident from this Figure. It can also be observed that spatial variations in microsphere concentration occurs over distance on the order of a few millimetres.

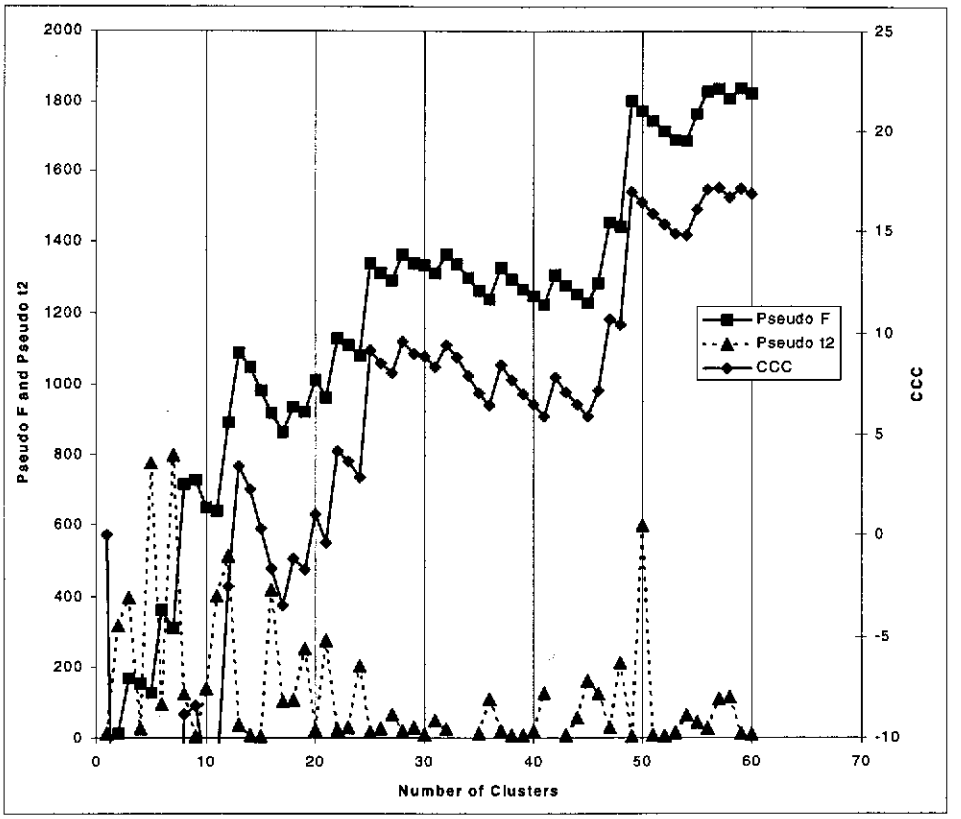

Figure 35. Variation of clustering parameters with number of clusters using the centroid clustering method for a tissue section containing the tumour normal tissue interface.

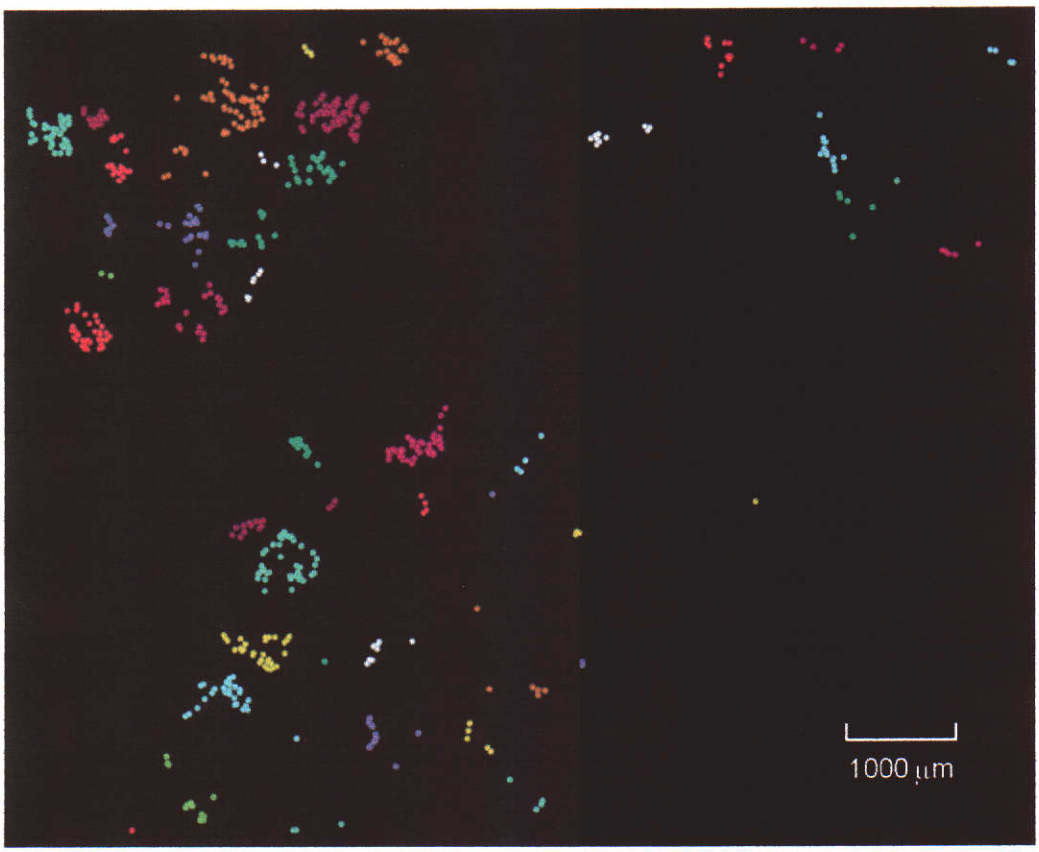

Figure 36. Example of cluster classifications for a tissue section containing the tumour normal tissue boundary. All microspheres shown are lodged within tumour tissues. The tumour boundary lies towards the left hand edge of the figure. Microspheres in different clusters are shown as different colours (colours have been reused for some non-adjacent clusters).

4.4.2.2 Cluster analysis applied to tumour-normal tissue interface data

Five of the sections that included an interface between tumour and normal tissue, were subjected to cluster analysis in order to classify microspheres into clusters and to determine parameters characterising the cluster population. The techniques discussed in the previous section were used and the variation of cluster parameters with number of clusters on a section were similar to those presented in Figure 35.

The sections encompassed nearly 5000 individual microspheres and the analysis clearly identified clusters, demonstrating that microspheres are not deposited randomly in this area of the tumour. The extent of each cluster, defined as the largest distance between any two microspheres of the cluster, the distance of

closest approach between clusters, and the number of microspheres in each cluster were determined. The results are presented in Figure 37 to Figure 39.

The distribution of cluster populations was skewed towards low numbers, as shown in Figure 37. It can be assumed that the clusters extend in the direction perpendicular to the plane of the section, so the number of spheres in the three dimensional clusters will be significantly greater than the figures given here. Figure 38 shows the histogram of the cluster extents, which is defined, for clusters consisting of more than a single microsphere, as the largest distance between any two microspheres in the same cluster. These varied over a wide range from 20 μm to 1500 μm. The distribution is fairly uniform in the range up to 1000 μm, falling away at higher distances. The minimum distances between clusters are shown in Figure 39. It can be seen that most clusters are less than 1200 μm apart.

The skewed nature of these distributions means that normal distribution theory parameters are not appropriate descriptors. The distributions are best described by use of percentiles. Table 6 summarises parameters describing the results for cluster populations, cluster extents and the minimum distance between clusters. The corner test of Olmstead and Tukey (Sachs, 1984) was used to test for independence between the cluster parameters. This test was chosen as it makes no assumptions about the underlying distribution of the quantities and allows for the effects of outliers that may bias other correlation measures. It was found that the measures for cluster population, cluster extent and minimum distance between clusters were not independent at the 0.5% level. There was a tendency for clusters with larger populations to have larger cluster extents and to be closer to another cluster. Figure 40 shows the relationship between cluster extent and cluster population. There are similarities between these results and those reported by Pillai et al. (1991), who found highly skewed distributions for cluster populations and the distances between clusters. However, different analysis techniques have been used here, so no direct comparison can be made with their results.

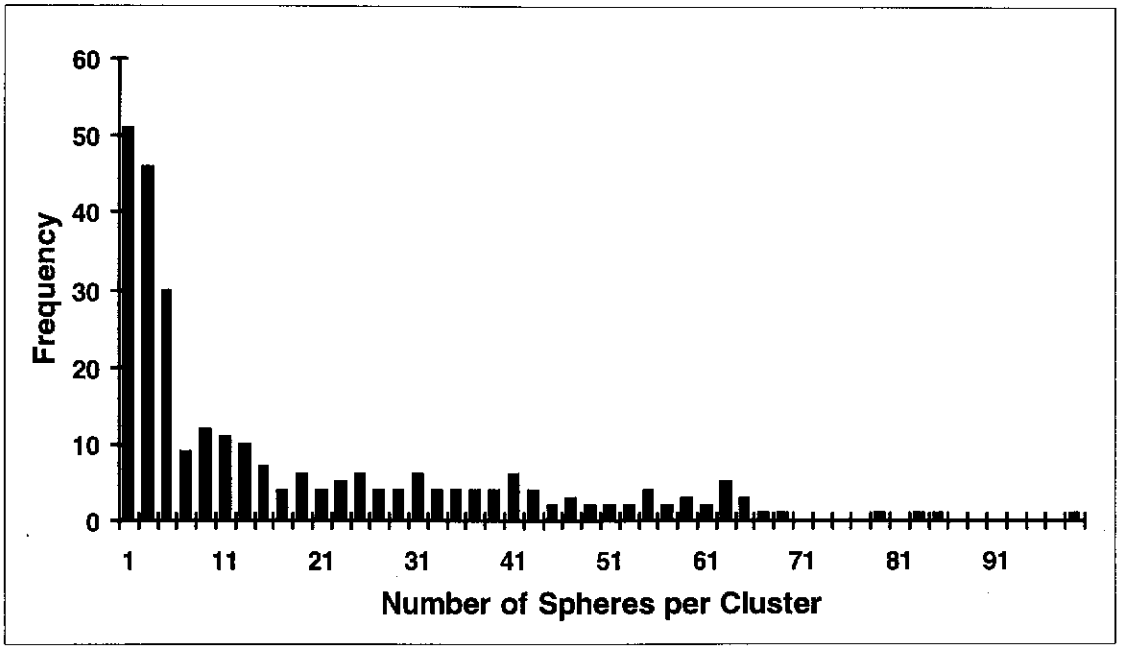

Figure 37. Histogram of the number of microspheres per cluster. (For tissue sections from the tumour-normal tissue interface that were subjected to cluster analysis.)

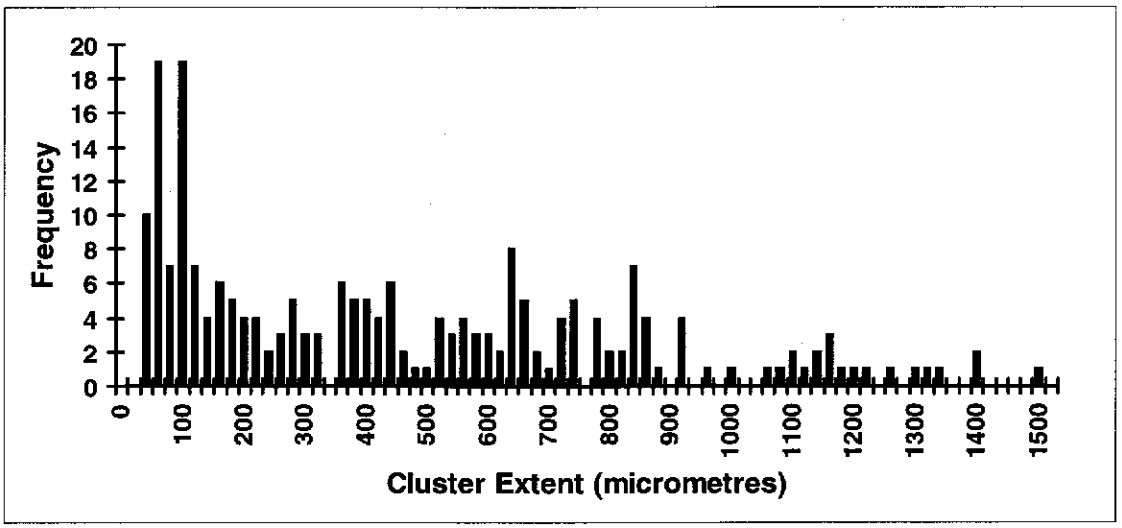

Figure 38. Histogram of cluster extents. (For tissue sections from the tumour-normal tissue interface that were subjected to cluster analysis.)

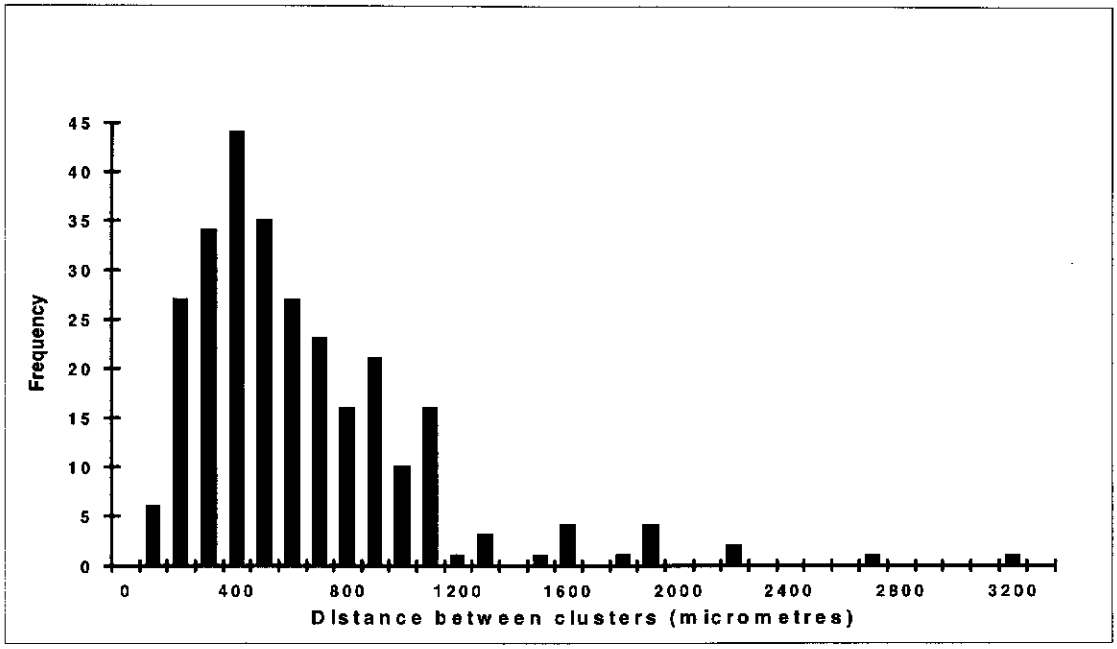

Figure 39. Histogram of the minimum distance between clusters. (For tissue sections from the tumour-normal tissue interface that were subjected to cluster analysis.)

Table 6. Summary of Cluster Analysis Results

	Cluster Population	Minimum Distance from another cluster (μm)	Cluster Extent (μm)
Median	8	470	337
25% percentile	2	303	101
75% percentile	29	774	690
minimum	1	89	21
maximum	98	3105	1489

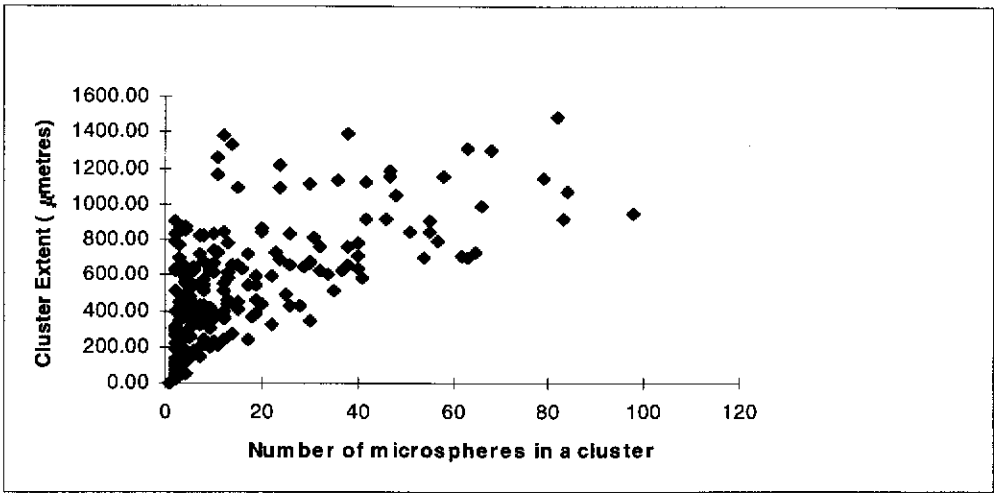

Figure 40. Plot of cluster extent against the number of microspheres in the cluster. (For tissue sections from the tumour-normal tissue interface that were subjected to cluster analysis.)

4.5 Randomness of microsphere deposition in normal liver

There was no visual evidence of clustering in normal liver tissue. In order to test whether or not the distribution of microspheres was random, the sample volume was divided into eight equal volumes. The number of microspheres observed in each volume will be the same if the distribution is random. The observed number was compared to the expected number and the randomness tested using a χ^2 test.

There was an expected number of 48 microspheres in each of the eight volumes into which the normal tissue sections were divided. The observed number ranged from 32 to 70 microspheres. The calculated χ^2 value was significant ($p<0.005$), indicating that the hypothesis of randomness should be rejected.

4.6 Discussion of microsphere distribution results

The delivery of microspheres via the hepatic artery, possibly in conjunction with a vasoconstrictive agent, is designed to achieve the preferential deposition of microspheres in tumour tissue. Microspheres are carried to their ultimate

deposition sites by blood flow, so it can be expected that deposition patterns will reflect blood perfusion. In this context, it can be noted that Anderson et al. (1992a) reported that a greater proportion of microspheres were delivered to tumours than would be expected from baseline arterial flow measurements. The results obtained here give support to these general expectations about microsphere deposition patterns in the tumour but indicated that deposition in normal liver was not uniform. The distribution of microsphere concentrations observed within the tumour is in agreement with blood flow patterns reported by Ariel and Padula (1982) for metastatic colorectal cancers. They reported larger tumours had an interior largely devoid of arterial supply, but a rich plexus of arterioles and capillaries in their outer perimeter.

The use of cluster analysis has confirmed in a statistically valid manner that microspheres do not deposit uniformly in the tumour periphery but form into clusters. It seems likely that the combination of the distended morphology and non-uniform concentration of blood vessels in the tumour periphery provide the mechanism by which microspheres deposit in clusters in this region of the tumour. Pillai et. al. (1991) found clustering occurred with 27 μm diameter polystyrene microspheres infused via hepatic injection in rabbits. This analysis has demonstrated similar behaviour occurring in a human subject. While Pillai et. al. (1991) defined a microsphere cluster as those microspheres separated from adjacent microspheres by a distance of less than 50 μm, and the statistical technique of cluster analysis to assign microspheres to clusters was employed here, the results are similar in character. The cluster population histogram presented in Figure 37 shows there is a preponderance of low population clusters. This does not however necessarily imply that a microsphere is more likely to be in a low population cluster as while there are many more clusters with low populations, the number of microspheres contained in these clusters will be a relatively small fraction of the total number of microspheres present. The results indicate that for a microsphere selected at random there is a 90% chance it will be in a cluster containing less than 65 microspheres. However there is a roughly equal probability of the actual cluster population being between anywhere in the range from one to 65. Pillai et. al. (1991) noted that microsphere clusters might

more appropriately represent sources of radioactivity for dosimetry calculations. Zavgorodni (1996) provided confirming evidence for this suggestion by modelling microsphere clusters as sources of radioactivity and obtained results in good agreement with those of Roberson et. al. (1992) who utilised microsphere locations using Pillai's data. This topic is explored further in Chapter 6.

The clusters identified in this study are a two-dimensional cross section through what is undoubtedly a three dimensional network of microspheres. The three dimensional shape of these clusters could not be ascertained, but some inferences can be made from the data. If the clusters were spherical and of uniform size, the distribution of cluster extents would be strongly skewed towards the cluster diameter. Figure 38 shows clearly that this is not the case. This implies that clusters are not uniform in size but have a range of sizes up to around 1400 μm.

In normal liver tissue microspheres were found to deposit non-uniformly. The size of the eight volumes used for the χ^2 test equate to cubes with sides of roughly 4000 μm, indicating that deposition is non-uniform over distances of this order. This means that radiation doses will be more heterogeneous than if microspheres deposited uniformly. Roberson et. al. (1992) performed normal tissue dosimetry calculations over a volume about 25 times smaller than the one analysed in this study. They found the large average normal liver doses estimated to be tolerable by this type of therapy could not be fully explained by their results and speculated the discrepancy could be resolved if the distribution of microspheres was more macroscopically non-uniform. These results support this conclusion. Detailed dosimetry calculations using the observed microsphere distributions are presented in Chapter 5.

Fox et al. (1991) reported a concentration higher concentration of microspheres of 40 mm^{-3} in normal liver tissue compared to the 3.5 mm^{-3} recorded in this study. Plots of microspheres positions in the paper by Fox et al. (1991) clearly indicate microspheres aggregating into short lines, of length on the order of 1 mm, along small vessels in the liver. The spatial distribution of microspheres was as a consequence very heterogeneous. The type of aggregations observed in that study were not apparent in the normal liver tissue sections examined in this

work, where it was unusual to find more than two microspheres within a 500 μm proximity. However, the liver studied by Fox had a significantly smaller tumour burden than the liver used in this study. It is likely that the concentration of spheres in normal tissue will depend on the tumour burden of the patient. Microspheres infused into a liver that has more tumours or larger tumours will have a greater tumour volume into which they can deposit. This would correspond to a smaller concentration of microspheres depositing into normal hepatic parenchyma.

Clearly there is scope for further work in this area in order to full characterise microsphere deposition patterns in normal liver tissue.

5. Radiation dose calculations for ^{90}Y labelled microspheres

5.1 Methods for calculating radiation doses on microscopic scales

Techniques for calculation of radiation doses from known microsphere positions normally assume that the microspheres behave as point sources of radiation (Roberson et al., 1992). The spatial distribution of radiation doses arising from a collection of microsphere sources can then be determined using the superposition principle and the dose distribution from a single point source emitter.

As a function of radial distance, r, the dose response to a point radiation source is called the dose kernel, k(r). Simpkin and Mackie (1990) state this may be thought of as the expectation value of the spatial distribution of the energy deposited in target volumes centred on a point source per mass of the target volume per decay of the point source. In an unbounded, homogeneous medium k(r) will be radially symmetric and have a singularity at the point of emission. This singularity is usually made tractable by scaling the kernel by the square of the distance from the emission point. It is also common practice to present the kernel using a scaled abscissa, r/X, where X is a predefined distance. A variety of scaling distances have been used including the continuous slowing down approximation (csda) range of the maximum energy electron emitted in a point source spectrum and X_{90}, the radius inside which 90% of the emitted energy is absorbed.

Dose point kernels are now commonly determined using Monte Carlo methods. Prestwich, Nunes, and Kwok (1989) calculated beta dose point kernels for radioisotopes of interest in radioimmunotherapy, including ^{90}Y, using Monte Carlo methods. Simpkin and Mackie (1990) derived the beta dose point kernel

for ^{90}Y and other isotopes using the parameter-reduced electron-step transport algorithm (PRESTA) version of the EGS4 Monte Carlo code. This algorithm includes secondary electron production and transport and was used for all dosimetry calculations presented in this work.

5.1.1 Dose-volume histograms

Calculation of radiation doses from observed microspheres locations throughout a three dimensional volume as performed by Fox et al. (1991) and Roberson et al. (1992) results in a large amount of dose information. The volume of information may make it difficult to interpret the data when displayed as isodoses on planes through the treatment volume, as three dimensional isodose surfaces or in some other form of three dimensional display. A method of condensing three dimensional dose data into a form that summarises radiation distribution information is via dose volume histograms. The technique was summarised by Drzymala et al. (1991) whereby a histogram may be plotted according to the usual mathematical definition, as the accumulated volume of those elements receiving dose in a specified dose interval against a set of equispaced dose intervals. This is referred to as a differential dose-volume histogram. Alternatively, it is possible to plot the dose data as the volume receiving a dose greater than or equal to a given dose against that dose over the expected dose range. In most cases the volume is specified as the percentage of the total volume of a structure receiving dose within each interval. This plot is referred to as a cumulative dose-volume histogram, or often a simply a dose-volume histogram.

Drzymala et al. (1991) noted that dose-volume histograms provide a graphical summary of dose distributions within a volume of interest (often an anatomical structure) but do so at the expense of losing information. While they provide information on the existence and magnitudes of hot (or cold) spots, they do not indicate where within the volume the hot spot occurred, nor whether it occurred in one place or several disconnected regions. For detailed information of this type, recourse must be made to other ways of visualising the dose data.

The shape of a dose-volume histogram (DVH) provides information about the distribution of dose within the volume. Drzymala et al. (1991) noted that when the volume represented by the histogram has a fairly uniform dose, the DVH approximates a step function, and that large steep drops in the DVH ordinate are indicative of a large percentage of the volume having a similar dose. In contrast, a DVH that has a relatively shallow and constant slope is indicative of a heterogeneous dose distribution in the volume of interest.

5.2 Software used for radiation dose calculations

Dosimetry calculations were performed using a personal computer running custom software written in the C programming language (Borland C++ Builder v1.0).

The volume over which radiation doses were determined was divided into a regular mesh. At each point of the mesh, the dose contribution from each microsphere was found and the total dose at that point determined using the superposition principle. Dose contributions from individual microspheres were determined by computing the distance of the microsphere from the mesh point and using the beta dose point kernel published by Simpkin and Mackie (1990) for ^{90}Y to find the radiation dose at that distance. The accuracy of the program was verified by determining the radiation doses from six sources over a mesh containing 75 points using the software and comparing the results with a manual calculation over the same volume.

The effect of the mesh size on calculated dose was investigated by performing calculations using three different mesh sizes. Mesh sizes of 0.05 mm, 0.1 mm and 0.2 mm were used. Radiation dose distributions arising from five microspheres positioned as depicted in Figure 43 were determined over a 4x4x4 mm^3 volume centred on the sources for each of the mesh sizes. The resulting dose volume histograms were virtually identical for each mesh size as can be seen in Figure 41. A mesh size of 0.1 mm was chosen for all radiation dose calculations.

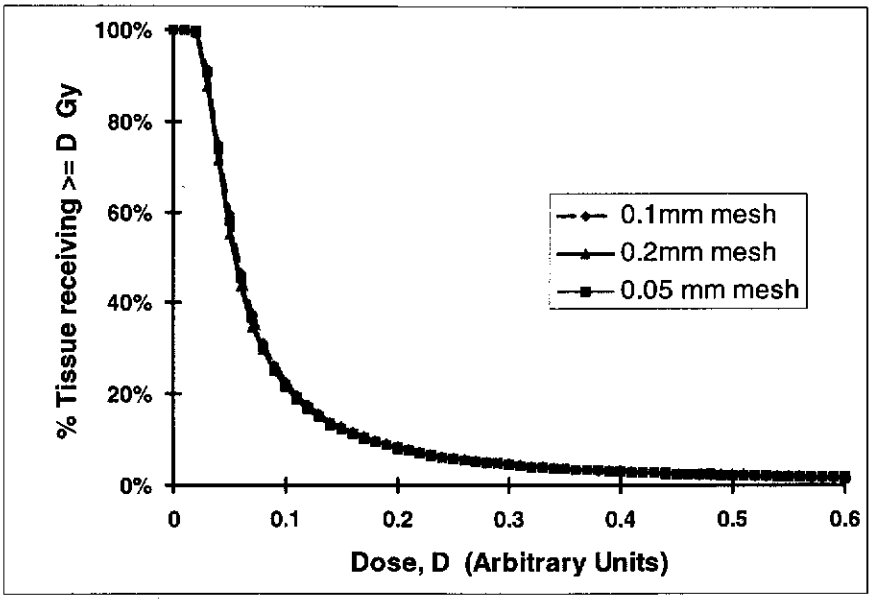

Figure 41. Effect of mesh size on radiation dose distributions.

5.3 Dose distributions for the observed microsphere positions

The three dimensional microsphere positions determined for each of the four tissue samples were used to calculate radiation dose distributions. For this calculation it was assumed each microsphere acted as a point source of radiation. Radiation dose calculations were carried out on each section plane for each of the sampled tissue volumes using an 0.1 mm grid. The activity per microsphere was taken as 50 Bq, which was the average activity per microsphere used in the treatment, and complete decay was assumed.

A problem arises for dosimetry calculations because beta emissions from microspheres lying outside the sample volume will make a contribution to the radiation dose within the sample volume. Ignoring this fact will cause calculated doses to be underestimated. Doses will be more severely underestimated closer to the edges of the sample volume. The contribution to radiation dose from microspheres lying outside the sample volume was allowed for in two different ways, depending on the location of these volumes with respect to the tumour boundary.

For volumes remote from the tumour boundary it was assumed that the sample was completely surrounded by tissue of the same type, and that microspheres deposited randomly in these tissues with the same densities as were observed for the samples themselves. A 10 mm margin was placed around each edge of the sample volume and microspheres placed randomly within this region with a density appropriate for the tissue. The radiation dose contribution from these spheres was then calculated for each of the calculation planes within the sample volume and this value added to the radiation doses calculated for sphere positions within the sample volume alone.

For volumes containing the tumour boundary the situation is more complex, since the microsphere concentration depends strongly on the distance from the boundary. It was necessary to devise a model which would allow for this non-uniform distribution. The method adopted for this model is illustrated in Figure 42. For the directions perpendicular to the boundary, the size of the sampled volume is such that at its edges, the microsphere concentration has fallen to a value characteristic of the adjoining tissue. Therefore, outside the sampled volume, the contribution to the dose can be modelled by placing microspheres at random in that volume with the concentration appropriate to the tissue. An extra 10 mm was added to the sample volume for this calculation.

This approach can not be used for the adjoining volumes which would include the tumour boundary. Since microspheres in these volumes will not contribute large local doses, but just generate doses varying relatively slowly with distance, it was assumed that sufficiently accurate modelling could be achieved by placing microspheres in positions obtained by reflecting the observed microsphere positions about the edge of the sampled volume. This was done for the two directions parallel to the tumour boundary. Note that for clarity only one of these directions is shown in Figure 42.

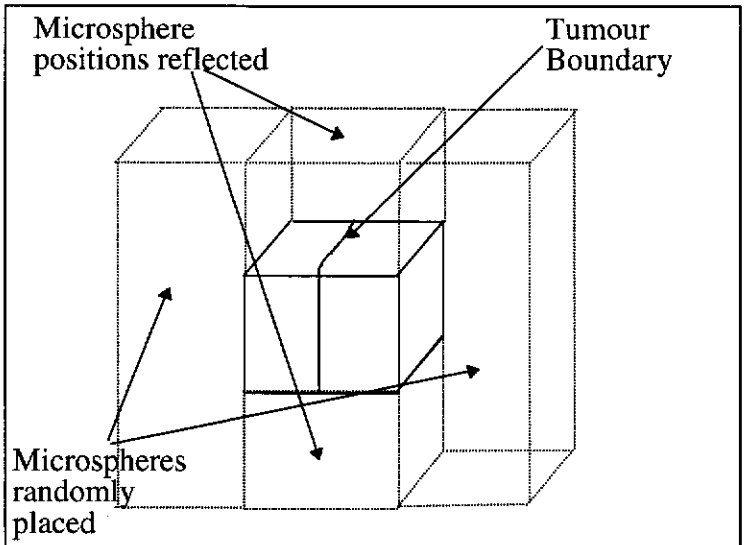

Figure 42. Placement of microspheres: Illustration of the methods used to add microspheres to the volume outside the sampled volume. Microspheres were also positioned in volumes in front of and behind the volume illustrated, but for clarity these have been omitted from this figure.

The fact that only every 20^{th} serial section was retained and analysed for microsphere locations must also be taken into account when determining radiation dose distributions. Fox et al. (1991) analysed microsphere positions in contiguous tissue sections taken from normal liver and noted that microspheres deposited in capillaries in short lines giving rise to considerable correlation of microsphere positions in adjacent sections. Strong correlation of microsphere positions in the tumour periphery was observed over distances on the order of 400 μm. Fox et al. (1991) reported that the correlation in microsphere positions leads to radiation dosimetry patterns for ^{90}Y being essentially unaltered if microsphere positions from sections at 500 μm intervals were used for dose calculations rather than the microsphere positions in contiguous sections. The 200 μm interval between sections analysed in this study is well within this distance. This indicates that calculated radiation dosimetry patterns should

accurately reflect those that would have been obtained if contiguous sections had been used.

For determination of absolute radiation doses, allowance must be made for microspheres lying in the volume between the sections in which microsphere positions were recorded. The work of Fox et al. (1991) indicates that if a microsphere is observed at a particular location in one tissue section then other microspheres would be expected to be found close to the same location in surrounding tissues. Absolute radiation doses can thus be estimated by scaling the activity of microspheres at the observed positions by a factor to allow for the microspheres in the intervening volume. The scaling factor will be the inverse of the fraction of the total number of microspheres present in the tissue volume that were observed in the sections analysed. The fraction of microspheres observed was 42/200, as discussed in section 4.3.1. The scaling factor is thus 200/42. This technique will overestimate radiation doses close to a microsphere but this will only affect a small fraction of the total volume in which radiation doses are determined.

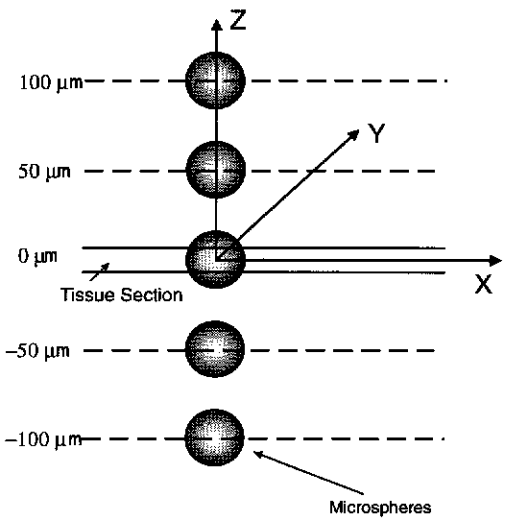

Figure 43. Geometry for assessing effect of the use of a scaling factor for absolute dose computations. The central microsphere is the one observed lying in the tissue section, the other microspheres are in tissue not included in the analysis.

The differences in dose caused by using the scaling factor can be estimated by recognising that an observed microsphere in a section represents $200/42 \approx 5$ microspheres in approximately the same position in a 200 µm thickness of tissue centred at the observed microsphere location, the geometry will be approximated by the arrangement of microspheres as

shown in Figure 43. Radiation dose patterns were calculated on a 0.2 mm mesh through a 20 x 20 x 20 mm^3 volume centred on the microspheres. The axes used for the calculations are shown in Figure 43. To estimate the affect of using the scaling factor radiation doses were calculated using all five sources and compared with scaled doses calculated using only the central microsphere (at the z= 0 μm position).

Cumulative dose volume histograms were determined for both cases and are shown in Figure 44. The percentage difference between doses calculated using all microspheres and the single scaled representation are shown in Figure 45 for the x-y plane and the x-z plane. Close to the sources quite large differences are apparent. At distances greater than 500 μm from the origin differences in dose using the scaled representation were less than 2%. This supports the expectation that the use of the scaling factor will only overestimate radiation doses to a relatively small fraction of the total tissue volume.

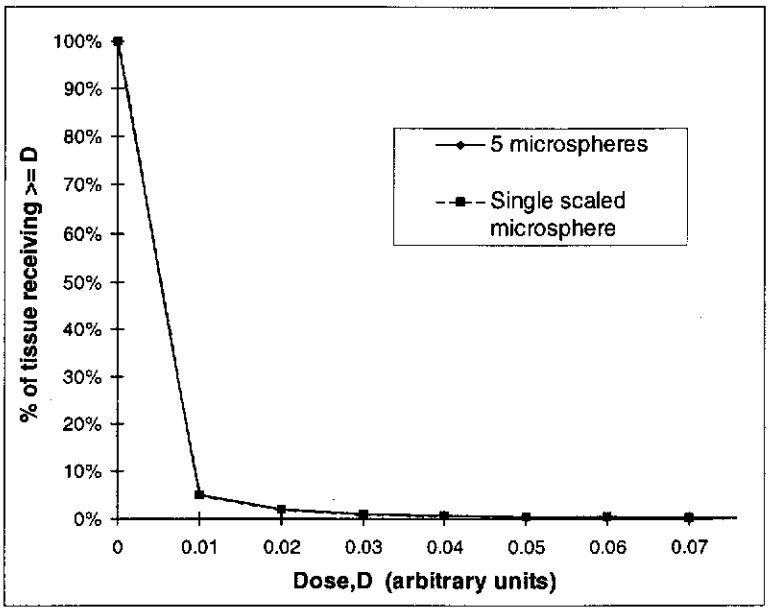

Figure 44. Cumulative dose volume histograms for all five microspheres and the single scaled case. The curves were virtually identical and cannot be separated on this plot.

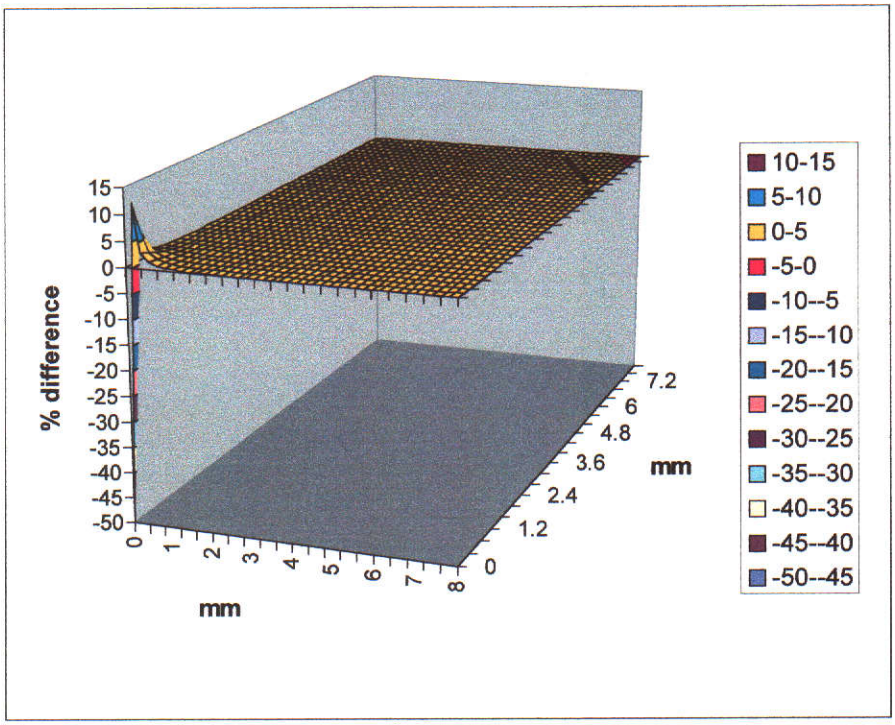

(a)

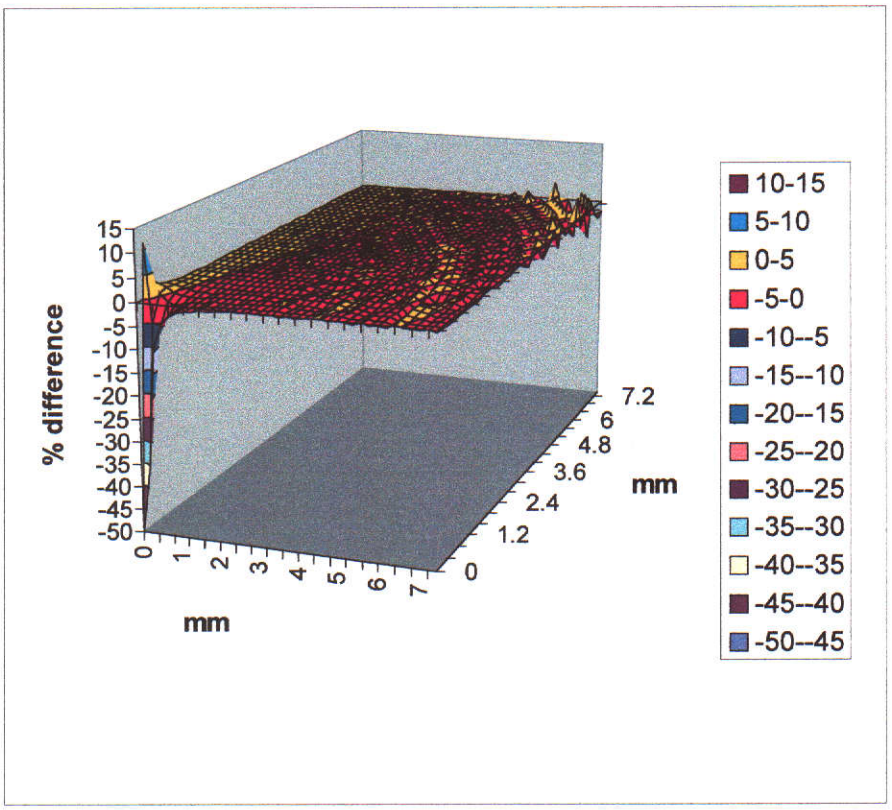

(b)

Figure 45. Percentage differences in radiation dose calculated using all microspheres and a single scale microsphere on (a) the x-y plane and (b) the x-z plane.

5.4 RESULTS

5.4.1 Normal Liver Tissue

Figure 46 shows the dose distribution on the central plane of the normal liver tissue block. Significant dose heterogeneity is evident with higher doses being delivered in the vicinity of a microsphere. Figure 47 shows the cumulative dose histogram for the tissues and displays features characteristic of dose inhomogenity (Drzymala et al. 1991). The mean tissue dose was 8.9 Gy and the minimum dose was 5.0 Gy.

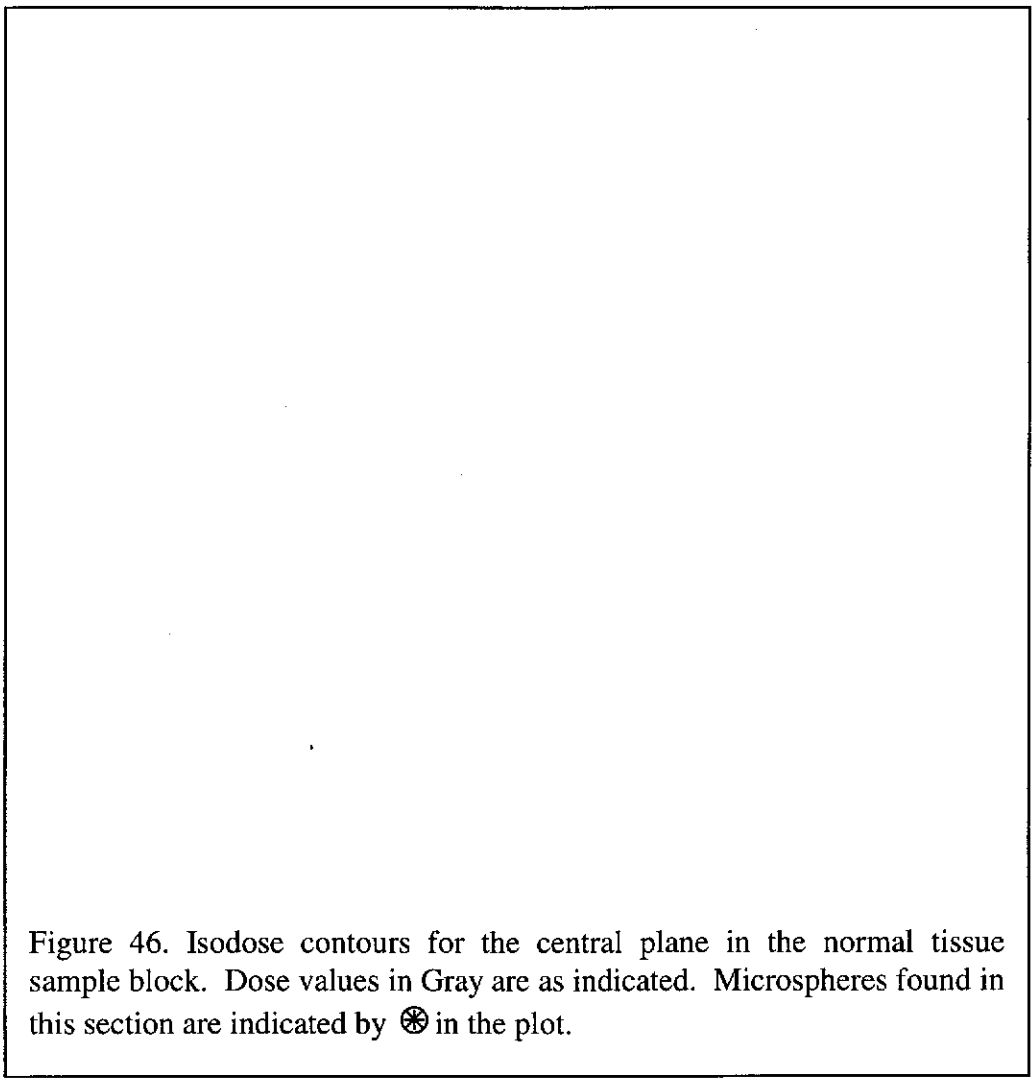

Figure 46. Isodose contours for the central plane in the normal tissue sample block. Dose values in Gray are as indicated. Microspheres found in this section are indicated by ⊛ in the plot.

If the same activity per unit volume as was deposited in this tissue had been homogeneously distributed throughout the tissue instead of being attached to

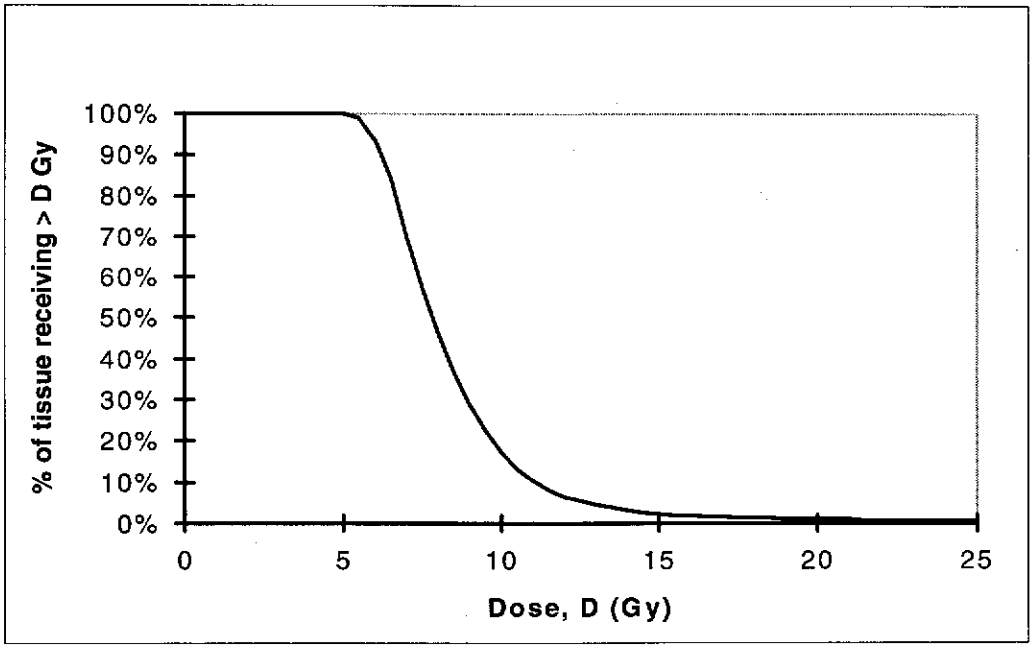

Figure 47. Cumulative dose volume histogram for normal liver tissue.

microspheres, then the radiation dose that would arise can be calculated by using the mean energy deposited per ^{90}Y disintegration (which is 0.936 MeV). This situation would result in a uniform dose of 8.9 Gy. It was calculated that 69.4% of the normal liver tissue volume receives less than this dose (see Figure 47). If all the infused activity had been assumed to deposit uniformly throughout the liver, as often assumed in calculations for absorbed dose to the liver, a delivered dose of around 80 Gy would have been calculated.

The fact that microsphere locations on sections at 200 μm spacings were used in the radiation dose calculations and then scaled to allow for microsphere positions in the intervening tissue volume, as discussed in section 5.3, potentially could lead to more non-uniform doses being calculated than if microsphere positions on contiguous planes had been used. While the considerations presented in section 5.3 lead to the expectation that such effects will be small, this was further investigated by repeating the dosimetry calculations using microsphere positions from every second tissue section analysed in the normal liver tissue sample volume. The spacing between tissue sections for this calculation was thus 400 μm. Comparison of the 200 μm and 400 μm section spacing results will

provide an indication of the effect allowing for microsphere positions in the intervening tissue volume by using a scaling faction will have on dose uniformity

Results are presented in Figure 48 It is apparent from the Figure that the cumulative dose volume histograms are almost identical. While there are some minor difference between the curves, the overall conclusions about dose heterogeneity would remain unchanged regardless of whether sections at 200 μm or 400 μm spacing were used. This gives confidence that using microsphere positions observed on planes with a 200 μm separation will not significantly alter calculated radiation dose distributions compared to those that would be calculated if microsphere positions on contiguous planes had been used.

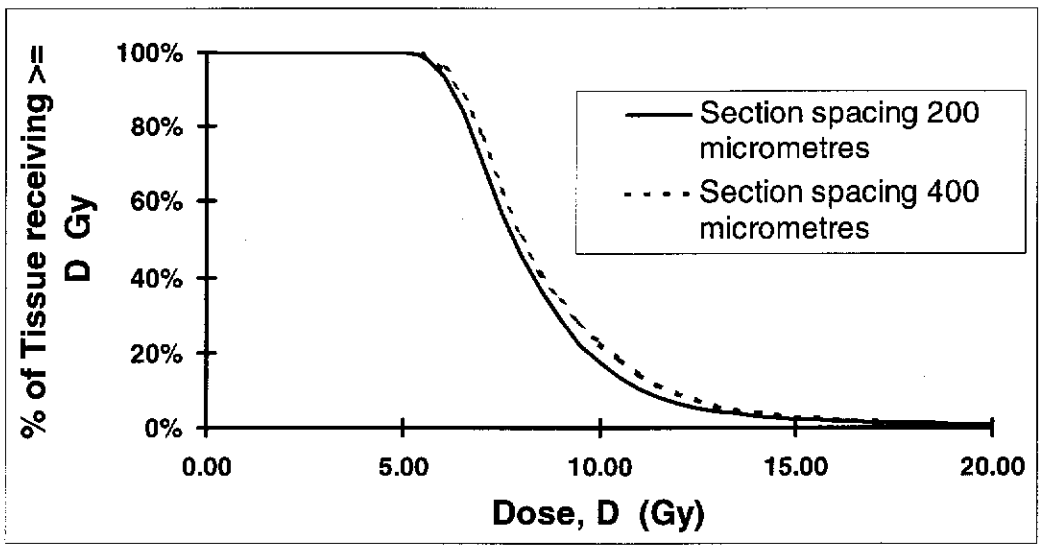

Figure 48. Cumulative dose volume histograms calculated for normal liver tissue using tissue sections at 200 μm and 400 μm spacing.

5.4.2 Tumour Centre Tissue

Results were similar in character to those for normal liver, although the slightly lower concentration of microspheres in this tissue results in lower average radiation doses. The cumulative dose volume histogram of Figure 49 again

indicates that a relatively broad range of doses is delivered. The minimum and average doses were 3.7 Gy and 6.8 Gy respectively. The dose delivered for a uniform distribution of activity would be 6.9 Gy and from the data presented in Figure 49 it was calculated that 68.2% of the tissue volume receives less than this dose.

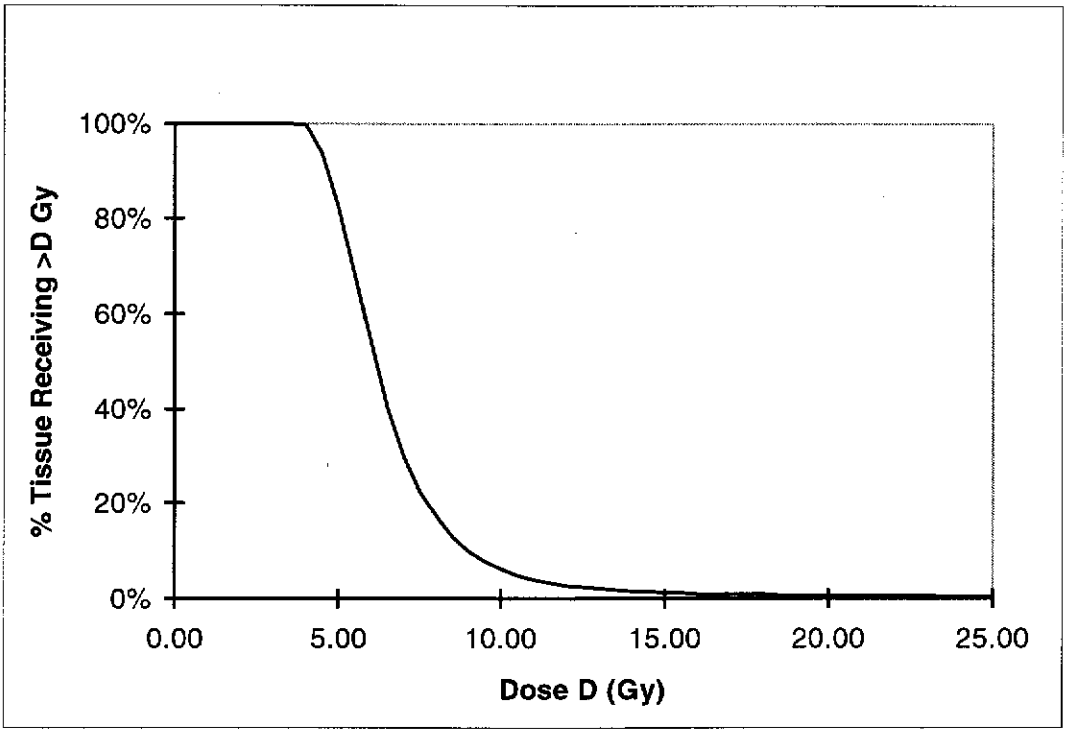

Figure 49. Cumulative dose volume histogram for tumour centre tissue block.

5.4.3 Tumour-Normal Tissue Boundary

Figure 50 shows an isodose plot for the section at the centre of the sample volume. The tumour boundary is drawn in as a dotted line which can be seen towards the left hand side of the plot. Normal liver tissue is to the left side of the boundary and tumour to the right. The isodose contours show their dose values in Gray and for clarity the 500 Gy isodose line is the highest shown. For the region enclosed by the inset box, isodose contours have been plotted up to 900 Gy and these are shown in Figure 51. This area contained a large aggregation of microspheres, which was the cause of the larger dose. The dotted line to the right of the tumour boundary in Figure 50 represents the edge of the vascular periphery of the tumour, as judged by the microsphere positions (see section 4.2 and

Campbell et. al., 2000) and is approximately 6 mm inside the tumour boundary. The region between this line and the tumour boundary contains over 90% of the spheres deposited in this section. Doses to the entire volume between this line and the tumour boundary are in excess of 120 Gy.

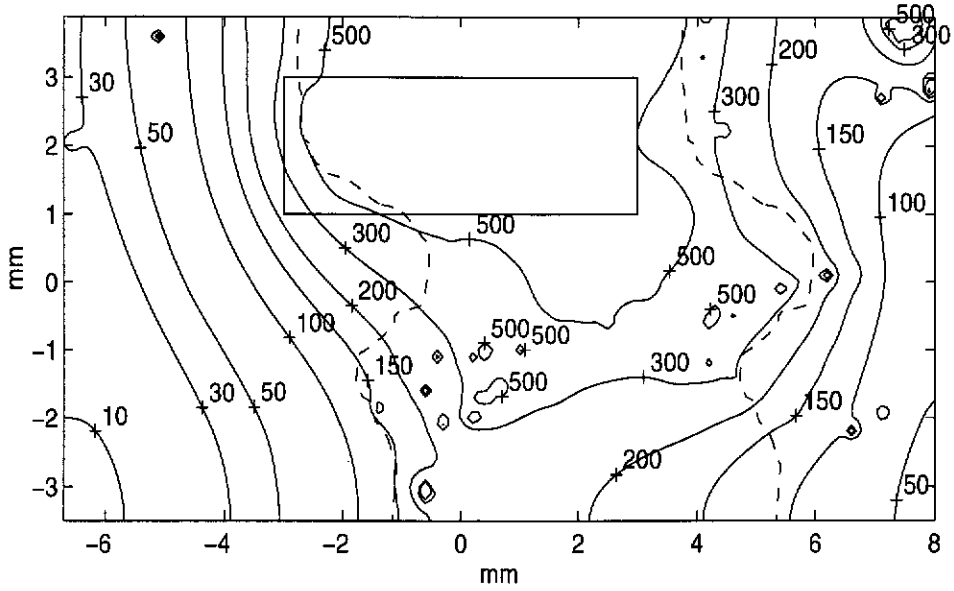

Figure 50. Selected isodose contours for central tissue section in the tumour-normal tissue boundary sample block. The dashed line on the left hand side is the tumour boundary and the line on the right is the edge of the tumour vascular periphery. More detailed isodose contours within the boxed area are shown in Figure 51.

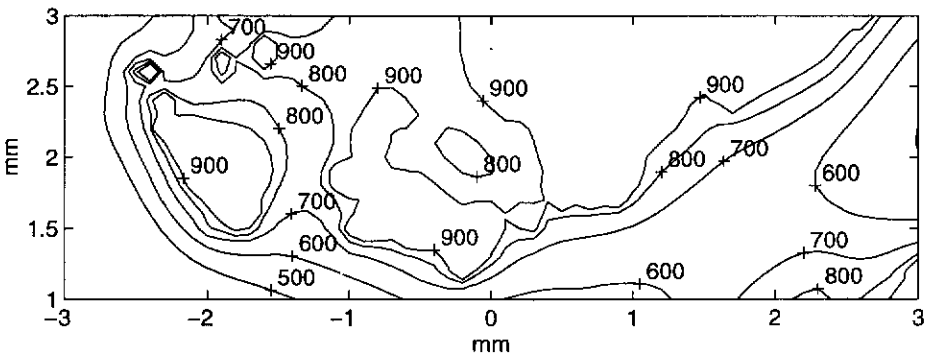

Figure 51. More detailed isodose plot of the boxed area in Figure 50.

Evaluation of the variation in radiation dose near the tumour boundary is made difficult by the fact that this boundary is not a straight line. In order to facilitate analysis of the dose distributions near the tumour normal tissue boundary, the boundary was 'straightened' by shifting the rows in each calculation matrix so that the tumour boundary was placed on the y-axis. The average and minimum radiation doses across the tumour-normal tissue boundary calculated for all sections are shown in Figure 52. Doses to normal tissues near the tumour edge fall quite quickly with distance away from the tumour. The average dose has fallen below 10 Gy at distances greater than 7.5 mm from the boundary.

In normal liver tissue the dose reduces quite rapidly with distance from the tumour boundary. It falls below the accepted safe whole liver exposure level a few millimetres from the boundary of the tumour. Moving toward the centre of the tumour away from the vascular periphery region, doses fall in a similar manner, although not as rapidly as they do in normal tissue. This is to be expected since the microsphere density in this volume of the tumour close to the vascular periphery is greater than in normal liver tissue. The increase in average

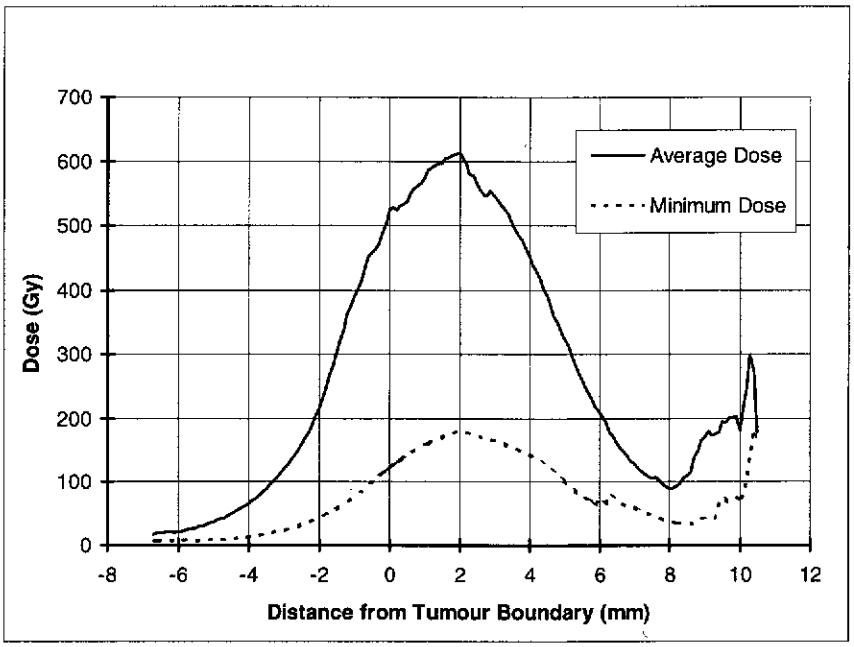

Figure 52. Average and Minimum doses across the tumour-normal tissue boundary. The tumour boundary is at 0 mm. Positive distances are inside the tumour.

dose apparent in Figure 52 at around 10 mm inside the tumour boundary is due to a cluster of microspheres. This illustrates the fact that while the general tendency is for microsphere concentration to fall with distance from the tumour boundary, there can be cases of localised microsphere concentration.

5.4.4 Serosal Surface

Dose distribution patterns showed inhomogeneties similar to those seen for the tumour-normal tissue boundary sections. Figure 53 shows an isodose plot for the section at the centre of the sample volume. The edge of the tumour is represented by the dotted line to the left side of the figure. Tumour tissue lies to the right of this line and isodose lines up to 500 Gy are labelled. The second dotted line to the right of the tumour edge represents the extent of the vascular periphery in this region of the tumour. Doses are slightly lower than those calculated for the tumour-normal tissue boundary, probably due to the slightly lower microsphere concentration in the serosal surface tumour periphery, but were still in excess of 150 Gy throughout the periphery of the tumour. Outside the tumour, doses are seen to fall rapidly. Figure 54 shows the variation of average and minimum tissue doses with the boundary region 'straightened' to lie on the x-axis using the same method as discussed for the tumour-normal tissue

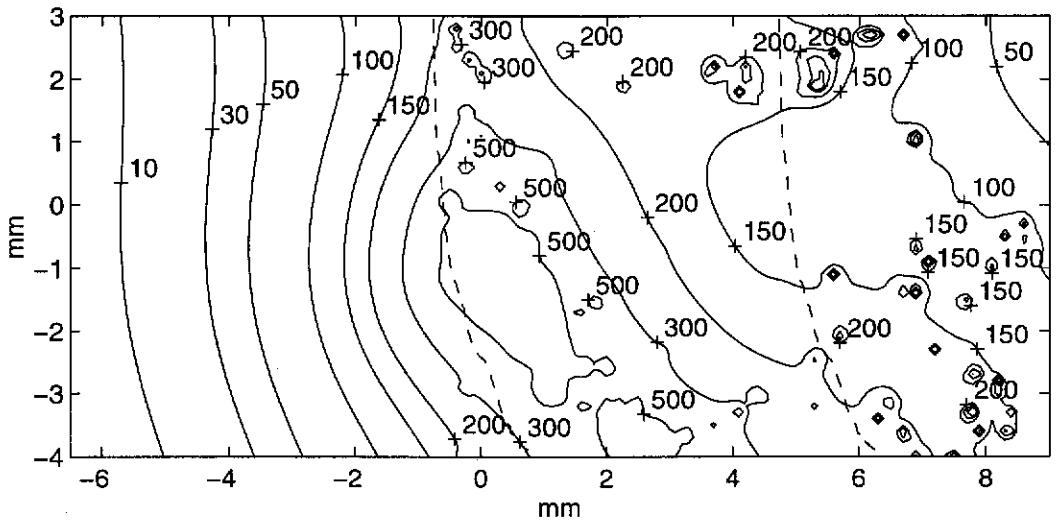

Figure 53. Selected isodose contours for the central tissue section in the serosal surface sample block. The dashed line on the left side is the tumour boundary and the line to its right is the edge of the tumour vascular periphery.

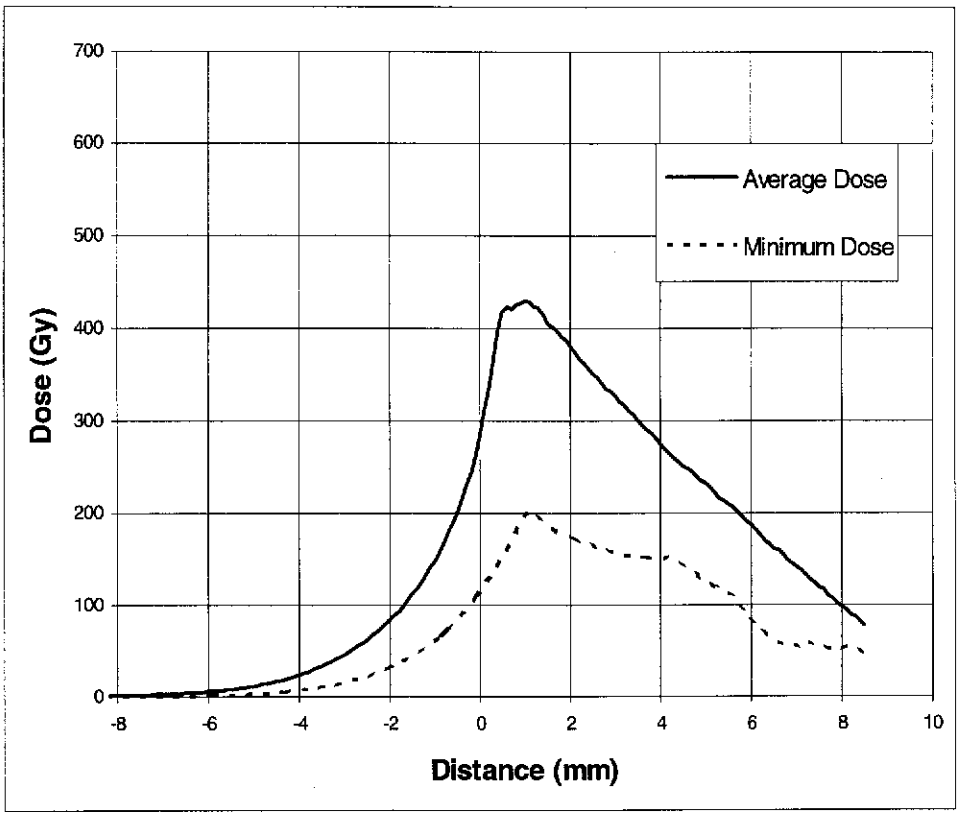

Figure 54. Average and Minimum doses across the 'straightened' serosal tumour boundary. The tumour boundary is at 0 mm. Positive distances are inside the tumour.

boundary sections. The average dose delivered outside the tumour has fallen below 5 Gy at distances greater than 6 mm from the boundary.

5.5 Discussion

The dose distributions calculated from the observed microsphere distributions have large variations within both normal hepatic parenchyma and the tumour. This is clearly evident in Figure 50 and Figure 53. Doses are greatest in the tumour periphery. The high concentrations of microspheres in the tumour close to the boundary led to high doses being delivered to the normal tissue immediately adjacent to the tumour boundary. The limited penetration of the beta radiation from ^{90}Y meant that the doses fell rapidly in the first few millimetres of normal tissue. At a distance equal to the range of the beta particles, which is 10 mm, the dose had fallen to the 8.9 Gy observed in the bulk

of the normal tissue. This normal tissue dose is in sharp contrast to the estimate of approximately 80 Gy that would be made using MIRD techniques and assuming all the activity infused spreads uniformly throughout the liver. Fox et al. (1991) also looked at the distribution of microspheres in normal liver and estimated that one third of normal liver will receive less than 33.7% of the dose predicted by assuming uniformly distributed activity. Using this estimate the expectation would be that one third of normal tissue would receive a dose less than 27 Gy in this case. It can be seen from Figure 47 that virtually the entire volume of normal liver tissue would receive a dose less than this value.

It was also clear that the dose in the tumour was a maximum in the highly vascularised tumour periphery, after which it decreased rapidly towards the centre of the tumour. Because the microsphere concentration in the centre of the tumour was slightly less than in normal tissue, the radiation dose in this region is slightly less than in normal tissue.

A closer examination of Figure 52 and Figure 54 reveals that average doses of 200 Gy or greater are delivered to tissue from 2 mm outside the tumour boundary to 6 mm inside the boundary. This shows clearly that the majority of the dose is delivered in the vicinity of the boundary, and that the tumour receives a substantial proportion of this dose. Since the diameter of this tumour was approximately 80 mm, it is apparent that 39% of the total tumour volume would receive an average dose in excess of 200 Gy. It must be noted however that the above discussion refers only to the average dose delivered to the tissues. Microspheres were not uniformly distributed, but tended to occur in clusters (see Chapter 4, also Campbell et al., 2000 and Pillai et al., 1991). Doses within clusters were greater than average, and away from the clusters, there was less dose. Aggregations of clusters also appear to occur in the tumour periphery leading to regions where the absorbed doses were far above the average (Figure 51 provides an example). Since the vascular beds of different parts of the tissue will be functionally perfused on a microscopic level at different times, these aggregations are likely to occur at random throughout the periphery. Examination of Figure 52 shows that within the 6 mm of tumour boundary,

which receives an average dose exceeding 200 Gy, the minimum doses range from 70 to 190 Gy. This dose distribution suggests that the tumour periphery will receive a therapeutic dose, but that further into the centre, doses will be sub-lethal.

Histological examination of the tissue sections that contained the tumour boundary revealed that tumour tissues within 6-7 mm of the tumour boundary were entirely necrotic. Tissue within the tumour periphery was almost enitrely fibrotic and there was some calcification present. Deeper into the tumour the histological appearance was similar to near the periphery, but there were a few areas where some active tumour cells were present. The tissue section from the centre of the sample block that contained the tumour-normal tissue boundary had a small region that contained some viable colorectal columnar cells. Isodose contours for this section are shown in Figure 50 and the viable tumour cells were observed in the area corresponding to the bottom right of the figure, where calculated radiation doses were 50 Gy or less. Tissue sections either side of this section had similar radiation dose distributions and also had viable tumour cells in a similar position to those observed on the central tissue section.

The patient also received chemotherapy in addition to treatment with ^{90}Y labelled microspheres and, while it is not possible to distinguish between cell necrosis and fibrosis caused by radiation from that caused by chemotherapy, the combination of the two treatments was apparently effective in killing active tumour cells in the vascular periphery of the tumour. The presence of active tumour cells deeper into the tumour may indicate that lower radiation doses have caused the combination of irradiation and chemotherapy to be less effective in killing cells in this region. This may well mean that multiple treatments will be required to successfully treat large tumours.

These conclusions are in agreement with the observations of Lau et al. (1998), who used this treatment method in patients with non-resectable hepatocellular carcinoma (HCC). Following treatment, Lau reported that tumours in four patients had become resectable. These were subjected to histological examination upon removal. All patients had large tumours similar to the one in

this study. Lau et al. (1998) reported that this examination revealed necrosis and fibrosis in the tumour peripheries, in a volume which also contained large concentrations of microspheres. In one case, viable HCC cells were found in the necrotic centre of the tumour, where only a small number of microspheres were observed.

It is not uncommon for patients to experience nausea and other complications following hepatic ^{90}Y microsphere therapy. For instance, Andrews et al. (1994) reported reversible gastritis or duodenitis in 4 out of 24 patients. Dancey et al. (2000) noted upper gastrointestinal tract ulceration in 15% of patients treated with ^{90}Y microspheres for hepatocellular carcinoma. Lau et al. (1998) reported 12 out of 59 patients had abdominal distension, discomfort, nausea and vomiting. The causes of these types of complication are not known. Figure 54 indicates that outside the tumour, average radiation doses between 50 Gy and 300 Gy occurred within 3 mm of the serosal tumour surface. This implies that tissues in contact with the serosal tumour surface would have received radiation doses of this order. The position of the liver within the abdomen means that, depending on the tumour position, parts of the diaphragm, stomach or intestinal wall could receive significant radiation doses. Such exposure could explain some of the post-procedure complications that occur following ^{90}Y microsphere infusions.

It is normally regarded that a dose of 30-35 Gy delivered to the whole liver is required to cause radiation hepatitis (Lawrence et al. 1995). The average dose to normal tissue was 8.9 Gy, well below this figure. Less than 1% of the normal tissue volume received a dose in excess of 30 Gy, and all of this volume was in the immediate vicinity of the tumour. Histological examination of tissue sections taken from normal liver tissue revealed the presence of some portal tract fibrosis, with evidence of stress on some of the viable cells. The fibrosis in normal liver parenchyma may be due to the chemotherapeutic treatment received by this patient, or be caused by external factors. As calculations indicate that normal liver received relatively low radiation doses, the fibrosis is less likely to be due to irradiation.

The concentration of microspheres in normal liver was less than that reported by Fox et al. (1991), who calculated an average microsphere concentration in normal liver tissue of 40 mm^{-3}, compared to the 3.5 mm^{-3} recorded in this study. However, the liver studied by Fox had a significantly smaller tumour burden than the liver used in this study. As discussed in section 4.6, this will most likely influence the concentration of microspheres in normal liver. Although this may be true on the macroscopic scale, it must be noted that the non-uniform deposition of microspheres into apparently uniform tissue will cause heterogeneous dose distributions on the microscopic scale.

It is interesting to compare dose volume histograms calculated here to those determined by Fox et al. (1991) in normal human liver and Roberson et al. (1992) in normal rabbit liver. As absolute dose is dependent on the activity per microsphere, to facilitate this comparison dose volume histograms are presented in normalised dose units. Normalisation was carried out by dividing absolute dose by Du, the dose that would have been obtained if activity were distributed uniformly throughout the liver with the same specific activity as observed in the tissue sample analysed in each study. The histograms are presented in Figure 55. All histograms show significant dose heterogeneity, however the dose volume histogram shape from Fox et al. (1991) indicates far more heterogeneous doses than the other curves, and the results from Roberson et al. (1992) show more heterogeneity than those from this study.

Roberson et al. (1992) determined microsphere positions in contiguous tissue sections 200 μm thick, while Fox et al. (1991) examined microsphere positions on 10 μm thick sections taken at 500 μm separations. This study followed a similar procedure to Fox, using 10 μm thick sections at 200 μm spacing. The influence on calculated dose homogeneity caused by the differing methods of determining microsphere distributions between the studies should be considered. The calculations presented in section 5.3 and section 5.4.1 indicated that for the normal liver tissue sample analysed in this study, allowing for microspheres in the intervening tissue volume between sections by using a scaling factor was unlikely to substantially affect dose heterogeneity. Fox et al. (1991) presented

similar calculations in their work. The technique employed by Roberson observed all microspheres, but as microsphere positions within a section were determined using transmission light microscopy, essentially a two dimensional distribution of microsphere positions was obtained, as there was no way to determine a microsphere's position in the direction of the thickness of a section. This would be expected to lead to an increase in dose inhomogeneity, but this is likely to be a small effect for reasons similar to those presented in section 5.3 in this thesis.

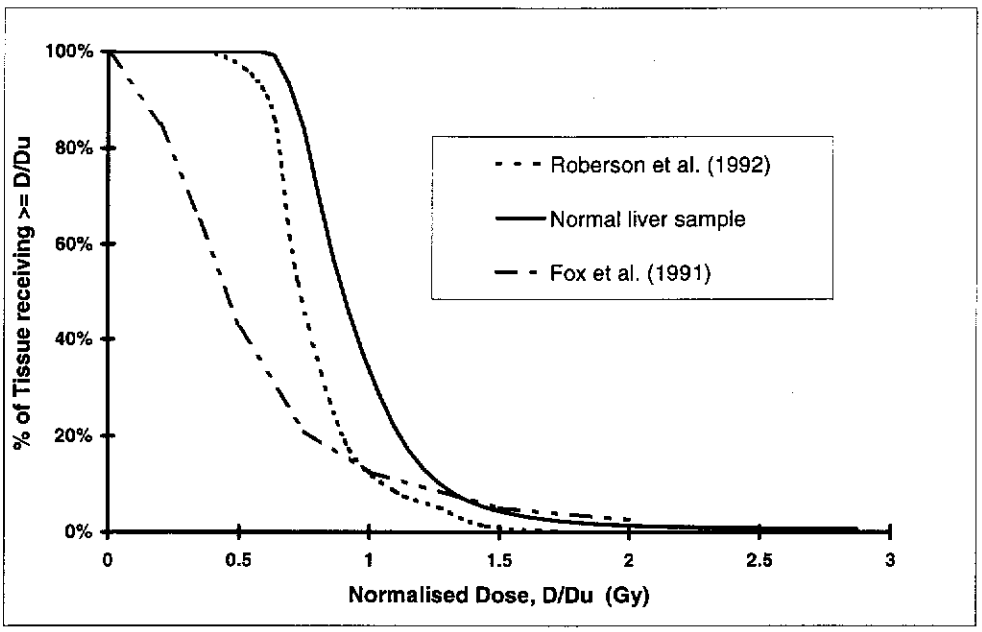

Figure 55. Cumulative dose volume histograms for the normal liver tissue sample compared with those published by Roberson et al. (1992) and Fox et al. (1991). Dose has been normalised by dividing by Du, the dose that would have been obtained if activity were distributed uniformly throughout the liver at the same specific activity as observed in the tissue sample for each study.

A micrograph of a normal liver tissue section presented in Roberson et al. (1992) suggested microsphere deposition patterns in their rabbit liver were similar to those observed in the normal liver sample analysed in this study. In both cases

microspheres were unlikely to deposit within a 500 μm proximity of another microsphere. Roberson et al. (1992) reported a microsphere concentration of 1.5 microspheres per mm^3, compared to 3.5 microspheres per mm^3 observed in this study. The differences between the dose volume histograms of Roberson and calculated for the normal liver sample analysis in this work are most likely due to this difference in microsphere concentration. In contrast, Fox et al. (1991) reported a microsphere concentration of 40 microspheres per mm^3 in normal liver. Additionally, microsphere position plots presented in Fox et al. (1991) suggest microspheres were depositing in short lines on the order of 1 mm in length, thus giving rise to a far more spatially non-uniform distribution of microspheres than observed in the other two studies. It appears clear that the greater dose heterogeneity calculated by Fox et al. (1991), compared with the other works, is due to the degree of spatial non-uniformity and the significantly greater microsphere concentration with which microspheres deposited in the tissue sample they analysed. As discussed in section 4.6, the influence of tumour burden on the deposition rate of microspheres in normal liver tissues maybe the underlying cause of the differences in radiation dose distributions seen amongst these studies, and warrants further investigation in future work.

The goal of hepatic microsphere therapy is to deposit the highest possible proportion of microspheres into tumour tissue in order to deliver a therapeutic dose of radiation to the tumour whilst sparing normal liver. The use of Nuclear Medicine techniques may allow an estimate of tumour uptake rate; and tumour volume could be estimated from CT scans in patients presenting with large isolated tumours (Ho et al., 1996). However such methods are unlikely to succeed in patients who have diffuse metastatic liver disease. As such, for many patients, it will most likely be difficult to calculate the optimum number of microspheres to infuse. The limiting factor will be the number of microspheres that deposit in normal tissue, but this is likely to depend on the size and number of tumours within the liver. Radiation doses to normal tissue calculated in this study were significantly lower than those that would have been expected if microspheres deposited in the same manner as observed by Fox et al.(1991).

This is possibly due to the larger tumour present in the patient accumulating a larger fraction of the total number of microspheres infused.

These observations could lead to the expectation that infusing a greater number of microspheres into patients with larger tumours could be more effective in treating the tumours without having any significant effect on the dose delivered to normal tissue. However, this may have limited benefit in terms of tumour control as it has been observed that infusion of a greater number of microspheres results not in a more uniform distribution, but in more microspheres aggregating in similar locations (Pillai et al. 1991). More importantly, since few microspheres deposit in the tumour centre, delivery of a sub-lethal dose to normal hepatic parenchyma will most likely result in sublethal doses towards the tumour centre for tumours whose dimensions are much larger than twice the range of the β particles emitted by ^{90}Y.

5.6 Comparison of dose distributions in normal liver tissue with a random distribution of microspheres

Visual examination of microsphere distributions in the normal liver tissue sample did not provide evidence of the clustering of microspheres observed in the tumour periphery. The results presented in section 4.5 however suggested that microsphere deposition in normal liver may not be random. This was investigated further by comparison of the radiation doses arising from a random distribution of microspheres with that observed in the normal liver sample.

Microsphere positions were generated randomly in space with the same concentration as observed in the normal liver tissue sample. Radiation doses were calculated over the same volume as used in the dose calculation presented in section 5.4.1 for the normal liver tissue sample. For the simulation, microsphere positions were generated through a volume large enough to allow for a 10 mm margin around the volume over which radiation doses were calculated. This allowed for dose contributions from microspheres lying outside the calculation volume to be included in the calculations.

Figure 56 presents the dose volume histogram for the simulation, along with that calculated using the microsphere positions observed in the normal liver tissue sample. The histogram that would arise if activity were homogeneously distributed throughout tissue, instead of being attached to microspheres is also shown in the figure. The closer a dose volume histogram is to this curve the more uniform the radiation dose.

While the simulation contains dose heterogeneity, it is clearly more uniform that that arising from the observed microsphere positions. This supports the results of section 4.5. The observed dose volume histogram for normal tissues could be explained if microspheres had a tendency to deposit near one another in normal tissue, rather than being found at random locations. Perhaps microspheres also cluster in normal liver, as well as in the tumour periphery. The low numbers of microspheres depositing in normal tissue make statistical analysis of the type presented in section 4.4.2 to characterise this behaviour impractical.

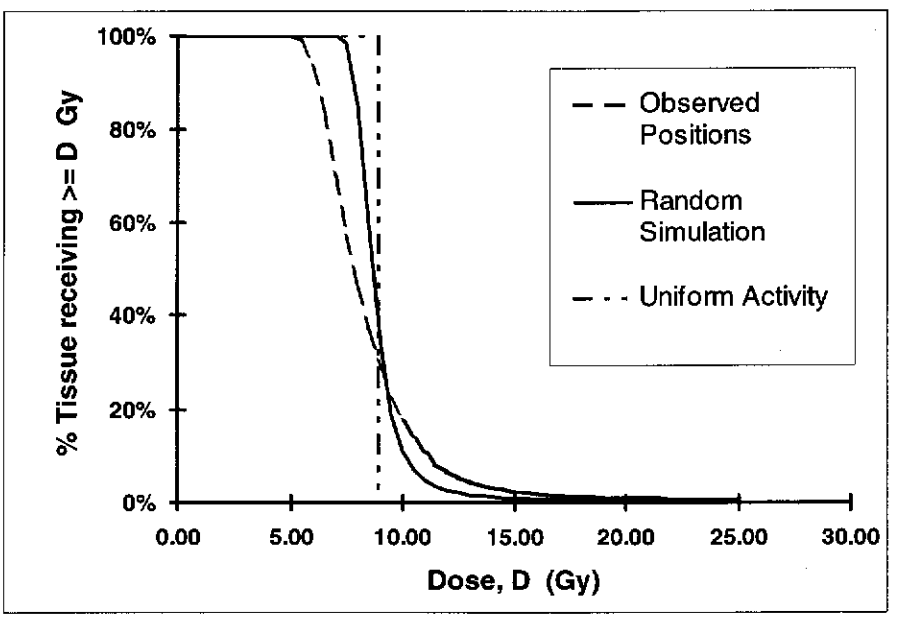

Figure 56. Dose volume histogram for randomly placed microspheres compared to the dose volume histogram calculated using observed microsphere positions in normal liver, and that arising from a uniform distribution of activity.

6. Modelling of Microsphere Deposition Patterns in the Tumour Periphery

The dosimetry calculations presented in Chapter 5 clearly demonstrated that considerable dose heterogeneity occurs in both normal and tumour tissues following hepatic ^{90}Y microsphere therapy. The application of standard MIRD approaches to the problem of dosimetry, with its implicit assumption of uniform activity distribution in tissues, will obviously be inaccurate in these circumstances. Radiation doses can be calculated using observed microsphere distribution patterns, such as reported in this work, and by Fox et al. (1991) and Roberson et al. (1992). However this approach relies on knowledge of the actual distribution of microspheres, which can only be determined retrospectively from the analysis of tissue samples. Calculations using observed microsphere positions also involve a large amount of computational time. For example, the calculations performed for each of the tissue samples taken from the tumour periphery reported in this work took in excess of 12 hours to complete running on a reasonably powerful personal computer (Intel Pentium III 350 MHz processor, 64MB RAM). It would be advantageous to have a model that could predict dose distributions a priori. Such a model would produce radiation dose patterns similar to those observed using measured microsphere distributions, preferably in a more acceptable computation time. This could be used to make dosimetry predictions for the treatment method employed.

This chapter presents an attempt at modelling microsphere distributions in the tumour periphery to try and generate realistic radiation dose distribution patterns. The model developed utilised the observation that microspheres aggregated into clusters in the tumour periphery (as discussed in section 4.4). Distributions of microsphere clusters were generated, rather than individual microsphere positions. The radiation dose contributions from all microspheres in a cluster were not considered individually. They were modelled as a single source of radiation positioned at the cluster's centroid and assigned an activity equal to the total activity of all microspheres in the cluster. This achieved a substantial reduction in the time taken for dosimetry calculations. The efficacy of the model

was evaluated against the criteria that the radiation dose distributions generated using the model should be similar to those produced using the observed microsphere positions.

6.1 Representing a microsphere cluster as a single radiation source

The microsphere distribution analysis presented in 4.4 demonstrated that within the tumour periphery, microspheres aggregated into clusters of varying sizes. Pillai et al. (1991) observed similar clustering in rabbit livers and suggested that, for radiation dosimetry purposes, it might be possible to replace a microsphere cluster by a single radiation source located at the cluster's centroid position. The activity of this source would be equal to the total activity of all microspheres in the cluster. Zavgorodni (1996) pursued this idea in modelling the microsphere distributions observed by Pillai et al. (1991) and obtained good matches with the radiation dose distributions published by Roberson et al. (1992) that were based on the microsphere distributions seen by Pillai. The same approach appeared promising for the simulation of microsphere distributions in the periphery of tumours in human liver. In order to gain some insight into how dosimetry patterns would be affected by replacing a cluster of microspheres by a single scaled radiation source, some initial modelling was performed. The dosimetry patterns of simulated clusters of microspheres were compared with the single equivalent source representation.

6.1.1 Initial Modelling

Clusters were simulated by placing microspheres randomly in space at distances up to a specified 'cluster radius' from a cluster centre. The extent of a simulated cluster will thus be roughly twice the cluster radius. Clusters having a range of extents were simulated. The cluster populations were chosen such that the relationship between cluster extent and cluster population was similar to the relationship observed for microsphere clusters in the tumour periphery (as shown in Figure 61). For each simulation the radiation dose along a diameter through

the cluster centre was found and compared with the dose profile for an equivalent single source placed at the cluster's centre. Microspheres were taken as having unit activity, and the activity of the single equivalent source was equal to the number of microspheres in the cluster. Figure 57 shows some typical results and demonstrated that close to the cluster centre doses from the equivalent source representation were higher than those calculated using actual microsphere positions. Deviations became larger as the cluster extent increased. For distances about 20% greater than the cluster radius (one half the cluster extent) agreement was within 15-20% in all cases.

6.2 Radiation dose patterns using single equivalent radiation source in the tumour periphery

The ability of single equivalent radiation sources to produce radiation dose patterns similar to those calculated using observed microsphere positions was investigated in the two tissue samples containing the tumour periphery. The radiation dose distributions arising when microsphere clusters were replaced by single equivalent radiation sources were calculated and compared with those determined using observed microsphere locations.

Doing such a comparison, perforce required identification of microsphere clusters in three dimensions. The microsphere clusters identified using cluster analysis (discussed in section 4.4.2) are two dimensional cross sections through a distribution of three dimensional clusters. Extension to three dimensional clusters may be possible but would require identification of clusters for each tissue section followed by identification of clusters that extend across multiple sections. Cluster analysis could be applied to all sections, but while cluster analysis objectively chooses clusters, selection of the number of clusters present in a data set is a subjective process (see section 4.4.2). Moreover, in some

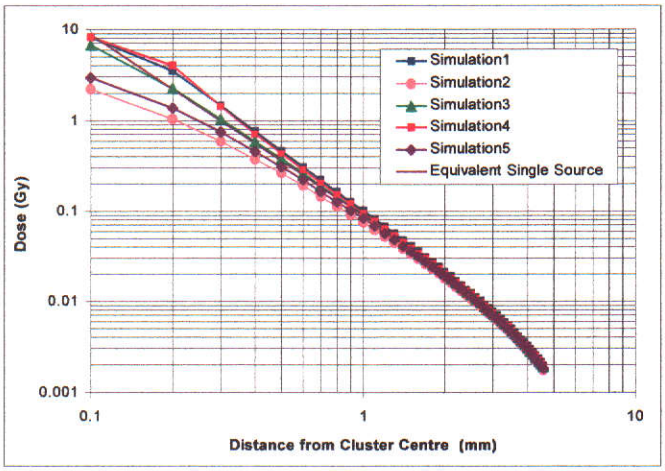

(a)

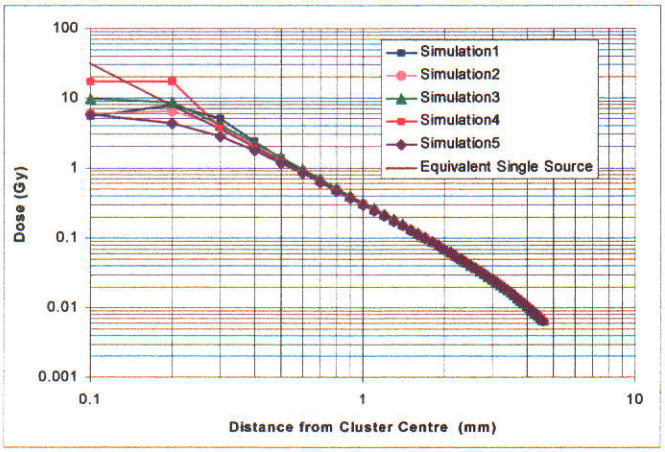

(b)

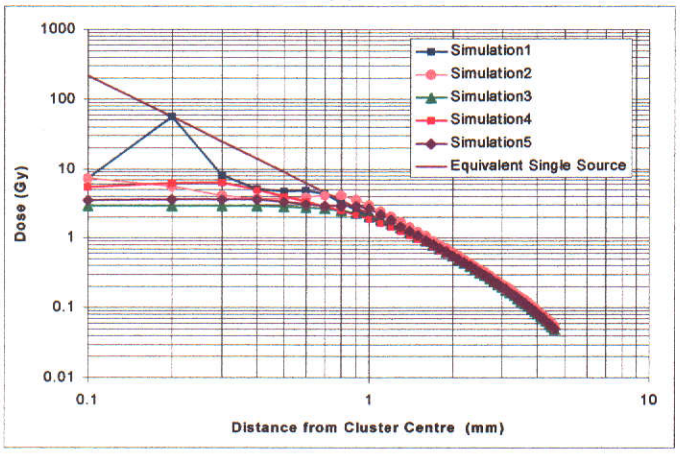

(c)

Figure 57. Comparison of simulated cluster dose profiles with a single equivalent activity source positioned at the cluster centre. (a) 2 microspheres, 250 μm cluster extent, (b) 7 microspheres, 500 μm cluster extent, (c) 50 microspheres,2000 μm cluster extent.

instances for the five sections analysed using this method, different clustering methods suggested slightly different numbers of clusters for the same section.

Selection of clusters using a cluster parameter, as used by Pillai et al. (1991), is a completely objective method and may be therefore a more suitable method for application to a large number of tissue sections. However, as pointed out in section 4.4.1, the choice of an appropriate value for the cluster parameter was not apparent from examination of the observed microsphere positions. By examination of the clusters chosen using cluster analysis it may be possible to infer a value for the cluster parameter such that the clusters chosen using the cluster parameter method closely match those determined by cluster analysis. The reasoning is a follows :

> Let the value of the cluster parameter be D. For all microspheres within the same cluster, the distance from any microsphere to its nearest neighbour must be less than D (from the definition of cluster selection using this technique). Examination of the nearest neighbour distances for microspheres within the same cluster should then provide an indication of a lower limit for D. The largest nearest neighbour distance seen over all identified clusters would be the smallest value of D consistent with the clusters selected.
>
> An upper limit for D can be established from the minimum distance between clusters. If D were greater than the smallest minimum distance observed then clusters with a separation smaller than D would merged into a single cluster.

A problem with the foregoing occurs if some microspheres were classified incorrectly by the cluster analysis process. Selection of the optimum number of clusters for each section analysed was subjective, and in some instances the total number of clusters on a section was equivocal by one or two clusters amongst the different clustering methods. This raises the possibility that some microspheres were incorrectly assigned to the 'wrong' clusters. This will have the effect of inflating the value of D indicated by nearest neighbour distances and decreasing the value suggested by consideration of the minimum distances between clusters.

The former effect can be reduced by considering all nearest neighbour distances for a cluster and choosing a distance below which most nearest neighbour distances are found. A few misclassified microspheres will then be less likely to bias the results. As a consequence of the latter effect, it should be regarded as acceptable for a small percentage of clusters identified by cluster analysis to lie closer together than the value of D.

6.2.1 Selection of a Cluster Parameter Value

The distribution of nearest neighbour distances was determined for all microspheres in the two dimensional clusters identified on the five tissue sections from the tissue sample containing the tumour-normal tissue interface that were subjected to cluster analysis, as discussed in Chapter 4. 277 clusters were analysed and the distribution of nearest neighbour distances is shown in Figure 58. Over 90% of the microspheres are within 85 μm of another microsphere, and over 95% of microsphere are within 165 μm of another microsphere. There are a small number where nearest neighbour distances exceed 300 μm, this is most likely due to a combination of the misclassification of microspheres and the presence of a number of isolated microspheres. Examination of this figure would suggest a value of D greater than 165 μm to be reasonable. Around 5% of clusters had a minimum separation distance below this distance. Performing clustering using a cluster parameter of 165 μm yielded too many small clusters compared with the clusters selected using cluster analysis, suggesting this value of D was too small. Use of a cluster parameter of 185 μm produced clusters that were a good match with those identified using cluster analysis. Figure 59 shows an example comparison of the clusters produced using both methods. In this case three microspheres were classified differently by the two methods, and these are indicated on the Figure. The differences would appear to be due to cluster analysis inappropriately including the three microspheres into larger clusters when they should have been classified as isolated microspheres. This value of D is also acceptable with respect to nearest neighbour distances; less than 9% of clusters had separations closer than this distance. A value for the cluster parameter of 185 μm thus appeared

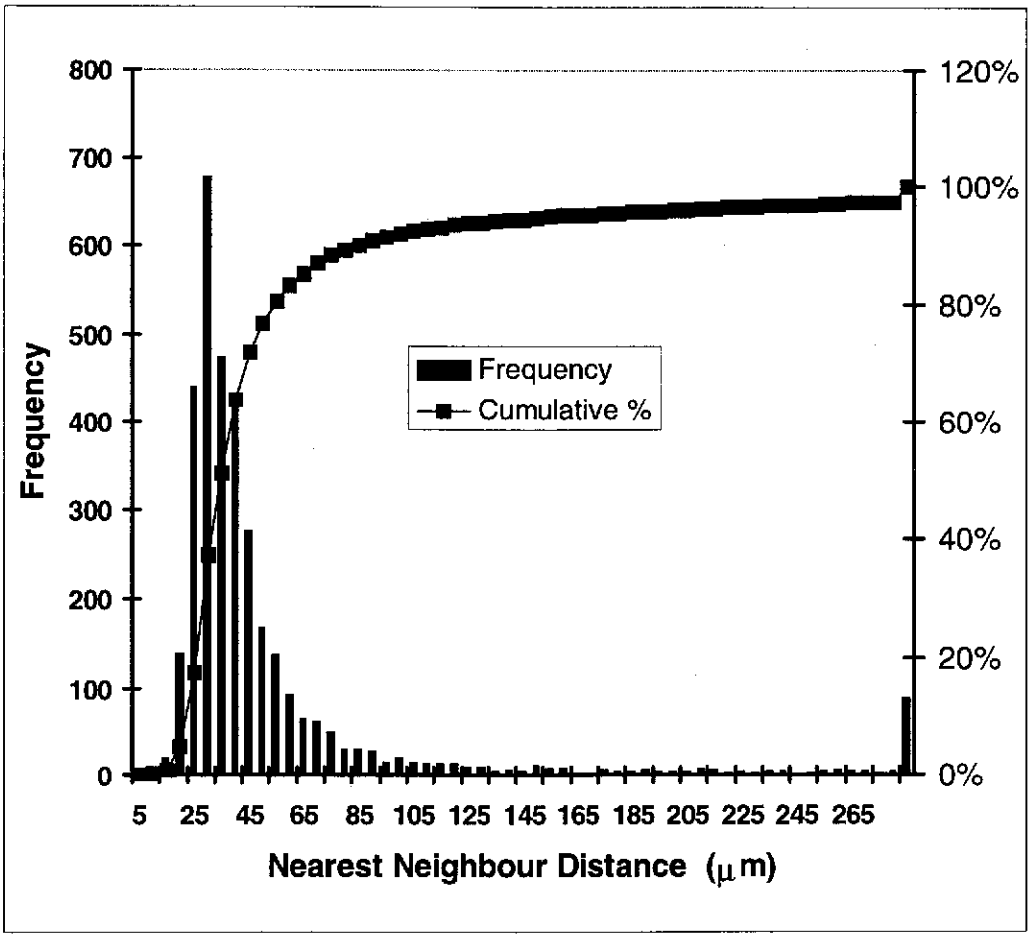

Figure 58. Distribution of nearest neighbour distances for microspheres in the same cluster.

appropriate for clustering of microspheres in the tumour periphery for human liver.

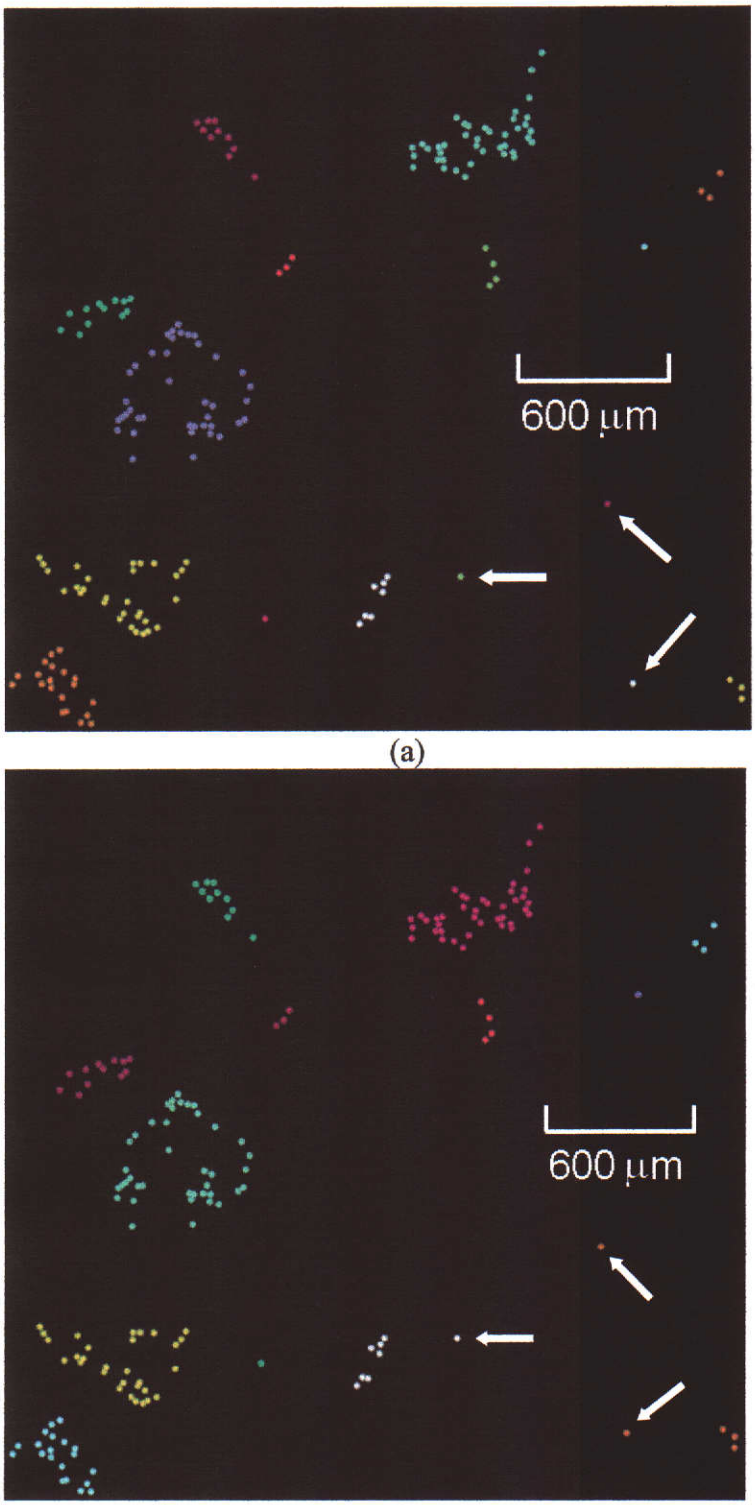

Figure 59. Comparison of microsphere clusters chosen using (a) a cluster parameter of 185 µm and (b) cluster analysis. Microspheres in different clusters are shown as different colours (colours have been reused for some non-adjacent clusters). Microspheres that have been classified differently by the two methods are marked with an arrow (←).

6.2.2 Identification of Clusters in Three Dimensions in the Tumour Periphery

Two dimensional clusters were identified for all sections in the tissue sample volumes that included the tumour's periphery (both the serosal surface volume and the volume containing the tumour-normal tissue interface). Clusters were chosen via a cluster parameter distance of 185 μm. Microsphere clusters are however undoubtedly three dimensional aggregations. Consequently it is to be expected that larger clusters will extend across more than one tissue section in some instances. In this case a large cluster would appear as a number of two dimensional clusters, each one a cross-section through the same three dimensional cluster and lying in a different tissue section. Such two dimensional clusters were amalgamated by assuming that the centroid of each cross-section should lie in a similar location on each tissue section. Two dimensional clusters lying on successive tissue sections were combined if their centroids were within one half of the largest cluster extent for either cluster. The resulting three dimensional clusters were viewed using data visualisation software capable of rendering three dimensional data and allowing interactive rotations, translations and magnifications. The clusters chosen appeared to be consistent with the natural groupings of the microspheres.

As with two dimensional cluster analysis, cluster populations were skewed towards low numbers. Again, as noted with the two dimensional case, the skewed nature of these distributions means that normal distribution theory parameters are not appropriate descriptors. The distributions can be described by use of percentiles and results are presented in Table 7 for the serosal surface sample volume and in Table 8 for the volume containing an interface between tumour and normal tissue. The cluster extent is the largest centre to centre distance between two microspheres in the same cluster. The minimum cluster extent was zero since clusters consisting of a single microsphere were taken to have a cluster extent of zero. The fact that the 25^{th} percentile cluster extent is also zero reflects the fact that many clusters consisted of a single microsphere (45% and 42% of clusters were single spheres for the serosal surface and tumour-

normal tissue interface samples respectively). The results are similar in character to those for two dimensional clusters.

Table 7. Three dimensional cluster analysis results for the serosal surface tissue sample. 2649 clusters were identified containing a total of 12 564 microspheres

	Cluster Population	Cluster Extent (μm)	Minimum Distance from another cluster (μm)
Mean	4.7	108	267
Median	2	34	233
Minimum	1	0	185
25^{th} percentile	1	0	207
75^{th} percentile	4	145	291
Maximum	405	2494	1244

Table 8. Three dimensional cluster analysis results for the tumour-normal tissue interface tissue sample. 1204 clusters were identified containing a total of 10 953 microspheres

	Cluster Population	Cluster Extent (μm)	Minimum Distance from another Cluster (μm)
mean	9.1	147	294
median	2	47	231
minimum	1	0	185
25% percentile	1	0	205
75% percentile	5	175	300
maximum	585	2514	2034

For purposes of representing a microsphere cluster by a single equivalent radiation source, the radiation field from a cluster consisting of a single microsphere will remain unaltered. It may therefore be more informative to examine cluster extents for clusters consisting of two or more microspheres. Table 9 contains information on the distribution of cluster extents for both sample volumes for clusters with populations greater than one. Figure 60 shows histograms indicating the distribution of cluster extents observed for these clusters. Both sample volumes showed similar distributions, although the tumour-normal tissue interface volume had a greater proportion of clusters with extents exceeding 1000 μm.

Table 9. Three dimensional cluster extents for clusters with populations of more than a single microsphere.

	Cluster Extent (μm)	
	Serosal Surface Sample Volume (1634 clusters)	Tumour-Normal Tissue Interface Sample Volume (649 clusters)
mean	195	255
median	133	148
minimum	32	32
25% percentile	60	71
75% percentile	243	296
maximum	2494	2514

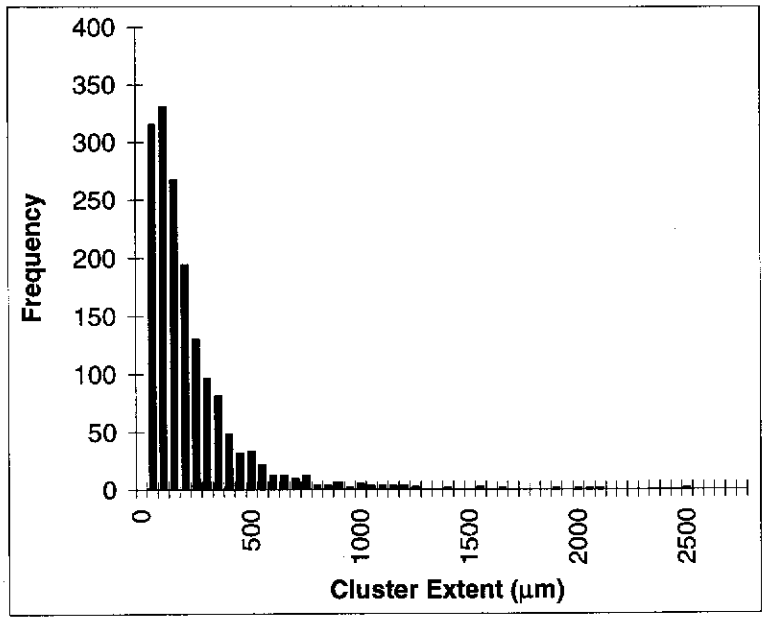

(a)

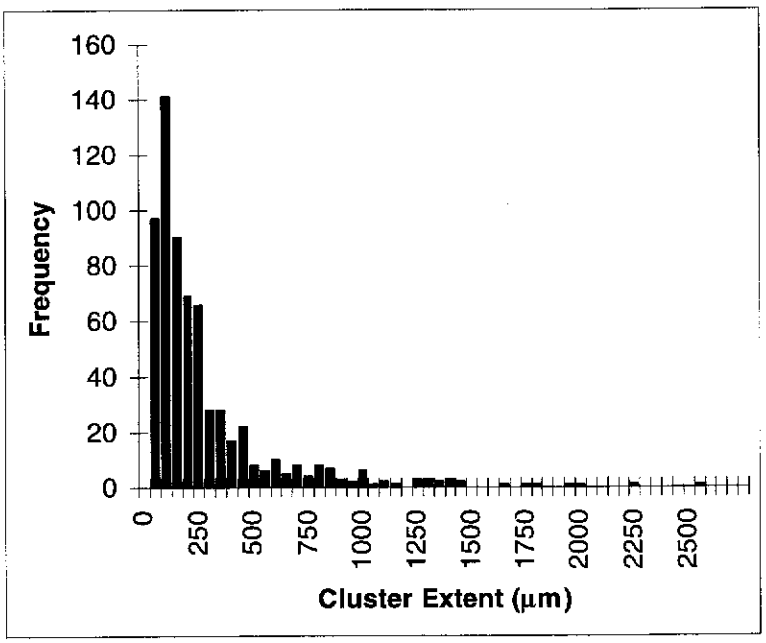

(b)

Figure 60. Cluster extent histograms for (a) serosal surface sample volume, and (b) tumour-normal tissue interface sample volume. Only clusters consisting of two or more microspheres were included in these histograms.

There was a strong correlation between cluster population and cluster extent. Clusters with larger extents contained more microspheres. This is clearly shown in Figure 61, where cluster population is graphed against cluster extent. It can also be seen from Figure 61 that the relationship between cluster extent and population was similar for both sample volumes.

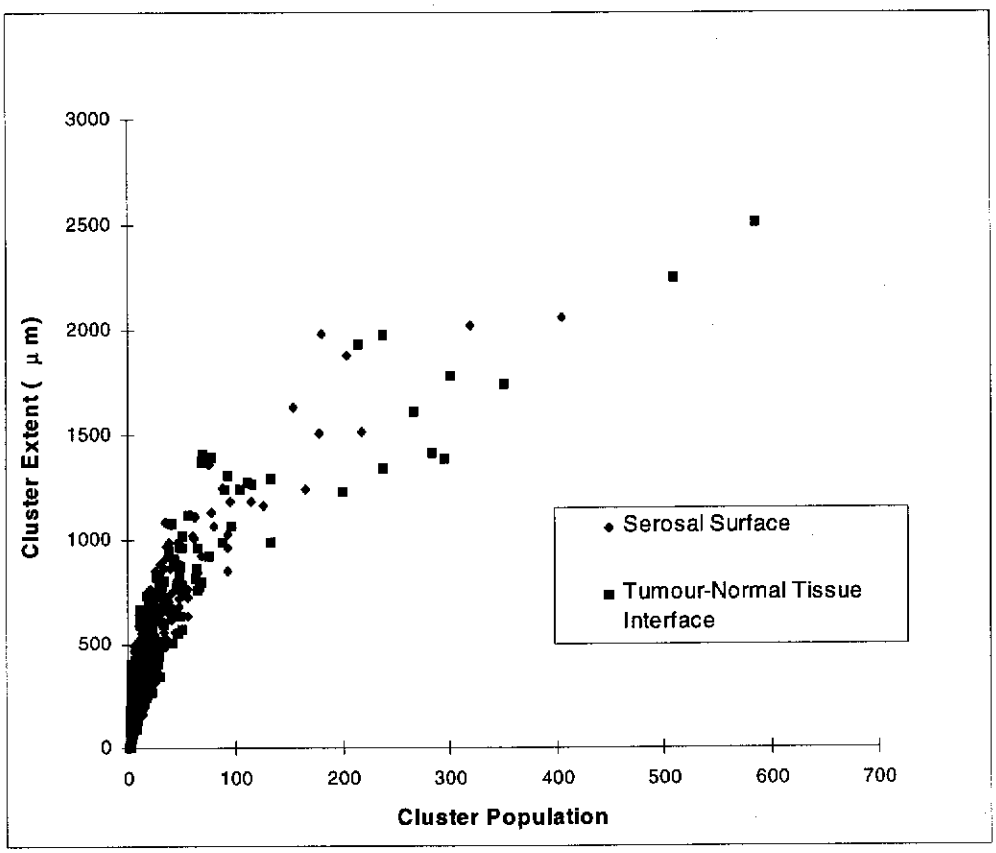

Figure 61. Correlation of cluster population with cluster extent.

The distance of a cluster from the tumour boundary and the number of microspheres in the cluster were also related. This is demonstrated in Figure 62, where the perpendicular distance of a cluster centroid from the tumour boundary is plotted against cluster population for the serosal surface tissue sample. It is clear from this Figure that the tendency was for larger clusters to lie closer to the tumour boundary. A similar relationship was observed in the tumour-normal tissue boundary tissue sample.

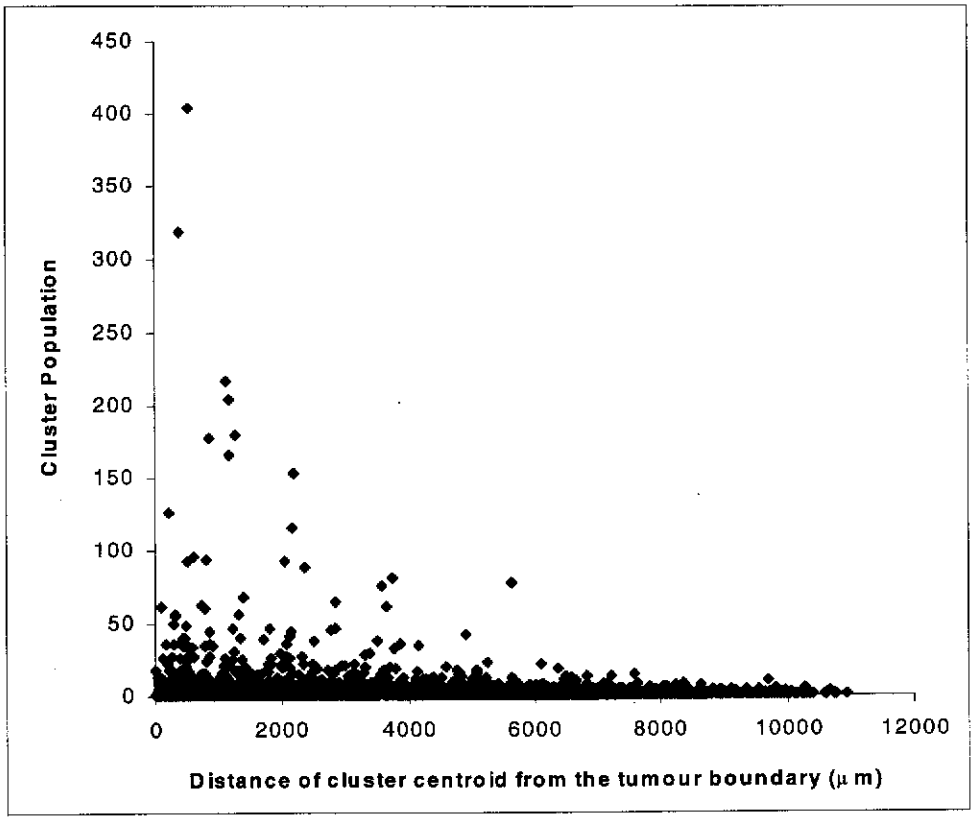

Figure 62. Plot of the distance of cluster centroids from the tumour boundary against cluster population for the serosal surface tissue sample .

6.2.3 Radiation dose calculations in the serosal surface and tumour-normal tissue interface sample volumes using single equivalent radiation sources

This section examines the use of single equivalent radiation sources in place of the observed microsphere positions in the tumour periphery. The initial modelling presented in section 6.1.1 suggested that at distances greater than 10% of the cluster extent from the cluster centroid, the radiation dose field produced by a cluster of microspheres and a single equivalent radiation source were similar. Examination of the three dimensional cluster extents in Table 9 reveals that for microsphere clusters consisting of more than a single microsphere, over 75% had an extent below 300 μm. This suggests that representing microsphere clusters by a single equivalent source positioned at the cluster centroid should produce dose deposition patterns in reasonable agreement with those generated

using individual microsphere positions. Over 40% of the observed microsphere clusters consisted of single microspheres whose radiation dose field will remain unaltered. For the other clusters, doses close to the cluster centroid will be overestimated, but as most clusters have extents less than 300 μm this will affect a relatively small fraction of the total tissue volume. Doses in the vicinity of clusters having a larger population and extent will be more poorly represented.

Microsphere positions observed in the sample volumes containing the tumour periphery were replaced with single equivalent sources of activity placed at the cluster centroids and dose deposition patterns calculated. These were compared to the patterns arising using the observed microsphere positions. Calculations were performed assigning a nominal activity of 50 Bq for each microsphere. In both cases, dose contributions from microspheres in the volume between tissue sections were allowed for by scaling the activity of the microspheres by the factor 200/42, as discussed in Section 5.3. In order to reduce computational time and complexity, only radiation dose contributions from microspheres contained within the sample volume were considered in this exercise. This means that absolute doses will be lower than would actually occur, especially near the edges of the sample volumes. The objective of this study was however to assess the efficacy of using an equivalent source representation in lieu of individual microspheres. Omission of dose contributions from outside the sample volumes will affect both cases equally and is therefore acceptable for comparative purposes.

The results are presented in Figure 63 to Figure 66. Figure 63 shows examples of radiation doses calculated on two different planes within the tumour-normal tissue interface sample volume. Figure 64 shows the cumulative dose volume histograms for the whole volume. Figure 66 and Figure 65 provide equivalent information for the serosal surface sample volume.

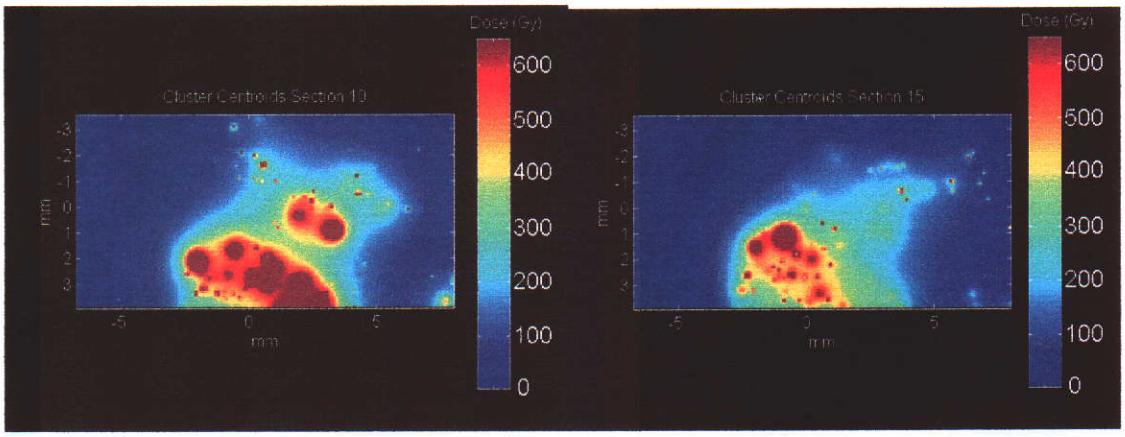

(a) (b)

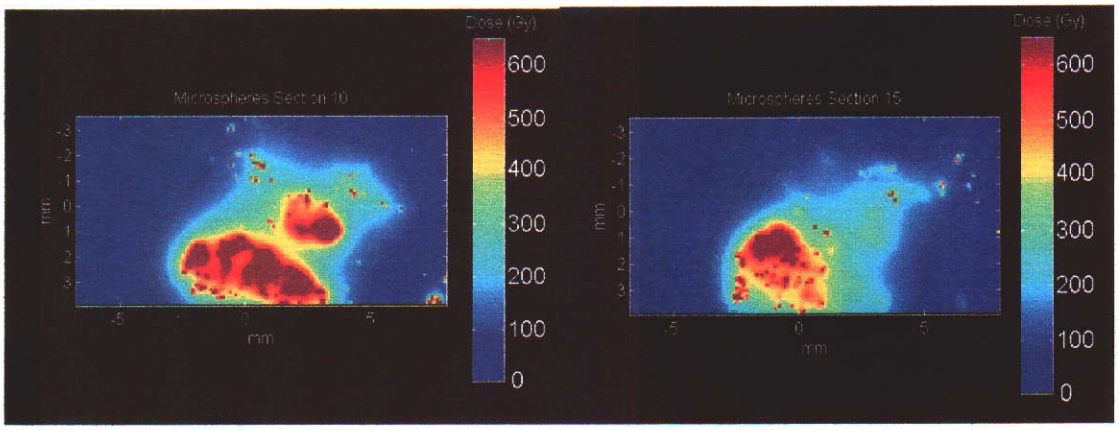

(c) (d)

Figure 63. Radiation dose distributions on two tissue sections in the tumour-normal tissue boundary tissue sample volume. Calculations were made using observed microsphere positions for (c) and (d); and single equivalent sources placed at cluster centroids for (a) and (b).

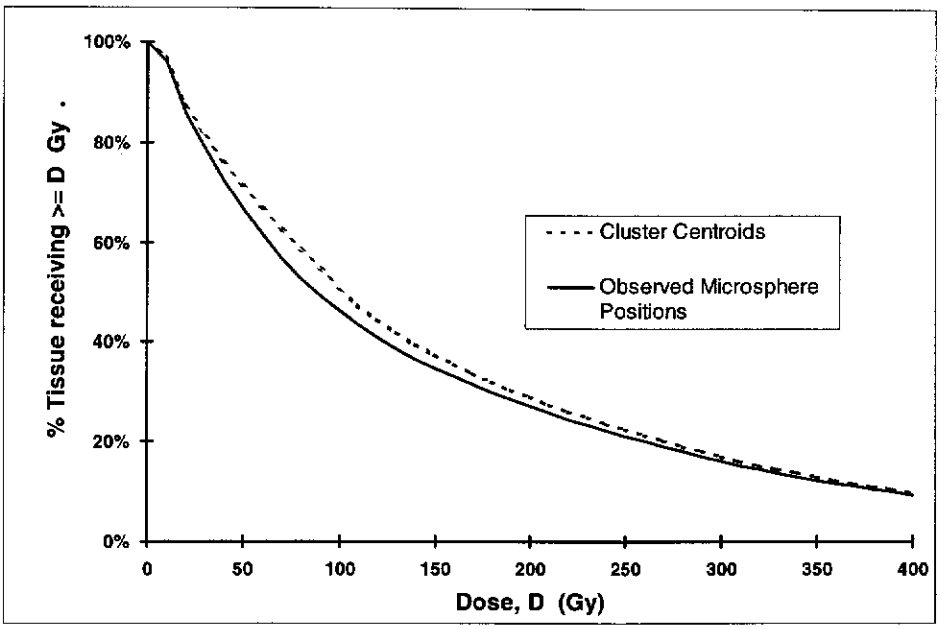

Figure 64. Cumulative dose volume histograms for the tumour-normal tissue boundary tissue sample volume.

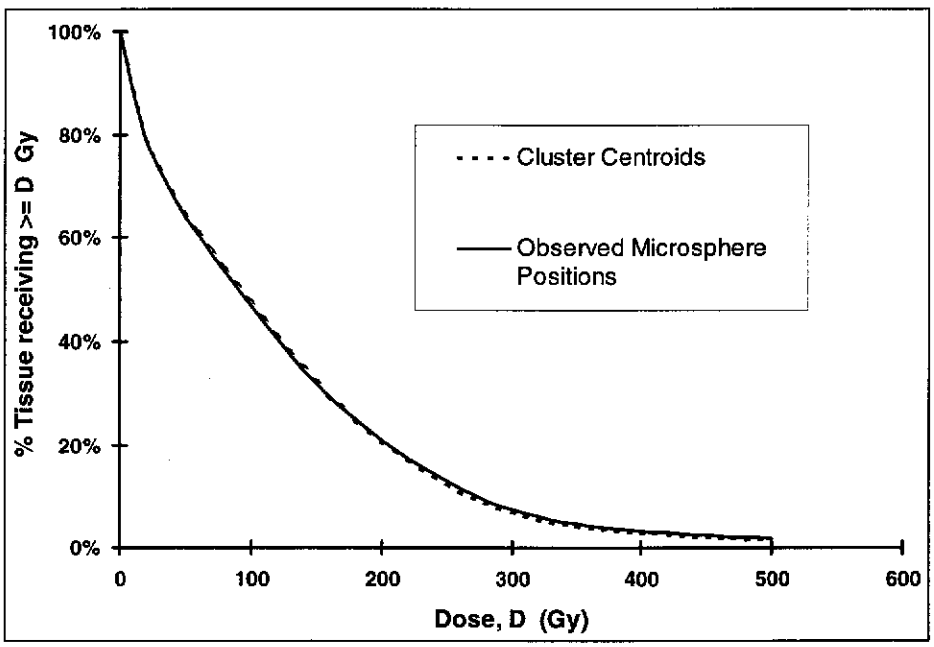

Figure 65. Cumulative dose volume histograms for the serosal surface tissue sample.

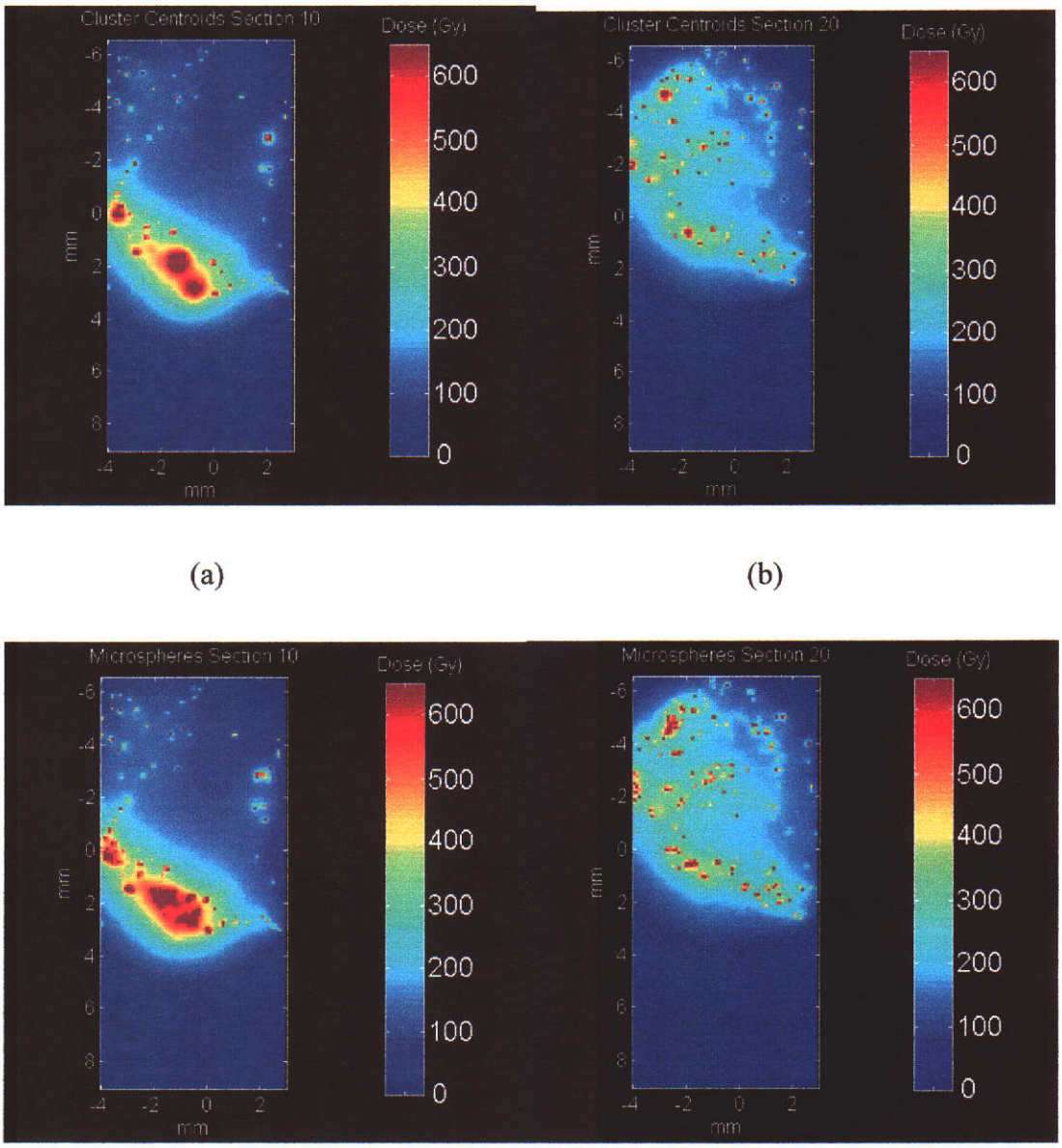

Figure 66. Radiation dose distributions on two tissue sections from the serosal surface tissue sample volume. Calculations were made using observed microsphere positions for (c) and (d); and single equivalent sources placed at cluster centroids for (a) and (b).

Dose distribution patterns appear more symmetrical when using single equivalent sources at the cluster centroids than those arising using observed microsphere positions. This was most noticeable in regions of high dose, corresponding to larger clusters. This was expected from the simulation studies. Cumulative dose volume histograms for the serosal surface volume were almost identical. In the tumour normal tissue interface sample, Figure 64 indicates that using equivalent sources placed at the cluster centroids resulted in a slightly larger tissue volume receiving radiation doses above approximately 30 Gy, but the difference in volumes of tissue receiving the same dose was still less than 5%. The larger discrepancy in dose volume histograms in the tumour-normal tissue interface volume compared with the serosal surface volume is most likely due to the fact that the former tissue sample contained a greater number of clusters with large extents than the serosal surface sample. The simulation studies discussed in section 6.1.1 demonstrated that the radiation field from clusters with larger extents was less well represented using the single equivalent source approach.

The radiation dose distributions calculated by modelling microsphere clusters as single equivalent radiation sources appear to be sufficiently similar to those calculated using the observed microsphere distributions to make it acceptable to treat a microsphere cluster as a single radiation source in dosimetry calculations. Modelling microsphere clusters in this manner also results in a substantial reduction in the number of radiation sources used in the dosimetry calculations. For instance, there were 12 546 microspheres in the serosal surface tissue sample and these grouped into 2649 clusters. Treating clusters as single equivalent radiation sources results in a reduction of the number of radiation sources by almost a factor of 5, with an equivalent reduction in dosimetry calculation time.

As a result of the conclusions presented in this section, microsphere deposition models were developed that generated distributions of microsphere clusters and modelled the radiation dose of a cluster as a single equivalent radiation source. These models are presented in section 6.4

6.3 Distribution of cluster centroids

In developing a microsphere distribution model based on single equivalent source cluster representations, it will be necessary to generate a spatial distribution of cluster centroids similar to that observed in the tissue sample volumes. Otherwise the radiation deposition patterns generated by the model will not closely approximate those calculated using observed microsphere positions. As the radiation dose from a cluster reduces quickly with increasing distance from the cluster, dose deposition patterns will depend strongly on the distance of a cluster centroid from its nearest neighbours. The relationship between neighbouring clusters can be examined using a histogram of the distribution of the distance between nearest neighbour clusters (Russ, 1995 pp 491-494).

Figure 67 presents the histogram of nearest neighbour distances for cluster centroids identified in the serosal surface and tumour-normal tissue interface sample volumes. Both are similar in character and their shape suggests that the cluster centroids themselves form clustered distributions (Russ, 1995 pp491-494). This supports the evidence of hierarchical clusters of microspheres discussed in section 4.4.2.1.2.

It is expected that a suitable model will produce microsphere distributions exhibiting nearest neighbour distance histograms similar to Figure 67, although this alone is not a sufficient condition for the generation of similar radiation dose distributions. For example, suppose cluster centroids distributed in a single large aggregation were divided into two halves and moved apart so as to form two aggregations separated by a distance that is large compared with the distances between clusters in the same aggregation. The nearest neighbour distance histogram for these two cases will be virtually identical. This is because that for the latter case the nearest neighbour of a cluster will be another cluster lying within the same aggregation - the large separation distance between the two aggregations will not feature in the histogram. However the radiation dose distribution patterns arising from the two situations will differ markedly.

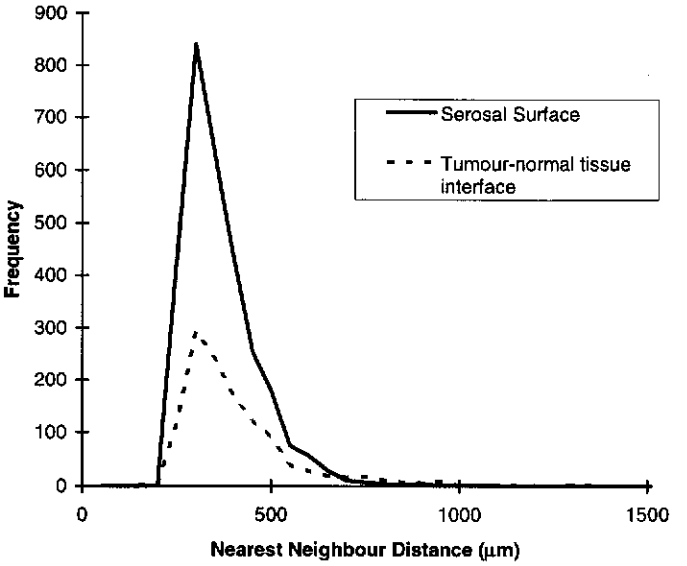

Figure 67. Histogram showing the distribution of nearest neighbour distances for cluster centroids in the serosal surface and tumour-normal tissue interface sample volumes.

6.4 Microsphere Deposition Models

Several microsphere deposition models were developed. These were all based on the single equivalent source representation of a microsphere cluster discussed in the previous sections of this chapter. The models placed microsphere cluster centroids in a 7 x 10 x 7.6 mm^3 volume of tissue whose dimensions were chosen to be approximately those of the tissue sampled from the serosal surface of the tumour. The objective was for the model to produce radiation dose patterns similar to those observed in the serosal surface sample.

The geometry used with all simulations is illustrated in Figure 68. The tumour boundary was taken as lying on the x-z plane so the y-axis ran perpendicular to the tumour surface, with y distances being positive towards the centre of the tumour. In tissue samples taken from the tumour periphery, microsphere concentration in the tumour showed a strong dependence on distance from the tumour boundary (see section 4.2). This feature was modelled by making the

concentration of microspheres vary with perpendicular distance from the tumour boundary to match the observed distribution for the serosal surface sample shown in Figure 14. The number of microspheres in a simulated cluster was chosen to match the relationship between cluster population and the perpendicular distance of the cluster from the tumour boundary observed in the serosal surface tissue sample (shown in Figure 62). This was done by examining the distribution of clusters identified in the serosal surface volume. The perpendicular distance from the tumour boundary was divided into 500 μm intervals and the population distribution in each interval determined. For a simulated cluster, the interval corresponding to the distance of the cluster from the boundary was determined, and a cluster population chosen randomly from the distribution observed for that interval.

The total number of microsphere clusters generated for a model was chosen to be approximately equal to the number of clusters observed in the serosal surface sample volume, which was 2649 (see Table 7). This technique ensured the total number of microspheres present in the simulation was approximately the same as the number detected in the serosal surface tissue sample (which was 12 564).

Radiation doses were calculated on a 0.1 x 0.1 mm grid on 38 planes parallel to the x-y plane. Z coordinate values for these calculation planes ranged from 0 to 7.6 mm in 0.2 mm increments. On each plane, doses were determined at grid points having x coordinates in the range -4 to +3 mm and y coordinates in the range 0 to +5.5 mm using the techniques described in Chapter 5. The chosen dose calculation volume matched that of the vascular periphery region observed for the serosal surface tissue sample, which facilitated comparison of simulations with dosimetry patterns calculated using observed microsphere positions.

6.4.1 Model Evaluation

Models were assessed by comparing the distribution of microsphere clusters and the calculated radiation dosimetry patterns against the observations made in the serosal surface tissue sample.

The distribution of microsphere clusters was assessed by comparing the histogram of the distance between nearest neighbour clusters for the model with the distribution observed in the serosal surface volume. The calculated radiation dose distribution pattern for each model was compared with that determined in the vascular periphery of the serosal surface sample volume in two ways. A global assessment was made by comparison of dose volume histograms for the model with those calculated for the vascular periphery region of the serosal surface sample. For this comparison, radiation doses for the serosal surface volume were calculated using observed microsphere cluster centroids as single equivalent sources of radiation in the same manner as the simulations. A visual

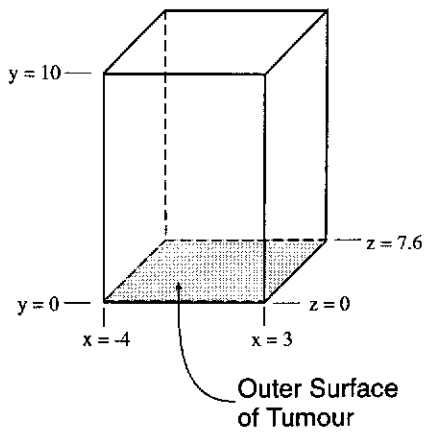

Figure 68. Geometry of the volume used for assessment of microsphere deposition models. The dimensions of the volume in which microsphere cluster centroids were generated were as indicated on this diagram. The tumour surface was taken to lie on the x-z plane, y distances are positive towards the tumour centre.

assessment of the spatial distribution of radiation doses on selected calculation planes was made using images such as those shown in Figure 70, where radiation dose is displayed in a false colour. For ease of comparison, the tumour boundary for the serosal surface sections was straightened to lie in the same plane as the model using the method discussed in section 5.4.3. For computational simplicity, dose contributions from microspheres lying outside the volume shown in Figure 68 were neglected for both the simulations and the serosal surface sample volume calculations. This is acceptable for the purposes of model assessment as dose contributions from microspheres lying outside this regions will vary relatively slowly across the calculation planes and would be anticipated to have a similar effect in both cases.

6.4.2 Quasi-Random Distribution of Microsphere Clusters

In the first attempt to develop a model, microsphere cluster centroids were placed randomly in the volume. Cluster centroids were generated by selecting x and z coordinates for each cluster from a uniform random distribution. The y-coordinate and the cluster population were chosen as discussed in section 6.4. If a generated cluster centroid position lay closer than 185 μm from a previously generated position it was rejected, as the analysis presented in section 6.2.2 demonstrated that separate clusters did not occur with separations below this distance.

The distribution of nearest neighbour distances obtained is shown in Figure 69, and is clearly different to the distribution observed in the serosal surface sample. For comparative purposes the curve have been normalised to have the same total cumulative frequency. Figure 70 shows a comparison of radiation dose distributions calculated using the model and using the microsphere clusters observed in the serosal surface sample volume. The calculation planes selected were chosen to illustrate the typical dose deposition patterns that occurred. The dose distributions generated by the model (Figure 70 (a) and Figure 70 (b)) appeared to be more uniform than those in the serosal surface periphery. The serosal tumour periphery showed significant variations in the spatial distribution

of radiation dose between calculation planes. A number of calculation planes had large areas where high doses were delivered, such as in shown in Figure 70 (c). There were also a number of regions that contained relatively large numbers of small area, high dose regions, an example of this is shown in Figure 70 (d). The model did not generate numerous, small area, high dose regions similar to Figure 70 (d) anywhere throughout the calculation volume. The cumulative dose volume histogram for this model, shown in Figure 71, supports these conclusions.

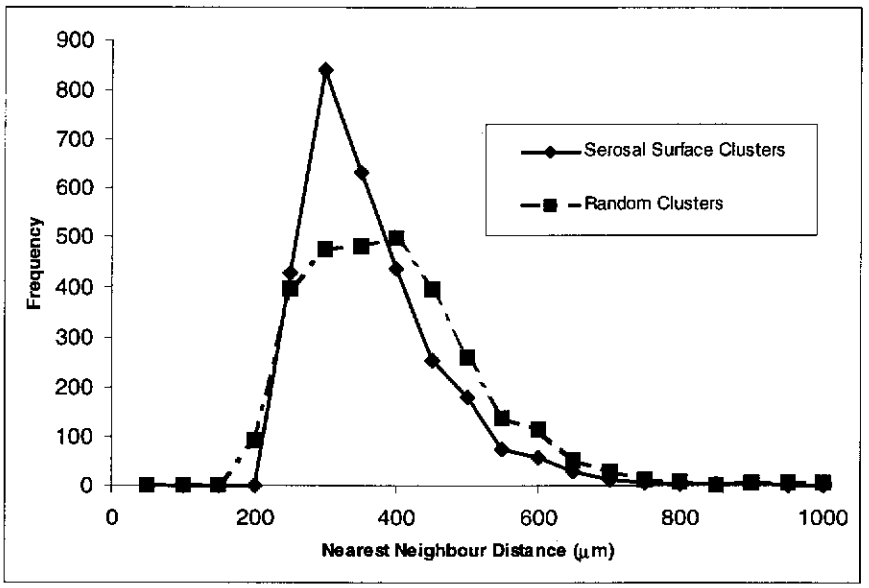

Figure 69. Comparison of the distribution of nearest neighbour cluster distances for the randomly placed cluster centres with that observed for the serosal surface sample volume.

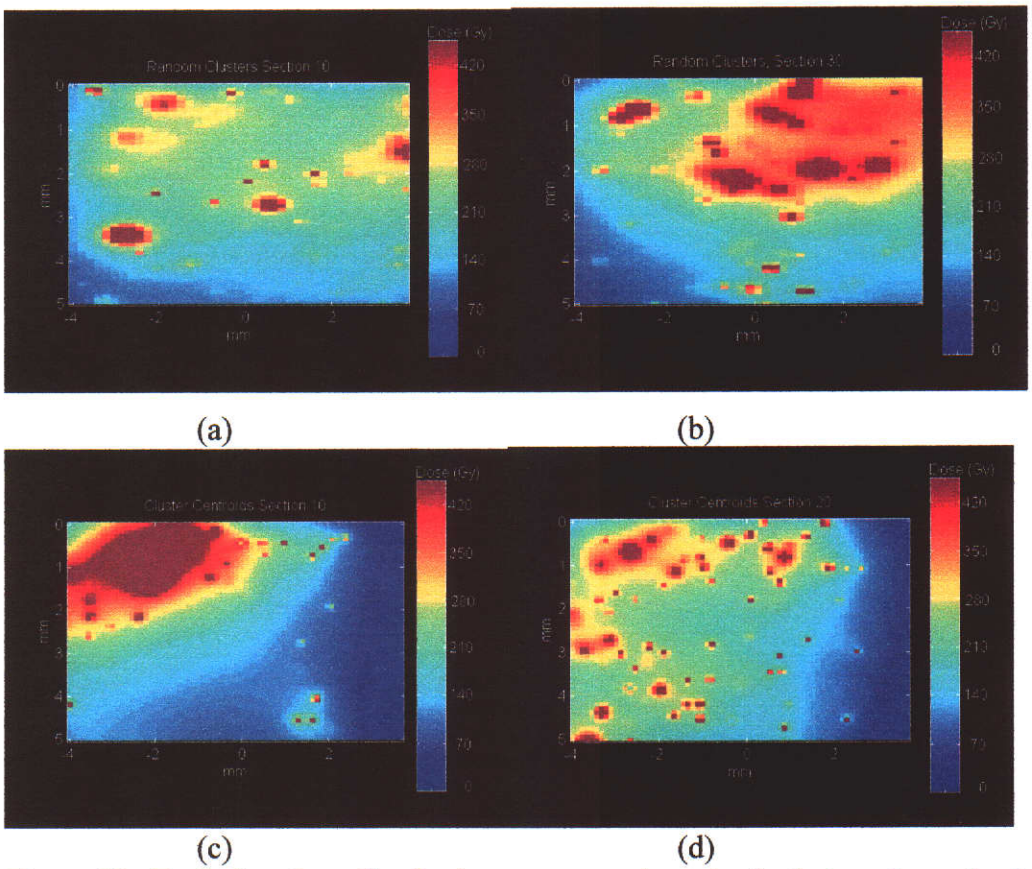

Figure 70. Radiation dose distributions on two selected calculation planes for the random cluster model, (a) and (b), and from the serosal surface tissue sample volume (c) and (d). Radiation dose in Gray is shown on the colour bar in each image. The tumour boundary is at the top of each picture.

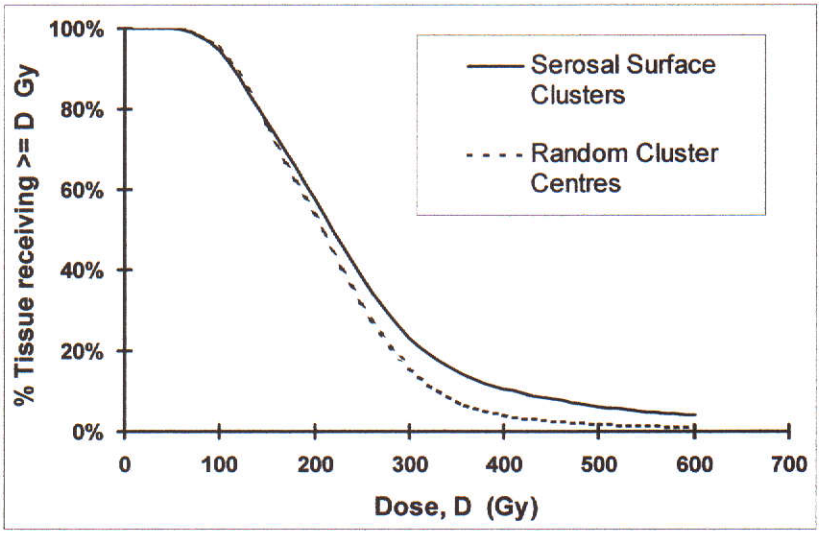

Figure 71. Cumulative dose volume histograms for the random cluster model and the serosal surface periphery.

6.4.3 Microsphere Superclusters

The cluster analysis results discussed in section 4.4.2.2 and the distribution of nearest neighbour cluster centroid distances both suggested that microsphere clusters were themselves clustered. Zavgorodni (1996) found that microsphere 'superclusters' consisting of approximately 5 clusters within a radius of 600 μm provided reasonable agreement with the experimental results of Pillai et al. (1991). The foregoing suggested that radiation dose distributions from microsphere superclusters may be able to match the observed distributions. Therefore the initial model was modified by grouping clusters into superclusters.

Superclusters were generated by distributing clusters constituting a single supercluster randomly in space about a supercluster centre. The clusters were placed up to a specified radius from the supercluster centre - the supercluster radius. Clusters were separated by at least 185 μm from any other cluster in the supercluster. The number of clusters in a supercluster was chosen randomly to be between one and a specified maximum supercluster population. The number of microspheres in each cluster was chosen as described in section 6.4.

Supercluster centres were positioned randomly throughout the calculation volume in the same manner as described for cluster centres in the previous section (section 6.4.2), except that in this case supercluster centres were separated by at least twice the supercluster radius. The total number of supercluster centres generated was used as an input parameter for a model, as were the supercluster radius and the maximum population of a supercluster. Models were generated for a variety of these parameters. Parameter values for a selection of these models are presented in Table 10.

The distribution of nearest neighbour distances for these models is shown in Figure 73, along with the distribution calculated for the serosal surface sample volume. From this figure it can be seen that simulations NS3, NS9 and NS14 matched the observed distribution quite well, with agreement within 20% of the serosal surface sample in the vicinity of the peak on Figure 73. For NS7 and NS8 the match was not as good.

Table 10. Supercluster Model Parameters

Simulation Code	Number of Superclusters	Supercluster Radius (μm)	Supercluster Population Range	Number of Clusters Generated	Number of Microspheres Simulated
NS3	200	500	1 - 26	2764	13083
NS7	200	600	1-27	2698	13837
NS8	430	600	1-11	2646	11075
NS9	100	700	1-52	2746	12529
NS14	200	600	1-32	3262	15757

The differential dose volume histograms generated by the models are shown in Figure 72. Figure 74 shows dose distributions on two selected planes for the models whose nearest neighbour distance distributions most closely matched those observed for the serosal surface sample. Radiation dose distributions generated by the models did not closely match those calculated for the serosal surface sample volume.

Because the models are the result of random cluster positioning with random cluster population selection, subject to the constraints specified by the model; two models generated using the same parameters would be expected to produce somewhat differing distributions of clusters, that would in turn lead to different radiation dose distributions. The extent of this variability was investigated by generating a number of distributions using identical model parameters. Figure 75 presents differential dose volume histograms for three simulations using the parameters for model NS14 from Table 10 and illustrates the variability typically observed between simulations. It can be see from Figure 75 that the variability of deposited dose is similar between simulations, but that the median delivered dose can shift by up to 50 Gy.

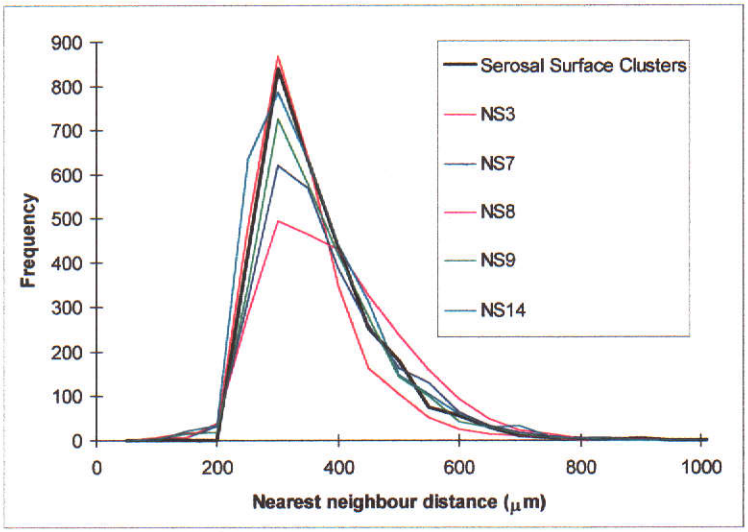

Figure 73. Distribution of nearest neighbour distances for supercluster models. The observed distribution for the serosal surface sample volume is provided for comparison.

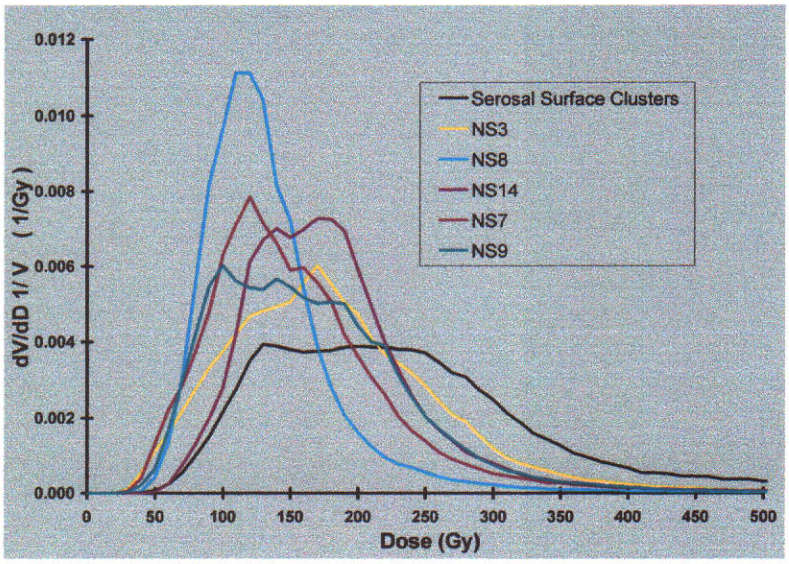

Figure 72. Differential dose volume histograms calculated for microsphere cluster models and using the observed serosal surface clusters.

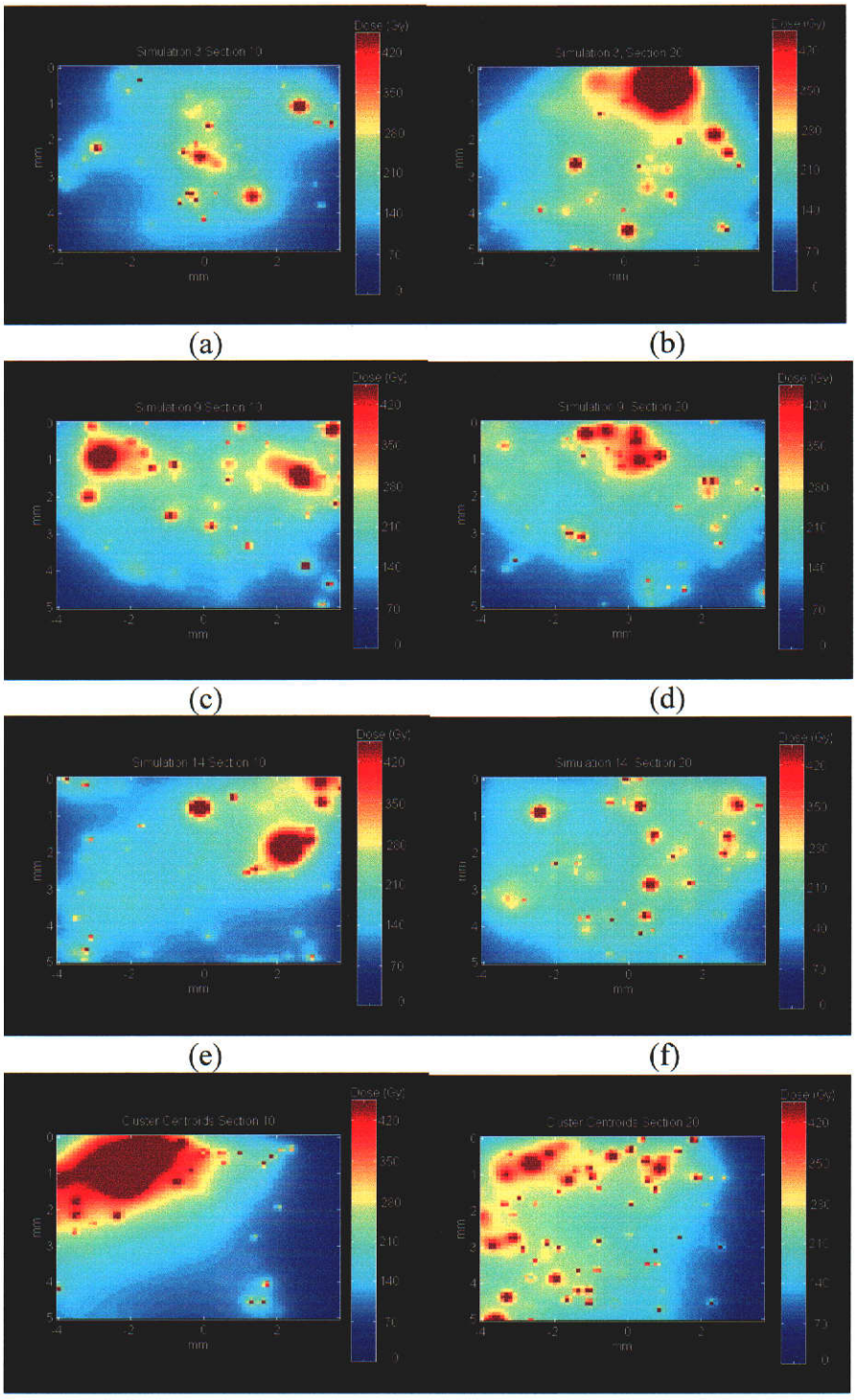

Figure 74. Example radiation dose distributions on selected calculation planes for supercluster models. (a) and (b), model NS3. (c) and (d), model NS9. (e) and (f), model NS14. (g) and (h), serosal surface sample volume. Radiation dose in Gray is shown on the colour bar in each image.

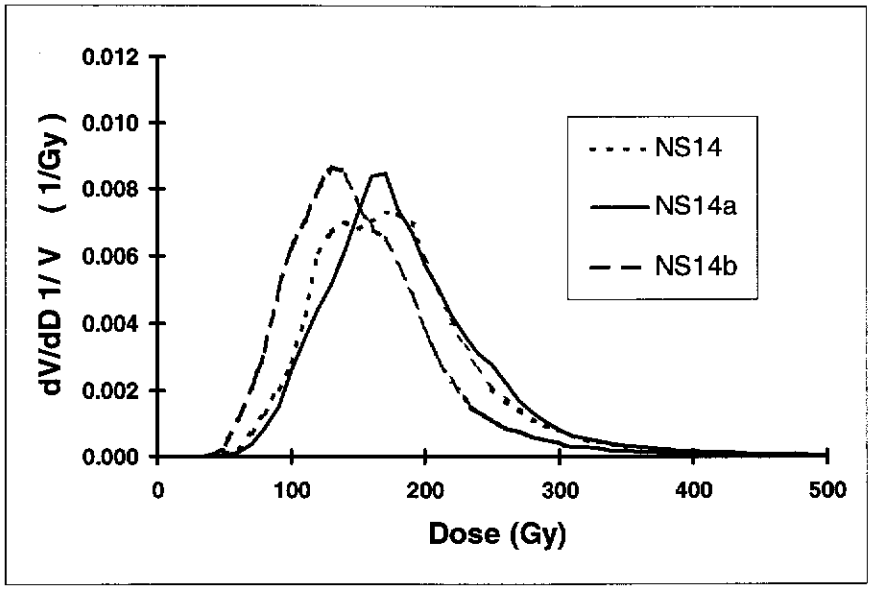

Figure 75. Differential dose volume histograms for three simulations using the parameters for model NS14 in Table 10 illustrating the variability typically observed between simulations having the same model parameters.

6.4.4 Discussion

None of the relatively simple models considered for microsphere deposition pattern in the tumour periphery produced radiation dose distributions that accurately matched those calculated for the serosal surface tissue sample.

The distribution of nearest neighbour distances for randomly distributed clusters did not match the experimentally observed distributions. A number of the supercluster models examined were able to produce nearest neighbour distance distributions that were a good match with observed distributions. However, this alone was not sufficient to produce radiation dose distributions that matched the experimentally observed patterns. Radiation dose distributions calculated using the experimentally observed microsphere clusters in the serosal surface tumour periphery varied substantially throughout the calculation volume, both parallel as well as perpendicular to the tumour boundary. Figure 74 (g) and Figure 74 (h) provide an example of this variation; these two calculation planes were separated by a distance of 1 mm. This gave rise to highly heterogeneous radiation doses being delivered throughout the tumour periphery. The differential dose volume

histogram for the serosal surface cluster positions shown in Figure 72 indicates that, for the measured sample, almost equal volumes of tissue received doses between 130 and 260 Gy. None of the models produced this degree of dose heterogeneity. Examination of the images in Figure 74 shows that while some models could generate dose distributions that resembled those calculated over some regions of the serosal surface volume, the variability of dose across the whole volume could not be simulated in a satisfactory manner.

The disagreement between modelled and reconstructed radiation dose distributions would appear to be due to the microsphere concentration varying significantly throughout the tumour periphery. Radiation dose patterns appeared to vary markedly over distances on the order of 2 to 3 millimetres, corresponding to variations in the underlying microsphere distribution over the same distance. While calculations presented in this chapter have concentrated on radiation dose patterns in the serosal surface sample volume, similar variations in radiation dose were also observed in the tumour periphery regions of the tumour-normal tissue sample volume. Effective modelling of microsphere distributions will require characterisation of the larger scale microsphere deposition variations. It would appear reasonable to expect that an assessment of microsphere distributions throughout a tissue volume having linear dimensions significantly larger that the distance over which microsphere concentrations occur would be needed to perform such a characterisation. As the linear dimensions of the volume sampled in this study were only approximately three times the distance over which large scale concentration variations appeared to be occurring, a meaningful quantitative assessment of this variation was not possible in this work.

7. Conclusions and Recommendations

This thesis has examined the distribution of microspheres and the resulting radiation dose deposition patterns in human liver following hepatic arterial infusion of ^{90}Y labelled microspheres as a treatment for liver cancer. Tissue samples from a patient who had received hepatic microsphere therapy to treat a large solitary metastatic liver tumour approximately 80 mm in diameter were used in the study. Representative samples from normal liver and tumour tissue were analysed to determine microsphere deposition patterns in the tissues. Radiation doses delivered to the sample volume were calculated using the observed microsphere positions.

Microspheres were found to deposit inhomogeneously in tissues, preferentially lodging in a region approximately 6 mm wide around the periphery of the tumour. Concentrations of around 200 microspheres mm^{-3} were observed in this region. This was 50 to 70 times the concentration observed in normal hepatic parenchyma, and 65 to 94 times that in the tumour centre. The deposition of microspheres in the tumour periphery was not uniform, and cluster analysis showed that microspheres could be classified into clusters. The number of microspheres in a cluster was skewed towards low numbers and cluster sizes of up to 1500 μm were observed.

The concentration of microspheres in normal liver tissue was measured to be 3.5 microspheres/mm^3. Examination of the numbers of microspheres found in 4 x 4 x 4 mm^3 volumes demonstrated that microsphere deposition in normal liver was non-uniform. Significant variations in microsphere density were occurring over distances on the order of 4 millimetres. This means that radiation doses will be more heterogeneous than if microspheres were deposited uniformly. This finding was supported by results obtained in modelling a uniform distribution of microspheres, the radiation dose distributions generated by the model being more uniform that those calculated using the observed microsphere positions. The concentration of microspheres was too low for cluster analysis to be used to

examine whether clustering of microspheres, as was found to occur in the tumour periphery, also occurred in normal tissues.

Radiation dosimetry calculations indicated that heterogeneous doses were delivered to both normal liver and tumour tissues. The mean dose of 8.9 Gy received by normal liver was well below the 30-35 Gy whole organ exposure dose needed to cause radiation induced liver toxicity. Normal liver tissue exposure is frequently calculated by assuming all the infused activity spreads uniformly throughout the liver. A normal liver absorbed dose of 80 Gy would have been calculated in this instance using this technique. This study clearly indicated that absorbed dose estimates made using this assumption of uniform specific activity would substantially overestimate the radiation dose delivered to the majority of normal hepatic parenchyma. As such they are meaningless in providing an indication of the biological effect to normal hepatic parenchyma following hepatic ^{90}Y microsphere infusion. Doses calculated in this manner reflect more on the total activity infused rather than the actual absorbed dose to normal liver tissues.

Calculations indicated that large radiation doses were delivered in the well vascularised tumour periphery. Absorbed doses of at least 70 Gy were given to the entire tumour periphery, and doses in excess of ten times this minimum value were delivered in the vicinity of large clusters of microspheres. The low concentration of microspheres in the avascular tumour centre resulted in this region receiving a mean radiation dose of only 6.8 Gy.

Doses outside the serosal surface of the tumour were in excess of 50 Gy within 3 mm of the tumour. The literature has not recognised that exposure of tissues in contact with serosal tumour may be a factor contributing to post procedure complications. The tacit assumption is that, as ^{90}Y is a beta emitter, no significant exposure to other organs from activity embolised within the liver will occur. The results of this study suggest that organs within 3 mm of the surface of tumours of the size analysed in this work could receive significant radiation doses.

The potential of performing dosimetry calculations in the tumour periphery using microsphere clusters as sources of radiation was investigated. Replacing observed microsphere positions with scaled sources of activity located at cluster centroids produced radiation dose deposition patterns that were in reasonable agreement with those calculated using actual microsphere positions, thus indicating that this is a viable approach for reducing dosimetry calculation times. Attempts to model the distribution of microsphere clusters using random distributions of clusters and microsphere superclusters were unsuccessful in producing radiation dose patterns similar to those observed. This was attributed to variations in the distribution of clusters (and hence the underlying microsphere concentrations) that occurred over distances on the order of a few millimetres. As the linear dimensions of the tissue samples containing the tumour periphery analysed in this work were of a similar order to this distance, meaningful modelling of these concentration variations could not be performed. This could be addressed by analysis of larger tissue samples in future work. The simulation studies presented in this work have presented evaluation criteria against which future models might be assessed.

The practical outcome of the radiation dosimetry calculations performed in this study is that a tumourcidal dose was delivered in the tumour periphery. The clustering of microspheres that was observed in the tumour periphery, while interesting, would have produced no significant effect on the biological outcome of the treatment. Radiation doses calculated for normal liver indicate it will be completely spared from any toxic side effects. The concentration of microspheres in the tumour centre was similar to that observed in normal liver. This indicates that delivering numbers of microspheres that will spare normal liver parenchyma may also result in sublethal does to malignant cells towards the tumour centre. As a result, multiple treatments may be required over time to successfully treat large tumours that often contain a necrotic centre.

7.1 Possibilities for future studies

The results presented in this work are for tissue samples from a single patient, and the extent to which they can be generalised is uncertain. In the published literature, only the studies of Pillai et al. (1991) and Fox et al. (1992) provide results with which the work presented in this thesis can be generally compared. Pillai et al. (1991) examined microsphere deposition in normal and tumour tissues in rabbit liver. They reported deposition patterns in normal liver similar to those observed in this study and also noted clustering of microspheres in tumour tissues. The similarity of their general conclusions and the results of this work provides encouragement that the microsphere deposition patterns observed in this work were not atypical. Fox et al. (1991) studied microsphere deposition in normal human liver tissues. They found microsphere concentrations approximately 10 times higher than observed in the normal liver sample analysed in this study, and a more heterogeneous spatial distribution of microspheres. As discussed in chapter 4, these variations may be due to differing tumour burdens of the two patients from which the tissue samples were taken, but clearly there is a need for further work to be done in order to characterise the role of tumour burden on microsphere deposition patterns. Additionally, while the volumes of tissue assessed in this study were larger than samples analysed in other published work, they were a small fraction of the total liver and tumour volumes. There exists a possibility that the tissue samples were not representative of the situation in all parts of the patient's liver. Variations in microsphere concentration also appeared to occur over distances on the order of a few millimetres in normal liver and around the tumour periphery

It would be clearly desirable to assess the distribution of microspheres in other patients, and to cover a variety of tumour sizes and types, as the distribution patterns might depend on these factors. Ideally larger volumes of tissue would be analysed, and more samples taken from additional sites in the same patient in future work. Such analysis may permit characterisation of larger scale microsphere concentration variations, and would increase the confidence that the

deposition patterns observed were indeed representative of those that normally occur.

The exposure of tissues in contact with the serosal surface of the tumour and the relationship of such exposure to post procedure complications also appears worthy of further investigation. It would be interesting to investigate whether there was a correlation between observed complications and exposure to organs in contact with serosal tumour.

The activity per microsphere reported in the literature for hepatic microsphere therapy varies from 10 Bq to several hundred Bq (Yorke et al., 1999). The 50 Bq per microsphere activity used to treat the patient from whom the tissue samples analysed in this study were taken is at the lower end of this range. The total activity normally infused for microsphere therapy does however remain fairly constant at around 3 GBq. It follows that use of microspheres having a greater activity per microsphere means fewer microspheres will be infused overall, reducing microsphere concentrations in tissues. Use of higher specific activity microspheres would therefore be expected to increase dose heterogeneity. This might not necessarily affect the tumourcidal results in the tumour periphery as Pillai et al. (1991) noted that while decreasing the number of microspheres infused reduced cluster populations, the overall number of clusters in tumour remained relatively constant. Doses in the vicinity of a cluster will thus most likely fall, but as these are already far in excess of the tumourcidal dose, this will be of no consequence. The likelihood is that a tumourcidal dose would still be delivered throughout the tumour periphery. Evaluation of the effects of infusing microspheres with a different specific activity could be a subject for further investigation.

8. References

Anderberg, M. R. 1973. "Cluster Analysis for Applications." Academic Press Inc., New York.

Anderson, J. H., Goldberg, J. A., Bessent, R. G., Kerr, D. J., McKillop, J. H., Stewart, I., Cooke, T. G., and McArdle, C. S. 1992. Glass yttrium-90 microspheres for patients with colorectal liver metastases. *Radiotherapy & Oncology* 25(2), 137-9.

Andrews, J. C., Walker, S. C., Ackermann, R. J., Cotton, L. A., Ensminger, W. D., and Shapiro, B. 1994. Hepatic radioembolization with yttrium-90 containing glass microspheres: preliminary results and clinical follow-up. *Journal of Nuclear Medicine* 35(10), 1637-44.

Archer, S. G., and Gray, B. N. 1990. Comparison of portal vein chemotherapy with hepatic artery chemotherapy in the treatment of liver micrometastases. *American Journal of Surgery* 159(3), 325-9.

Archer, S. G., and Gray, B. N. 1989. Vascularization of small liver metastases. *British Journal of Surgery* 76(6), 545-8.

Ariel, I. M. & Padula, G. 1982, Treatment of asymptomatic metastatic cancer to the liver from primary colon and rectal cancer by the intraarterial administration of chemotherapy and radioactive isotopes, Journal of Surgical Oncology, vol. 20, no. 3, pp. 151-6.

Ballantyne, G. H., and Quin, J. 1993. Surgical treatment of liver metastases in patients with colorectal cancer. *Cancer* 71(Suppl), 4278-92.

Bichsel, H. 1968. Charged Particle Interactions. 2nd ed. *In* "Radiation Dosimetry" (F. Attix and R. WC., eds.), Vol. 1, pp. 157-224. 3 vols. Academic Press, New York.

Blue Histology - Accessory Digestive Glands [Online]. (2000) Available http://www.lab.anhb.uwa.edu.au/mb140/CorePages/Liver/Liver.htm [2001, April 5].

Burton, M. A., and Gray, B. N. 1995. Adjuvant internal radiation therapy in a model of colorectal cancer-derived hepatic metastases. *British Journal of Cancer* 71(2), 322-5.

Burton, M. A., Gray, B. N., and Coletti, A. 1988. Effect of angiotensin II on blood flow in the transplanted sheep squamous cell carcinoma. *European Journal of Cancer & Clinical Oncology* 24(8), 1373-6.

Burton, M. A., Gray, B. N., Jones, C., and Coletti, A. 1989a. Intraoperative dosimetry of Y-90 in liver tissue. *International Journal of Radiation Applications & Instrumentation - B, Nuclear Medicine & Biology* 16, 495-498.

Burton, M. A., Gray, B. N., Klemp, P. F. B., Kelleher, D. K., and Hardy, N. 1989b. Selective internal radiation therapy: Distribution of radiation in the liver. *Eur. J. Canc. Clin. Oncol.* 25, 1487-1497.

Burton, M. A., Gray, B. N., Self, G. W., Heggie, J. C., and Townsend, P. S. 1985. Manipulation of experimental rat and rabbit liver tumor blood flow with angiotensin II. *Cancer Research* 45(11 Pt 1), 5390-3.

Campbell, A. M., Bailey, I. H., and Burton, M. A. 2000. Analysis of the distribution of intra-arterial microspheres in human liver following hepatic yttrium-90 microsphere therapy. Phys. Med. Biol. 45(April), 1023-1033.

Casinu, S., Catalano, V., Baldelli, A.M., Scartozzi, M., Battelli, N., Graziano, F. and Cellerino, R. (1998). Locoregional treatments of unresectable liver metastases from colorectal cancer. *Cancer Treatment Reviews* 22, 355-363.

Caudry, M., Causse, N., Trouette, R., Recaldini, L., Maire, J. P., and Demeaux, H. 1993. Radiotoxic model for three-dimensional treatment planning. Part 1: Theoretical basis. *International Journal of Radiation Oncology, Biology, Physics* 25(5), 907-19.

Chang, A., Schneider, P. D., Sugarbaker, P. H., Simpson, C., Culane, M., and Steinberg, S. 1987. A prospective rangomized trial of regional versus systemic continuous 5 fluorodeoxyuridine chemotherapy in the treatment of colorectal liver metastases. *Ann. Surg.* 206, 685-93.

Ciftci, K., Hincal, A. A., Kas, H. S., Ercan, T. M., Sungur, A., Guven, O., and Ruacan, S. 1997. Solid tumor chemotherapy and in vivo distribution of fluorouracil following administration in poly(L-lactic acid) microspheres. *Pharmaceutical Development & Technology* 2(2), 151-60.

Codde, J. P., Lumsden, A. J., Napoli, S., Burton, M. A., and Gray, B. N. 1993. A comparative study of the anticancer efficacy of doxorubicin carrying microspheres and liposomes using a rat liver tumour model. *Anticancer Research* 13(2), 539-43.

Cravalho, E. G., Fox, L. R., and Kan, J. C. 1980. The application of the bioheat equation to the design of thermal protocols for local hyperthermia. *In* "Thermal Characteristics of tumours: Applications in detection and treatment" (R. K. Jain and P. M. Gullino, eds.), Vol. 335, pp. 87-97. The New York Academy of Sciences, New York.

Dancey, J. E., Shepherd, F. A., Paul, K., Sniderman, K. W., Houle, S., Gabrys, J., Hendler, A. L., and Goin, J. E. 2000. Treatment of nonresectable hepatocellular carcinoma with intrahepatic Y-90-microspheres. *Journal of Nuclear Medicine* 41(10), 1673-1681.

Donath, D., Nori, D., Turnbull, A., Kaufman, N., and Fortner, J. G. 1990. Brachytherapy in the treatment of solitary colorectal metastases to the liver. *J. Surg. Oncol.* 44(1), 55-61.

Drzymala, R. E., Mohan, R., Brewster, L., Chu, J., Goitein, M., Harms, W., and Urie, M. 1991. Dose-volume histograms. *International Journal of Radiation Oncology, Biology, Physics* 21(1), 71-8.

Ebert, M. A. & Zavgorodni, S. F. 2000, 'Modelling dose response in the presence of spatial variations in dose rate', *Medical Physics,* vol. 27, no. 2, pp. 393-400.

Endrich, B. & Vaupel, P. 1998, 'The role of the microcirculation in the treatment of malignant tumours: Facts and fiction', in *Blood perfusion and microenviroment of human tumors - Implications for Clinical Oncology*, eds. M. Molls & P. Vaupel, Springer-Verlag, Berlin, pp. 19-39.

Fawcett, D. W. 1986. "A Textbook of Histology." 11 ed. W. B. Saunders Company, Philadelphia.

Feinendegen, L. 1994. Microdosimetric considerations of hepatic radioembolization. *Journal of Nuclear Medicine* 35(10), 1644-1645.

Fox, R. A., Klemp, P. F., Egan, G., Mina, L. L., Burton, M. A., and Gray, B. N. 1991. Dose distribution following selective internal radiation therapy. *International Journal of Radiation Oncology, Biology, Physics* 21(2), 463-7.

Fukumura, D., Yuan, F., Monsky, W. L., Chen, Y. & Jain, R. K. 1997, 'Effect of host microenvironment on the microcirculation of human colon adenocarcinoma.', *American Journal of Pathology,* vol. 151, no. 3, pp. 679-688.

Gitman, I., and Levine, M. D. 1970. An algorithm for detecting unimodal fuzzy sets and its application as a clustering technique. *IEEE Transactions on Computing* C-19(7), 583-593.

Goldberg, J. A., Thomson, J. A., Bradnam, M. S., Fenner, J., Bessent, R. G., McKillop, J. H., Kerr, D. J., and McArdle, C. S. 1991. Angiotensin II as a potential method of targeting cytotoxic-loaded microspheres in patients with colorectal liver metastases. *British Journal of Cancer* 64(1), 114-9.

Gray, B., Anderson, J., Burton, M., van Hazel, G., Codde, J., Morgan, C., and Klemp, P. 1992. Regression of liver metastases following treatment with yttrium-90 microspheres. *Aust and New Zealand Journal of Surgery* 62, 105-110.

Gray, B. N., Burton, M. A., Kelleher, D. K., Metz, L., and Klemp, P. 1990. Tolerance of the liver to the effects of yttrium-90 radiation. *International Journal of Radiation Oncology, Biology, Physics* 18, 619-623.

Groen, K. A. 1999, 'Primary and metastatic liver cancer', *Seminars in Oncology Nursing,* vol. 15, no. 1, pp. 48-57.

Halley, S. 1999. The distribution of microspheres and histopathological changes in malignant liver tissue and normal parenchyma following selective internal radiation therapy with hepatic perfusion chemotherapy. Honours Thesis. Charles Sturt University.

Hamilton, R. 1999. "Liver Histology". [on line]. Available http://128.218.123.161/IDS_100/liver/chapter18.html [2000, July 26] .

Hardy, A. 1996. On the number of clusters. *Computational Statistics & Data Analysis* 23, 83-96.

Hayes, A. J., Li, L. Y. & Lippman, M. E. 2000, 'Anti-vascular therapy: A new approach to cancer treatment', *Western Journal of Medicien,* vol. 172, no. 1, pp. 39-42.

Hearn, D., and Baker, P. 1986. "Computer graphics." Prentice Hall, New Jersey.

HB134 - Liver (high power) [Online]. (1998) Available http://virtual.curtin.edu.au/curtin/dept/biomed/teach/hubiol/134hrliverh.html [2000, August 28].

HB134 - Liver (low power) [Online]. (1998) Available http://virtual.curtin.edu.au/curtin/dept/biomed/teach/hubiol/134hrliverl.html [2000, August 28].

Ho, S., Lau, W. Y., Leung, T. W. T. & Johnson, P. J. 1998, 'Internal radiation therapy for patients with primary of metastatic hepatic cancer', *Cancer,* vol. 83, no. 9, pp. 1894-1907.

Ho, S., Lau, W. Y., Leung, T. W., Chan, M., Ngar, Y. K., Johnson, P. J., and Li, A. K. 1996. Partition model for estimating radiation doses from yttrium-90 microspheres in treating hepatic tumours. *European Journal of Nuclear Medicine* 23(8), 947-52.

Hunstberger, and Billingsley 1981. "Elements of statistical inference" 5th ed. Allyn and Bacon Inc., Boston.

Jain, R. K. 1994. Barriers to drug delivery in solid tumours. *Scientific American* 271(1), 42-49.

Kienle, P., Weitz, J., Klaes, R., Koch, M., Benner, A., Lehnert, T., Herfarth, C. & von Knebel Doeberitz, M. 2000, 'Detection of isolated disseminated tumors cells in bone marrow and blood samples of patients with hepatocellular carcinoma', *Archives of Surgery,* vol. 135, no. 2, pp. 213-8.

Kondering, M. A., van Ackern, C., Fail, E., Steinberg, F. & Streffer, C. 1998, 'Morphological aspects of tumor angiogenisis and microcirculation', in *Blood perfusion and microenviroment of human tumors - Implications for Clinical Oncology*, eds. M. Molls & P. Vaupel, Springer-Verlag, Berlin, pp. 5-17.

Last, R. J. 1978. "Anatomy: Regional and Applied." 6th ed. Churchill Livingston, Edinburgh.

Lau, W. Y., Ho, S., Leung, T. W., Chan, M., Ho, R., Johnson, P. J., and Li, A. K. 1998. Selective internal radiation therapy for nonresectable hepatocellular

carcinoma with intraarterial infusion of 90yttrium microspheres. *International Journal of Radiation Oncology, Biology, Physics* 40(3), 583-92.

Lau, W. Y., Leung, W. T., Ho, S., Leung, N. W., Chan, M., Lin, J., Metreweli, C., Johnson, P. & Li, A. K. 1994, 'Treatment of inoperable hepatocellular carcinoma with intrahepatic arterial yttrium-90 microspheres: a phase I and II study', *British Journal of Cancer,* vol. 70, no. 5, pp. 994-9.

Lawrence, T. S., Robertson, J. M., Anscher, M. S., Jirtle, R. L., Ensminger, W. D., and Fajardo, L. F. 1995. Hepatic toxicity resulting from cancer treatment. *International Journal of Radiation Oncology, Biology, Physics* 31(5), 1237-48.

Lawrence, T. S., Ten Haken, R. K., Kessler, M. L., Robertson, J. M., Lyman, J. T., Lavigne, M. L., Brown, M. B., DuRoss, D. J., Andrews, J. C., and Ensminger, W. D. 1992. The use of 3-D dose volume analysis to predict radiation hepatitis. *International Journal of Radiation Oncology, Biology, Physics* 23(4), 781-8.

Leavers, V. F. 1992. "Shape detection in computer vision using the Hough transform." Springer-Verlag, London.

Leen, E., Goldberg, J. A., Angerson, W. J. & McArdie, C. S. 2000, 'Potential role of doppler perfusion index in selection of patients with colorectal cancer for adjuvant chemotherapy', *The Lancet,* vol. 355, no. 9197, pp. 34-37.

Li, C. Y., Shan, S., Huang, Q., Braun, R. D., Lanzen, J., Hu, K., Lin, P. & Dewhirst, M. W. 2000, 'Initial stages of tumor cell-induced angiogenesis: evaluation via skin window chambers in rodent models.', *Journal of the National Cancer Institute,* vol. 92, no. 2, pp. 143-7.

Lin, W. Y., Tsai, S. C., Hsieh, J. F., and Wang, S. J. 2000. Effects of Y-90-microspheres on liver tumors: Comparison of intratumoral injection method and intra-arterial injection method. *Journal of Nuclear Medicine* 41(11), 1892-1897.

Ling, C. C. L. 1992. Permanent implants using Au-198, Pd-103 and I-125: Radiobiological considerations based on the linear quadratic model. *Int. J. Radiation Oncology Biol. Phys.* 23, 81-87.

Lowry, S. 1974. "Fundamentals of Radiation Therapy and Cancer Chemotherapy." English Universities Press, London.

McGinn, C. J., Ten Haken, R. K., Ensminger, W. D., Walker, S., Wang, S. & Lawrence, T. S. 1998, 'Treatment of intrahepatic cancers with radiation doses based on a normal tissue complication probability model', *Journal of Clinical Oncology,* vol. 16, no. 6, pp. 2246-52.

Meade, V. M., Burton, M. A., Gray, B. N., and Self, G. W. 1987. Distribution of different sized microspheres in experimental hepatic tumours. *European Journal of Cancer & Clinical Oncology* 23(1), 37-41.

Moss, W. T., Brand, W. N., and Batifora, H. 1973. "Radiation Oncology: Rationale, Techniques, Results." 4th ed. C.V. Mosby Company, St. Louis.

Mould, R. 1994a. Radium Brachytherapy: Historical Review. *In* "Brachytherapy from Radium to Optimization" (R. Mould, J. Battermann, A. Martinez and B. Spieser, eds.), pp. 1-9. Nucletron International, The Netherlands.

Mould, R., Battermann, J., Martinez, A., and Spieser, B., eds. 1994b. Brachytherapy from radium to optimization. The Netherlands: Nucletron International.

Mumper, R. J., Ryo, U. Y., and Jay, M. 1991. Neutron-activated holmium-166-poly (L-lactic acid) microspheres: a potential agent for the internal radiation therapy of hepatic tumors. *Journal of Nuclear Medicine* 32(11), 2139-43.

Nahum, A. E. 1996. Microdosimetry and radiocurability: modelling targeted therapy with beta-emitters. [Review] [34 refs]. *Physics in Medicine & Biology* 41(10), 1957-72.

Nijsen, J. F. W., Zonnenberg, B. A., Woittiez, J. R. W., Rook, D. W., Swildens-van Woudenberg, I. A., van Rijk, P. P., and Schip, A. D. V. 1999. Holmium-166

poly lactic acid microspheres applicable for intra-arterial radionuclide therapy of hepatic malignancies: effects of preparation and neutron activation techniques. *European Journal of Nuclear Medicine.* 26(7), 699-704.

Paton, R. 1999. "Computing at the tissue/organ level" [online]. Available http://www.csc.liv.ac.uk/~biocomp/reports/tissue_comp/tissue.html [2000, Aug 3].

Pillai, K. M., McKeever, P. E., Knutsen, C. A., Terrio, P. A., Prieskorn, D. M., and Ensminger, W. D. 1991. Microscopic analysis of arterial microsphere distribution in rabbit liver and hepatic VX2 tumor. *Selective Cancer Therapeutics* 7(2), 39-48.

Prestwich, W. V., Nunes, J., and Kwok, C. S. 1989. Beta dose point kernels for radionuclides of potential use in radioimmunotherapy [published erratum appears in J Nucl Med 1989 Oct;30(10):1739-40]. *Journal of Nuclear Medicine* 30(6), 1036-46.

Ridge, J. A., Bading, J. R., Gelbard, A. S., Benua, R. S., and Daly, J. M. 1987. Perfusion of colorectal hepatic metastases. Relative distribution of flow from the hepatic artery and portal vein. *Cancer* 59(9), 1547-53.

Roberson, P. L., Ten Haken, R. K., McShan, D. L., McKeever, P. E., and Ensminger, W. D. 1992. Three-dimensional tumor dosimetry for hepatic yttrium-90-microsphere therapy. *Journal of Nuclear Medicine* 33(5), 735-8.

Robertson, J. M., Lawrence, T. S., Andrews, J. C., Walker, S., Kessler, M. L. & Ensminger, W. D. 1997, 'Long-term results of hepatic artery fluorodeoxyuridine and conformal radiation therapy for primary hepatobiliary cancers.', *Int J Radiat Oncol Biol Phys,* vol. 37, no. 2, pp. 325-330.

Russ, J. C. 1995. "The image processing handbook." 2nd. ed. CRC Press, Florida.

Russell, A. H., Clyde, C., Wasserman, T. H., Turner, S. S., and Rotman, M. 1993. Accelerated hyperfractionated hepatic irradiation in the management of patients

with liver metastases: results of the RTOG dose escalating protocol. *International Journal of Radiation Oncology, Biology, Physics* 27(1), 117-23.

Russell, A. H., Pelton, J., Reheis, C. E., Wisbeck, W. M., Tong, D. Y., and Dawson, L. E. 1985. Adenocarcinoma of the colon: an autopsy study with implications for new therapeutic strategies. *Cancer* 56(6), 1446-51.

Ruszniewski, P. & Malka, D. 2000, 'Hepatic arterial chemoembolization in the management of advanced digestive endocrine tumors.', *Digestion*`, vol. 62 Suppl. 1, pp. 79-83.

Sachs, L. 1984. "Applied Statistics: A Handbook of Techniques." 2nd ed. Springer-Verlag, New York.

SAS, I. 1982. Introduction to SAS clustering procedures. *In* "SAS User's Guide: Statistics", pp. 417-422. SAS Institute Inc., Cary, NC.

SAS, I. 1988. The cluster procedure. *In* "SAS/STAT User's Guide, Release 6.03", pp. 283-357. SAS Institute Inc., Cary, NC.

Scheele, J., Stangl, R., Altendorf-Hofmann, A. & Gall, F. P. 1991, 'Indicators of prognosis after hepatic resection for colorectal secondaries', *Surgery,* vol. 110, no. 1, pp. 13-29.

Schilling, M. K., Redaelli, C., Friess, H., Blum, B., Signer, C., Maurer, C. A. & Buchler, M. W. 1999, 'Evaluation of laser Doppler flowmetry for the study of benign and malignant gastric blood flow in vivo', *Gut,* vol. 45, no. 3, pp. 341-5.

Sheehan D.C. and Hrapchak B.B. 1980. *Theory and practice of hitsotechnology.* C.V. Mosby: St Louis, pp. 227-228.

Shen, S., DeNardo, G., Yuan, A., DeNardo, D., and DeNardo, S. 1994. Planar gamma camera imaging and quantitation of yttrium-90 bremsstrahlung. *Journal of Nuclear Medicine* 35, 1381-1389.

Simpkin, D. J., and Mackie, T. R. 1990. EGS4 Monte Carlo determination of the beta dose kernel in water. *Med. Phys.* 17(2), 179-86.

Song, C. W. 1998, 'Modification of Blood Flow', in *Blood perfusion and microenviroment of human tumors - Implications for Clinical Oncology*, eds. M. Molls & P. Vaupel, Springer-Verlag, Berlin, pp. 193-207.

Synder, W. S., Ford, M. R., Warner, G. G., and Watson, S. B. 1975. "S" absorbed dose per unit cumulative activity for selected radionuclides and organs. *NM/MIRD Pamphlet No. 11* .

Tortora, G. 1983. "Principles of Human Anatomy." 3rd ed. Harper & Row, New York.

Trott, N. G., ed. 1987. Radionuclides in Brachytherapy: Radium and After. British Journal of Radiology: British Institute of Radiology Supp 21.

Turner, J. H., Claringbold, P. G., Klemp, P. F., Cameron, P. J., Martindale, A. A., Glancy, R. J., Norman, P. E., Hetherington, E. L., Najdovski, L., and Lambrecht, R. M. 1994. 166Ho-microsphere liver radiotherapy: a preclinical SPECT dosimetry study in the pig. *Nuclear Medicine Communications* 15(7), 545-53.

Walter, J., Miller, H., and Bomford, C. K. 1979. "A short textbook of radiotherapy." 4th ed. Churchill Livingston, Edinburgh.

Wang, S. J., Lin, W. Y., Chen, M. N., Chi, C. S., Chen, J. T., Ho, W. L., Hsieh, B. T., Shen, L. H., Tsai, Z. T., Ting, G., Mirzadeh, S., and Knapp, F. F. 1998. Intratumoral Injection Of Rhenium-188 Microspheres Into an Animal Model Of Hepatoma. *Journal of Nuclear Medicine* 39(10), 1752-1757.

Weaver, M.L., Atkinson, D. and Zemel,R., 1995. Hepatic cryosurgery in treating colorectal metastases. *Cancer* 76, 210-214.

Yoo, H. S., Park, C. H., Suh, J. H., Lee, J. T., Kim, D. I., Kim, B. S., and Madsen, M. T. 1989. Radioiodinated fatty acid esters in the management of hepatocellular

carcinoma: preliminary findings. *Cancer Chemotherapy & Pharmacology* 23(Suppl), S54-8.

Yorke, E. D., Jackson, A., Fox, R. A., Wessels, B. W., and Gray, B. N. 1999. Can current models explain the lack of liver complications in Y-90 microsphere therapy? *Clinical Cancer Research (Suppl.)* 5, 3024s-3030s.

Zavgorodni, S. F. 1996. A model for dose estimation in therapy of liver with intraarterial microspheres. *Physics in Medicine & Biology* 41(11), 2463-80.